University of Birmingham

AC Railway Power Network with Integration of Renewable Energy Sources

by

Nakaret Kano

A thesis submitted to
the University of Birmingham
for the degree of
DOCTOR OF PHILOSOPHY

Department of Electronic, Electrical and Systems Engineering
College of Engineering and Physical Sciences
University of Birmingham, UK
March 2023

Abstract

Currently, 25 kV 50/60 Hz AC electrical railway systems are the global standard for mainline and high-speed rail. However, high-speed trains consume substantial energy from the power supply, contributing to carbon emissions and climate change. Most electricity is generated by fossil fuel-based steam turbine generators, including power for railways. To reduce carbon emissions, it is crucial to decrease reliance on fossil fuels and explore renewable energy sources. While studies exist on integrating renewables into the power grid, few have examined their connection to railway power supply systems. This thesis aims to identify a suitable scheme for integrating renewable energy and an energy storage system to decarbonize the traction power network.

The thesis reviews the AC railway traction power supply system, including transformer connections and feeding arrangements. It explores solar PV farms, wind farms, and energy storage systems. A simulation model is developed to verify the findings using a case study of a high-speed railway route.

Proposed renewable integration schemes for the AC railway traction network are presented and simulated. The case study results show that connecting the RES to a three-phase railway power network yields the lowest power losses, requires less investment, and provides greater long-term cost savings. Furthermore, all schemes based on a 400 kV transmission system meet the UK's restriction of 1.5% voltage unbalance factor (VUF). Integrating 120 MW of RES in the case study reduces CO2 emissions by 50%.

A scheme integrating solar PV farms and large-scale energy storage into the railway power supply is introduced. It studies energy flow, storage benefits, and renewable sources. The main control strategy is to reduce system energy costs by using regenerative braking energy and purchasing low-priced energy. Results show effective utilization of captured regen energy, though not all can be absorbed. The scheme with energy storage exhibits lower electricity costs and carbon emissions compared to the benchmark scheme. Integration of PV farms in the benchmark scheme reduces net electricity cost and carbon tax. Employing both PV farms and energy storage achieves the lowest electricity cost and carbon emissions.

A concept to decarbonize electric railways by integrating solar PV farms, wind farms, and an energy storage system (ESS) has been proposed. An energy management system was developed to calculate energy flow and cost, considering contact wire loss and conversion loss. The Brute Force Algorithm was used to optimize the capacity and location of the PV farm, wind farm, and ESS for the lowest daily expenses. The High Speed 2 Railway in the UK was used as a case study. Implementing ESS and renewable energy sources (RESs) significantly reduced global cost and carbon emissions. The ESS alone eliminated around 1.3% of the global cost by absorbing and reusing regenerative energy. Including PV and wind farms increased this figure to 10% and 62% respectively. Taking all factors into account, establishing a wind power plant was found to be the more cost-effective option. The study also showed that the ideal installation sites for the plants and ESS varied depending on the scenario.

Acknowledgements

Firstly, I would like to sincerely express my gratitude to my supervisors Prof. Stuart Hillmansen and Prof. Clive Roberts for their help advising me on my PhD research project as well as for supporting me throughout my PhD. I would not have come this far if I had not known Dr. Zhongbei Tian who sacrificed valuable time to advise and guide me to the correct way. Your guidance has helped me to accomplish another level of achievement.

Secondly, I would like to express my appreciation to my wife (Bongkot Mahayotsanan) and my family for cheering me up and giving me the strength to challenge myself. I would also like to thank my sponsor for supporting my scholarship throughout the four years of this study. Studying at the University of Birmingham was a memorable opportunity that opened up my world, teaching me lessons not only in relation to a particular academic topic but also in life.

Lastly, I would like to express my gratitude to Nutthaka Chinomi for her help in journal article writing. I am also deeply grateful to Ngamjit Kongsupon for her meticulous assistance in correcting my thesis. Additionally, I extend my sincere appreciation to all my friends in Thailand and the UK who provided unwavering emotional support throughout this journey, with special recognition to Jitpisute Chunthorng-Orn, Ngamjit Kongsupon, Hattaya Benya-aphikul, Adjabhak Wongviriya, Ni-Asri Cheputeh, Teerapong Iamcheerangkoon, Punya Promhuad, Siwanon Rattanakanokchai, and Chutiphon Moranon. Together, we embarked on an extraordinary journey spanning hundreds of miles, traversing from the vibrant southern landscapes to the awe-inspiring beauty of lakes and towering mountain peaks. Our expedition even led us to conquer the majestic summits of the United Kingdom, encompassing the lofty peaks of England and Wales.

Table of Contents

List of Figures

List of Tables

List of Acronyms

Term	Explanation / Meaning / Definition
3Ph	Three Phase
AC	Alternating Current
AT	Autotransformer
BES	Battery Energy Storage
BF	Brute Force
BT	Booster Transformer
CO2	Carbon Dioxide
DC	Direct Current
ESS	Energy Storage System
FES	Flywheel Energy Storage
LV	Low Voltage
MV	Medium Voltage
PCC	Point of Common Coupling
POC	Point of Connection
PV	Photovoltaic
PWM	Pulse Width Modulation
RES	Renewable Energy Source
SOC	State of Charge
UC	Ultracapacitor

Note: International System of Units is used throughout this thesis without statement.

Chapter 1 Introduction

1.1 Background

Rail transport is one of the most popular modes of transport. It is a significant means of transportation utilised for passenger and cargo transit. Passenger and freight activity is anticipated to more than double by 2050. Such growth is a sign of social and economic success, but it is accompanied by an increase in energy demand, CO_2 emissions, and air pollution. Rail networks transport 8% of the world's motorised passenger movements and 7% of the world's freight, but only 2% of the transportation sector's energy use. Less than 0.6 million barrels per day of oil (about 0.6% of global oil consumption) and around 290 terawatt-hours (TWh) of electricity (more than 1% of global power consumption) are utilised by rail services. They are responsible for roughly 0.3% of direct CO_2 emissions from fossil fuel combustion and the same proportion (0.3%) of fine particulate matter emissions connected to energy ($PM_{2.5}$) [1]. With the rapid expansion in high-speed train operation and more railway routes will be electrified in the future, rail transport sector will require more energy than ever before, and those figures are expected to increase. Generally, rail transit is seen as a more environmentally friendly means of transportation than other modes, such as road or air travel. Nevertheless, depending on several variables, such as the type of train, the distance travelled, and the energy mix used to power the trains, the precise quantity of carbon emissions from rail transportation can vary. For instance, compared to diesel-powered trains, electric trains fueled by renewable sources emit substantially less carbon dioxide.

Carbon emissions, and more specifically carbon dioxide emissions, are a major factor in global warming. Burning fossil fuels like coal, oil, and gas for energy generation releases CO_2 into the atmosphere, where it acts as a greenhouse gas and contributes to global warming, which is already having significant impacts on the planet. Many nations and institutions are working to minimise their carbon footprints by switching to renewable energy sources, including wind, solar, and hydropower. Emissions from transportation, manufacturing, and construction are all targets of new laws and regulations. In 2019, with the aim of reaching a carbon-neutral economy by 2050, the European Union (EU) proposed the European Green Deal, which is a comprehensive plan to shift to a sustainable, low-carbon economy and address the challenges of climate change. There are also three key targets for 2030: at least a 40 per cent reduction in greenhouse gas emissions, at least 32 per cent of renewable energy share and at least 32.5 per cent energy efficiency improvement. Another vital project from the green deal is to make the railway the backbone of transportation [2].

In order to mitigate the climate change impacts, which are expected to intensify in the near future, decarbonisation must be implemented in all industries. Switching from diesel-fueled trains to electric trains powered by renewable energy sources such as wind or solar power is one of the most effective ways to decarbonise rail transportation. This can be accomplished through the application of technologies, such as batteries, ultracapacitors and other types of energy storage devices, and the expansion of electrified rail networks. Nevertheless, there are only a few projects that integrated renewable energy sources into the traction power network in real work. Therefore, this research aims to present ways to utilise renewable energy sources as a power hub for the traction system. Furthermore, the energy storage system will be studied. This work also investigates the advantages and disadvantages of those renewables and energy storage systems.

1.2 Motivation

- Most studies exclude large-scale plants and concentrate on PV farms as the sole form of renewable energy for railway power system integration. To accelerate decarbonisation, the proportion of supplied energy from renewable sources must be increased. This can be accomplished by incorporating additional renewable plant types and increasing plant size. Some studies suggest that structural modifications to the traction power supply system may be required to effectively integrate renewable sources, which entails substantial investment costs.
- The combined use of energy storage systems and renewable energy sources for traction power networks has not been thoroughly assessed in terms of performance and energy flow. Existing studies primarily examined transient analysis within a short time frame (seconds) to evaluate power quality.
- Numerous researchers in the field of power system analysis are focused on determining the optimal capacity of PV farms, wind farms, and energy storage.

For the electrified railway power system, however, very little work has been completed. In addition, previous studies lacked optimisation to determine the optimal location for installing renewables and energy storage along a railway route, taking contact wire loss into account.

1.3 The objectives are to study

- Literature about AC railway connection schemes and the integration of renewable energy sources into the AC traction power system is reviewed. The benefits and drawbacks of each scheme are compared.
- Based on the literature review, a model of a 25-kV AC railway power network can be developed and used as a based model.
- Renewable integration schemes for AC railway should be proposed. Models of solar PV farms and wind farms will be built to integrate with based model according to configurations of each proposed scheme. The energy evaluation and performance of each scheme can be assessed to perform an in-depth comparison between different proposed schemes.
- The energy storage system will be studied and modelled with the aims to capture the excess energy from regenerative braking and renewable energy sources.
- An optimisation problem must be formulated to find the optimal capacity and location of renewable energy sources and energy storage in which total cost is minimal. A contact wire loss model will be included in the optimisation problem.

1.4 Thesis Structure

The detailed structure of the thesis is given as follows:

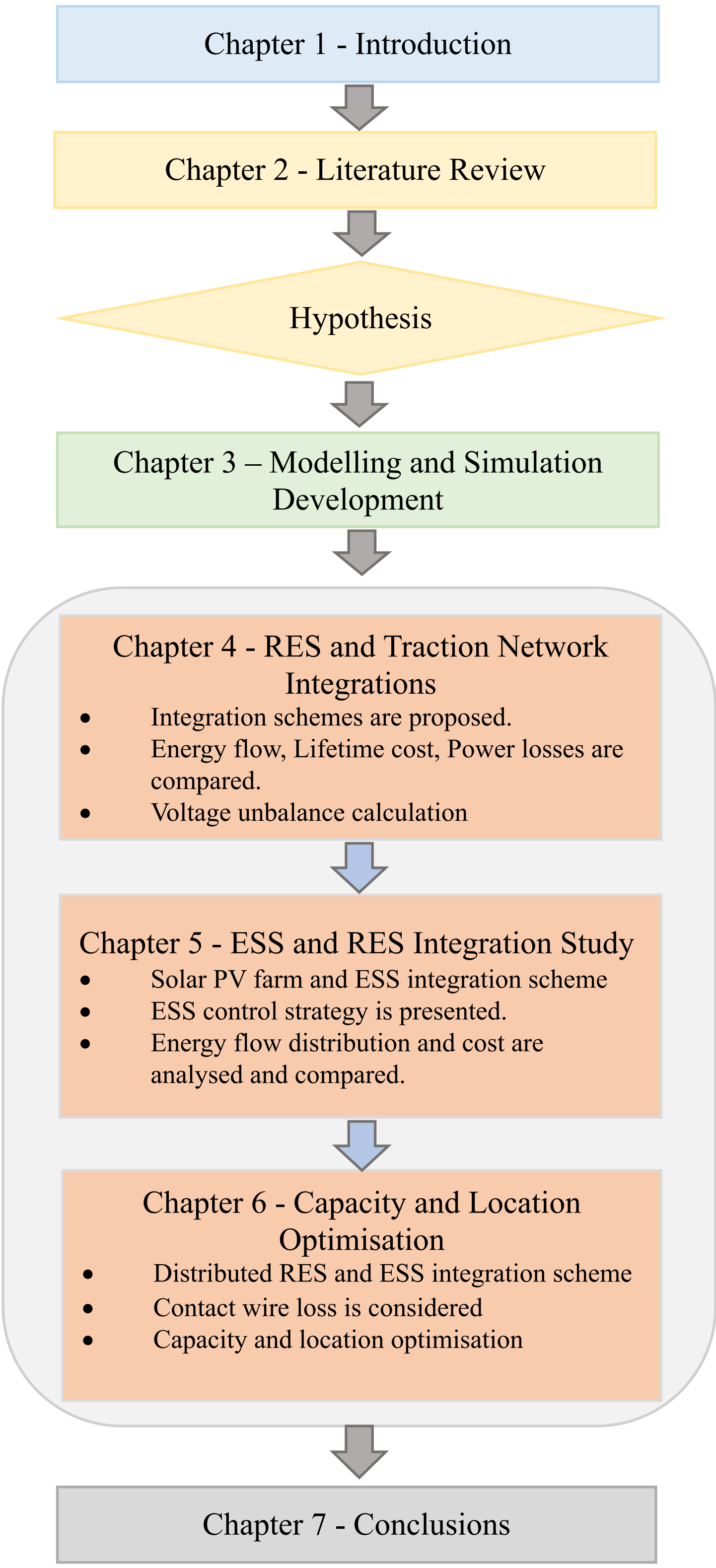

Figure 1-1 Thesis structure

Chapter 1 provides a general introduction related to the railway energy background. Moreover, the motivation, the objectives and thesis structure are presented.

Chapter 2 gives a review of different AC railway transformer connections and feeding connections followed by fundamentals of solar PV energy system and wind energy system. Additionally, energy storage technologies and their application in the electrified railway are studied. The literature related to railway energy systems and existing methods to bring toward low carbon emission railways are reviewed and analysed to identify the research gap.

Chapter 3 presents the procedures that are used to create the simulation model. This includes the derivation of the train power profile, AC railway power system development and renewable energy sources and energy storage modelling.

Chapter 4 compares several aspects of newly proposed schemes for integrating solar PV farms and wind farms. The voltage unbalance factor and lifetime cost of each proposed scheme are investigated and analysed.

Chapter 5 introduces the integration of energy storage devices and solar PV farms into the three-phase transmission line. In order to reduce the total electricity cost, the control strategy of energy storage is introduced.

Chapter 6 presents the optimisation to find the capacity and location of energy storage, PV farms and wind farms to be equipped on the contact wire of one of the proposed schemes to minimize global cost. Moreover, this chapter considered the copper loss on the contact wire.

Chapter 7 concludes all the work that has been done in this research and suggests future work that is worth to further study.

1.5 Innovation and Publications

- **Challenges and Innovation**

Even though many challenges have been found while conducting this research, there are innovations that are created while completing the research. Furthermore, part of the accomplishment is presented by publications. The innovations and challenges for the main chapters are listed below:

- Chapter 3: Building integration schemes for traction networks and other energy sources using phasor-type simulation is challenging. However, this type of simulation enables us to construct the model for train operation and energy management with small time steps over a significant time horizon. This will make the simulation models able to capture regenerative braking power which will last less than 60 seconds and the entire day's energy flow is obtained and analysed.

- Chapter 4: Constructing the train power profile based on the chosen case study is time-consuming because both directions (up and down) of train services are considered. Moreover, with the integration of the renewable energy sources, the simulation time for each model becomes large. Total simulation time to obtain the complete results is tremendous owing to 60 months of meteorological data being used.

- Chapter 5: Design control strategy for energy storage systems is difficult and a comprehensive study needs to be carried out to make sure that all scenarios are taken into account in energy storage control strategy. Furthermore, when there are more energy sources and loads, the energy flow pattern is more complex.

- Chapter 6: Regarding the contact wire loss calculation, a number of equations arise due to the complex power flow pattern, especially in cases with both renewable energy source and energy storage included. Furthermore, due to the nature of the optimisation problem in this study, most of the optimisation algorithms are not suitable to solve the problem.

- **Publication list:**

[1] N. Kano, Z. Tian and S. Hillmansen, “Integration of energy storage and renewable energy sources into AC railway system to reduce carbon emission and energy cost,” *IEEE Veh. Power Propuls. Conf. VPPC 2020 - Proc.*, 2020.

[2] N. Kano, Z. Tian, N. Chinomi, and S. Hillmansen, “Comparison of renewable integration schemes for AC railway power supply system,” *IET Electr. Syst. Transp.*, vol. 12, no. 3, pp. 209–222, 2022. (Chapter 4 is reproduced by this paper)

[3] N. Kano, Z. Tian, N. Chinomi, X. Wei and S. Hillmansen, “Renewable Sources and Energy Storage Optimization to Minimize the Global Costs of Railways,” *IEEE Transactions on vehicular technology, 2023.* (Chapter 6 is reproduced by this paper)

Chapter 2 Literature Review

2.1 Introduction

Due to a growth in railway traffic, particularly on the electrified railway, trains consume a substantial quantity of energy, and this tendency will continue to rise. Not only is there concern regarding the shortage of electric energy to power the trains, but also the climate effect caused by the trains' carbon emissions. Moreover, it is not a simple operation to construct new power-generating plants for the network in order to expand the railroad system. Renewable energy is an alternate answer to this problem; in comparison to other sources of energy, it has a number of advantages that make it an attractive choice. It is a source of energy that is not only clean but also sustainable and abundant, and it can help cut emissions of greenhouse gases and ameliorate the effects of climate change. It is also helpful in diversifying the energy mix and reducing dependence on fossil fuels, both of which can improve energy security and lower energy prices over the long run. During braking, certain types of electric trains have the ability to recycle energy, which is referred to as regenerative braking energy. Therefore, if both of these sources of energy are controlled efficiently, the demand for energy from the power plant will be lower. However, energy storage devices are required in order to manage the power generated by renewable sources and regenerative braking systems.

An overview of the AC railway power system is given in this chapter, followed by the literature on renewable integration into the traction power system. Additionally, the use of an energy storage system for the rail system is reviewed. After the research gaps are found, the hypothesis is developed.

2.2 AC Railway Traction Power Systems

The majority of high-speed electric trains and intercity rail lines are powered by alternating current (AC) power system, which is transmitted to the train through an overhead contact wire. The overhead contact wire is supported by poles or other structures along the tracks, and the train is fitted with a pantograph, a mechanism that links the train to the overhead wire and enables it to draw power from it.

2.2.1 AC Power Supplies

The use of AC power enables the transmission of electricity to trains over large distances with minimal loss. Two types of single-phase alternating current traction systems are available for mainline railroads: 25 kV 50/60 Hz and 15 kV 16.7 Hz. The first system is a standard supply and the most popular in use today [3]. Some European nations, including Germany, Austria, Switzerland, Sweden, and Norway, continue to employ the latter. Before electric current consumes by the electric train, it travels from the power sources through several stages and components. The main component of the standard 25 kV AC traction network is the traction transformer equipped at the traction substation, which steps down three-phase high voltage currents, typically 132, 275 and 400 kV in the UK, to single-phase 25 kV at feeding sections. As shown in Figure 2-1, a typical structure of a 25 kV AC feeding system is comprised of various parts. Each transformer at the feeder station (traction substation) supplies the load on its side under normal conditions. Nevertheless, in case of emergency, the transformer located opposite will also be able to supply a total load of both sides by operating the circuit breaker at the middle between both transformers. Furthermore, in the worst-case scenario when there is a failure of the traction substation, the circuit breaker at Mid-point track sectioning cabin will be switched on to let the power from another traction substation supply the load [4].

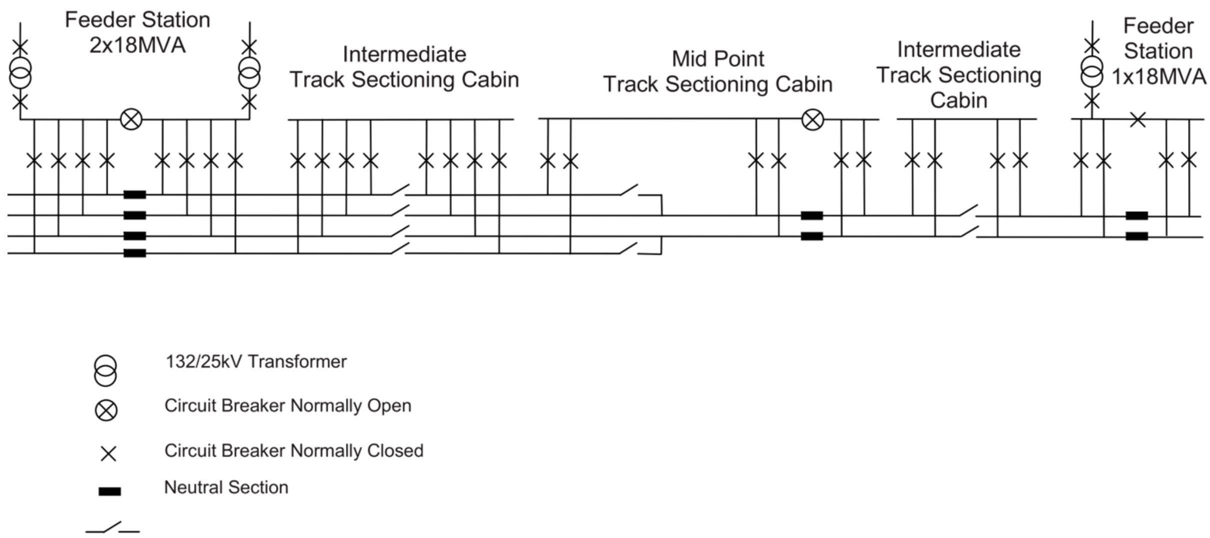

Figure 2-1 Typical 25 kV AC Feeding Section created by R.D. White [4]

2.2.2 Transformer Connections

Due to the nature of traction load, which is normally supplied by single-phase AC power in a railroad system, it might contribute to the possibility of imbalance problems. This is due to the fact that traction load is often a highly dynamic load with power requirements that can fluctuate dramatically based on a variety of factors, including the speed of the trains, their weight, and the grade of the track. This might make maintaining a properly balanced power supply across all three phases problematic. There are many special transformer connections created and used in the real world to alleviate the issue of the imbalance from the railway side.

2.2.2.1 Single-phase Connection

In this configuration, a transformer is connected by a cyclic permutation of phases. A single transformer is provided with two phases from the three-phase transmission line as shown in Figure 2-2a. This configuration is suitable for low-traffic railway lines with small power demand [5].

2.2.2.2 V/V Connection

Two single-phase transformers are required in the traction substation. The primary side of each is connected to a pair of phases from the high-voltage power supply. Therefore, there are two single-phase 25 kV feeders on the secondary side. Due to the phase shift on the output, the neutral zone is inevitable to separate the contact wires [5].

2.2.2.3 Scott Connection

The Scott transformer is comprised of two single-phase transformers, which are typically referred to as the main transformer (M) and the teaser transformer (T), and they feature unique winding ratios. This transformer is coupled to a three-phase system [6].

2.2.2.4 Le Blanc Connection

Three single-phase transformers are used to convert three-phase power to three single-phase outputs in a Le Blanc transformer connection. Then, these three single-phase outputs are joined to provide a balanced three-phase system. This permits the traction motor to receive the required three-phase electricity while still utilising single-phase transformers [6].

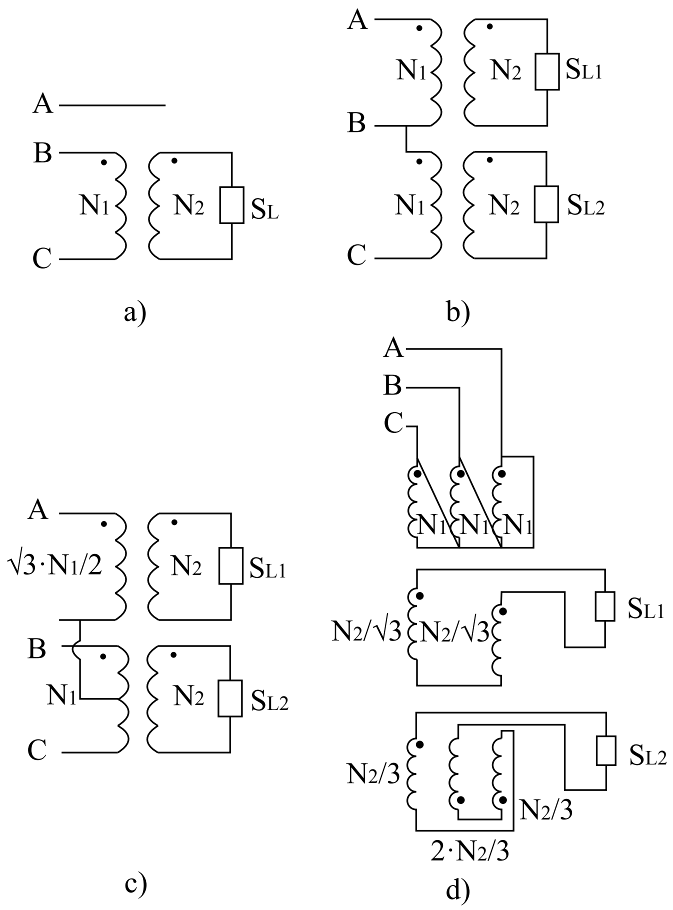

Figure 2-2 Traction Transformer Connections: a) Single-phase connection, b) V/V connection, c) Scott connection and d) Le Blanc Connection [5] [6].

2.2.3 AC Railway Feeding Arrangement

2.2.3.1 Direct Feeding

The least capital-intensive way of feeding power is by direct connection of the traction feed transformer secondary to the catenary and rail at each substation (Figure 2-3(a)). The disadvantages are high feeding impedance with large losses, high rail-to-earth voltage (a potential safety hazard) and the production of earth currents which can cause interference in adjacent telecommunications circuits [3].

2.2.3.2 Direct Feeding with Return Conductor

The addition of a return conductor connected to the rails at regular intervals, typically 5 or 6 km, provides a lower impedance traction current return path (Figure 2-3(b)) [3].

2.2.3.3 Booster Transformer Feeding

Booster transformers (BTs), rated at about 150 kVA, were first used on the Tokaido Shinkansen (Japan) in 1964. They are placed along the catenary at 3-4 km intervals and represent a further improvement in the feeding circuit [3]. The BT primary is connected across a gap in the contact wire and the secondary is connected to a return conductor as shown in Figure 2-3(c).

2.2.3.4 Autotransformer Feeding

Autotransformer supply schemes are increasingly used for high-speed AC electrification. The supply takes advantage of the 50 kV (2x25 kV) yet being able to utilise the standard 25 kV traction equipment. The autotransformer works on the principle that the train is supplied between the +25 kV and rail with a parallel feeder at -25 kV as shown in Figure 2-3(d). The AT winding is connected between the catenary and auxiliary feeder, with the rails tied to an intermediate point [4].

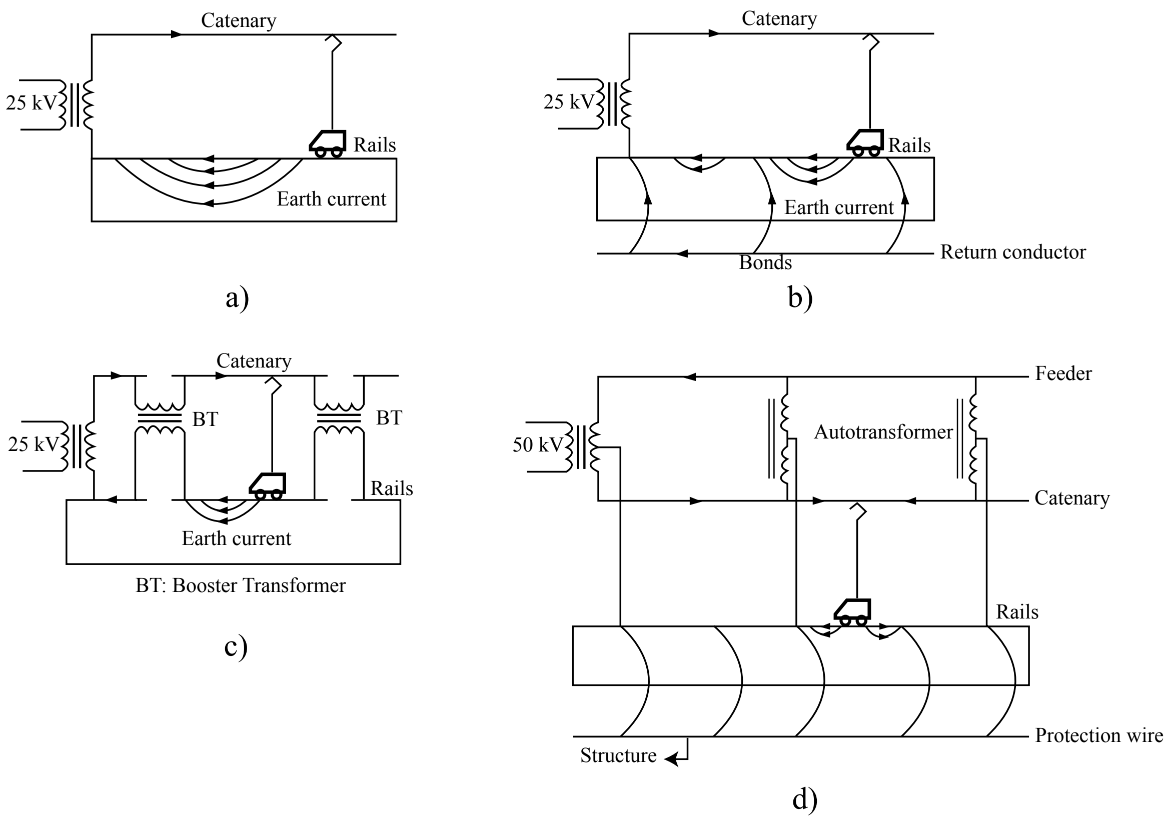

Figure 2-3 Most common AC railway feeding arrangement [3]

2.2.4 Railway Energy Flows

- **Regenerative Braking**

Pulse-width modulated (PWM) inverter circuits with induction motors are used by the majority of modern traction drives. Because these traction converters are capable of operating in all four quadrants, they handle both motor control directions as well as motoring and generation. Consequently, they are often set to offer some degree of braking while regenerating kinetic energy into the traction power system. Modern AC propulsion systems, as depicted in Figure 2-4, comprise of a three-phase AC induction traction motor, a three-phase traction inverter, and a four-quadrant converter (PWM) coupled to the inverter through a direct current (DC) link. This combination is intrinsically regenerative and is capable of feeding back the regenerated energy to the supply. Regeneration begins with the traction motors, which transform the kinetic energy of the rail car into electric power. The traction inverter then transmits the electricity that was generated by the traction motor to the DC link. It functions as a bidirectional interface for power transfer in both motoring and regenerative modes. Connected to the opposite end of the DC link is the four-quadrant (4Q) converter. The secondary side of the on-board transformer converts the regenerated power from the DC link into 50 Hz AC [7]. Regenerative braking energy is typically absorbed by other trains on the 25 kV section. However, in the case that the section does not contain a motoring train, the extra regenerated power flows back through the feeder station and grid supply point [8].

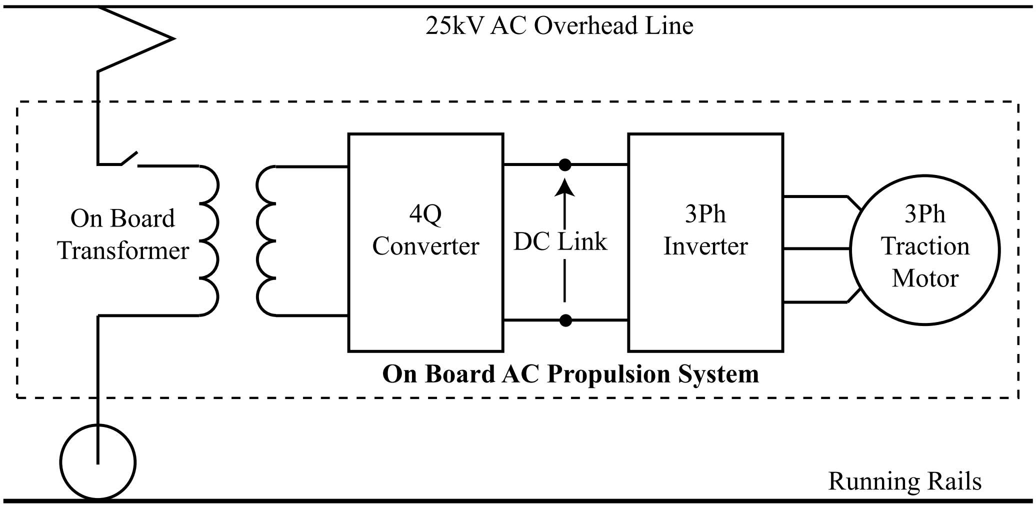

Figure 2-4 Onboard AC propulsion system [7]

- **Traction Energy Demand**

Electric trains require power to drive traction motors during running in traction mode in order for them to move. Traction energy demand refers to the quantity of electrical energy required to operate trains, trams, and other electrically powered modes of transportation. This demand is contingent on a number of variables, including the type of vehicle, its speed, acceleration, grade, and the number of vehicles on the network. In traction mode, the power flows in the opposite direction of that in the regenerative braking mode which is illustrated in Figure 2-4. The electrified trains receive the power from the overhead catenary system and the onboard transformer adjusts the voltage to appropriate level before entering the converter. The inverter collects the power via DC link and then convert it to AC to supply the traction motor.

2.3 Renewable Energy Sources

In recent years, renewable energy sources have expanded fast, and this trend is anticipated to continue in the future. Government incentives, technological improvements, and increased consciousness of the need for clean energy have all contributed to the expansion of renewable energy sources. It is anticipated that renewable energy will continue to gain popularity and eventually become the primary energy source surpassing coal in many regions of the globe [9]. Moreover, forecasts indicate that wind and solar PV will contribute 42% of total electricity output by 2030, leading to a shift [10]. Therefore, in this chapter, the solar PV energy system and wind energy system are reviewed.

2.3.1 Solar PV Energy System

A PV cell, commonly referred to as a photovoltaic cell, is the fundamental component of a solar panel that transforms sunlight into energy. A group of PV cells are connected in parallel and series to create a PV module. Solar panels are collections of structural and electrical components PV modules that have been wired together in series. Arrays refer to groups of panels that have been assembled and wired together in series, whereas a PV generator refers to many arrays wired together in parallel to generate electricity [11].

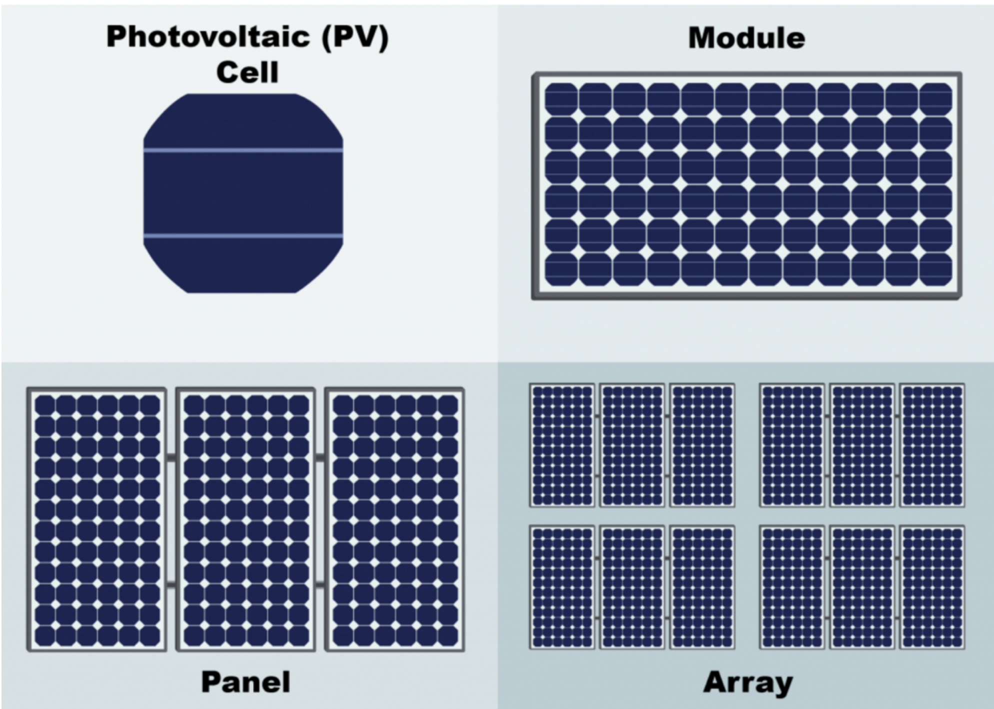

Figure 2-5 PV components [12]

2.3.1.1 Power Converter Topologies

Solar power systems are designed with multiple PV inverter topologies. Two of the most prevalent topologies for utility-scale PV farms are described below and shown in Figure 2-6 [13].

- **Central Inverter**

This is the most frequent and typical inverter topology found in large-scale solar power installations. A central inverter is a single huge inverter that is connected in parallel to many PV arrays. All of the arrays' DC electricity is aggregated into a single DC input for the inverter, which subsequently transforms the DC power into AC power.

- **String Inverter**

A string inverter, which is comparable to a central inverter, is used in medium-sized solar power systems. A string inverter, on the other hand, joins numerous PV arrays in series to form a string of panels. Each string's DC power is pooled and sent into the inverter.

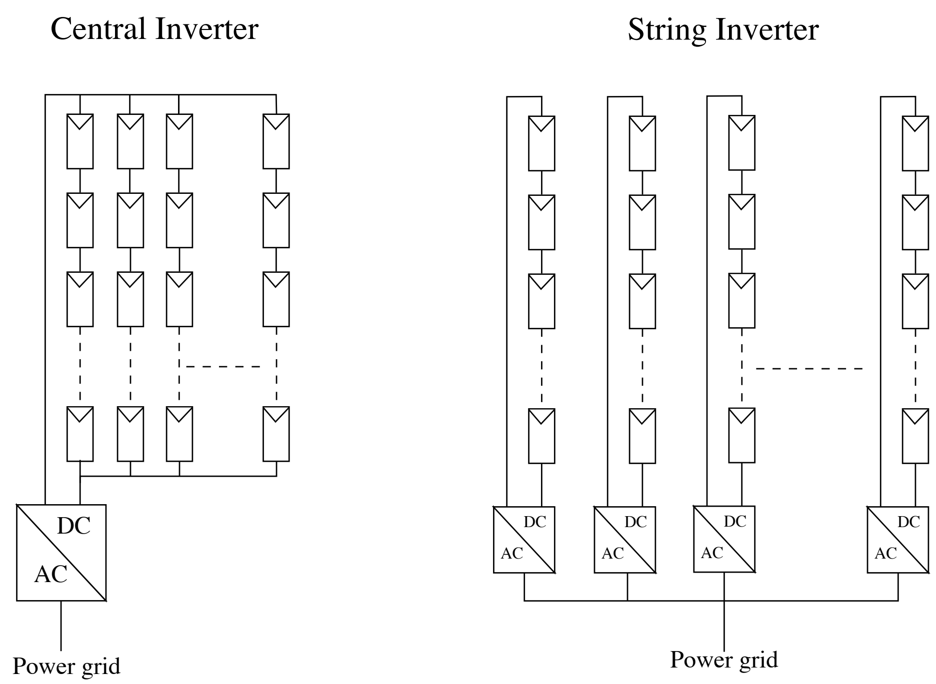

Figure 2-6 Central inverter and string inverter topologies [14]

2.3.1.2 PV Integration System

Two major categories can be used to describe PV systems:

- **Standalone (off-grid) PV system**

Standalone photovoltaic (PV) systems, often known as off-grid solar systems, are solar power installations that are not connected to any larger power grid. An array of solar panels, a battery bank, a charge controller, and an inverter make up the system [11]. This method is typically employed in rural locations, where the availability of a reliable energy supply may be limited. In the event of a power loss, they can be used as backup generators to keep homes and businesses operational. A simplified diagram of the off-grid PV system is depicted in Figure 2-7.

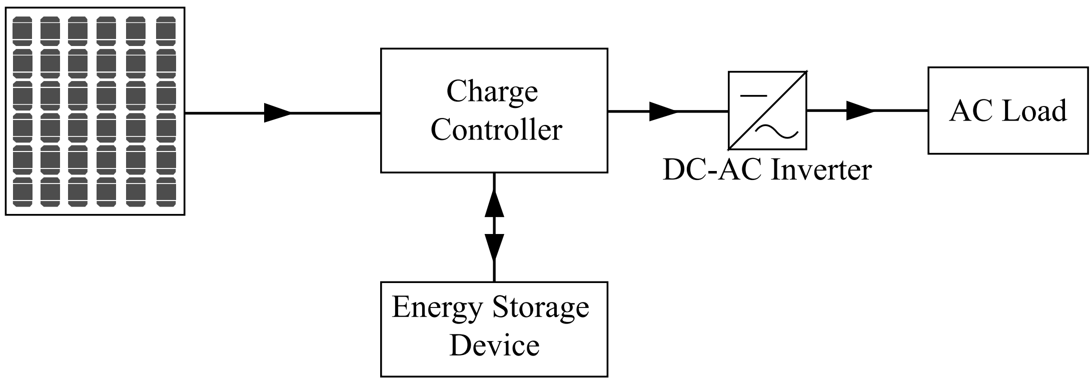

Figure 2-7 Simplified diagram of off-grid PV system [11]

- **Grid-connected (on-grid) PV system**

A grid-connected photovoltaic (PV) system, also known as a grid-tied solar (or grid-tied PV) system, is a solar energy system that is tied into the traditional power grid. An array of solar panels, an electrical inverter, and a power metre make up the system [11]. Figure 2-8 illustrates example of a grid-connected solar PV system with central inverters utilised.

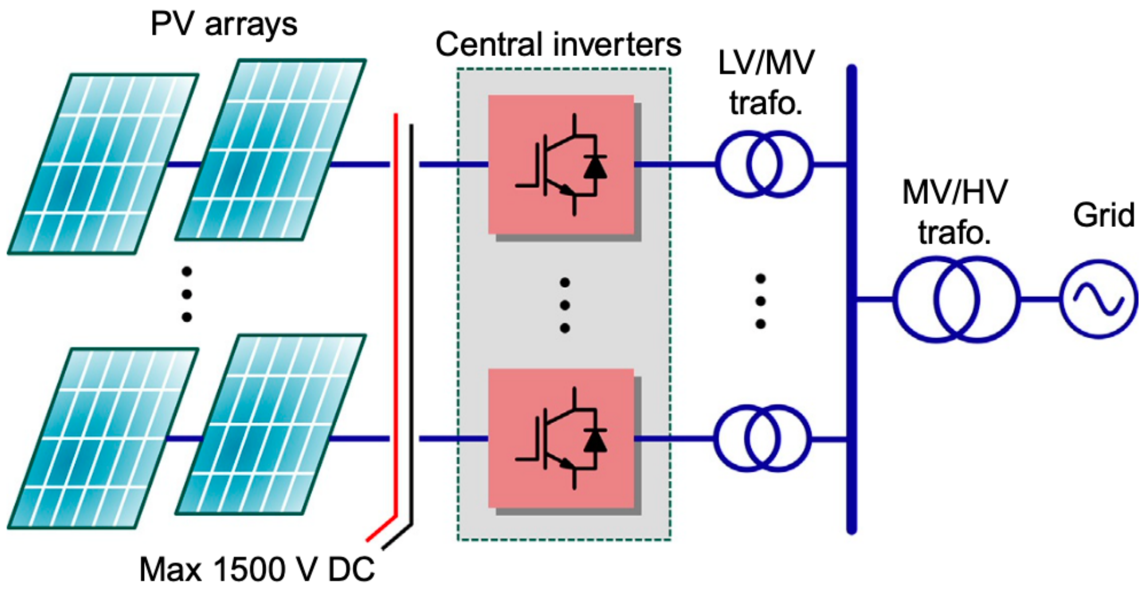

Figure 2-8 Grid-connected PV system [15]

2.3.2 Wind Energy System

The wind energy system consists of at least one wind turbine that converts the kinetic energy of the wind into mechanical energy, which is subsequently used to run an electric generator. The main components of a wind turbine include rotor blades, rotor hub, gearbox, and generator as illustrated in Figure 2-9. The rotor blades are constructed to collect wind and rotate around the rotor hub. The gearbox increases the rotor's spinning speed, which in turn drives the generator. The generator turns mechanical energy into electrical energy, which is subsequently transmitted to the transformer, which is often positioned at the wind turbine's base or nacelle.

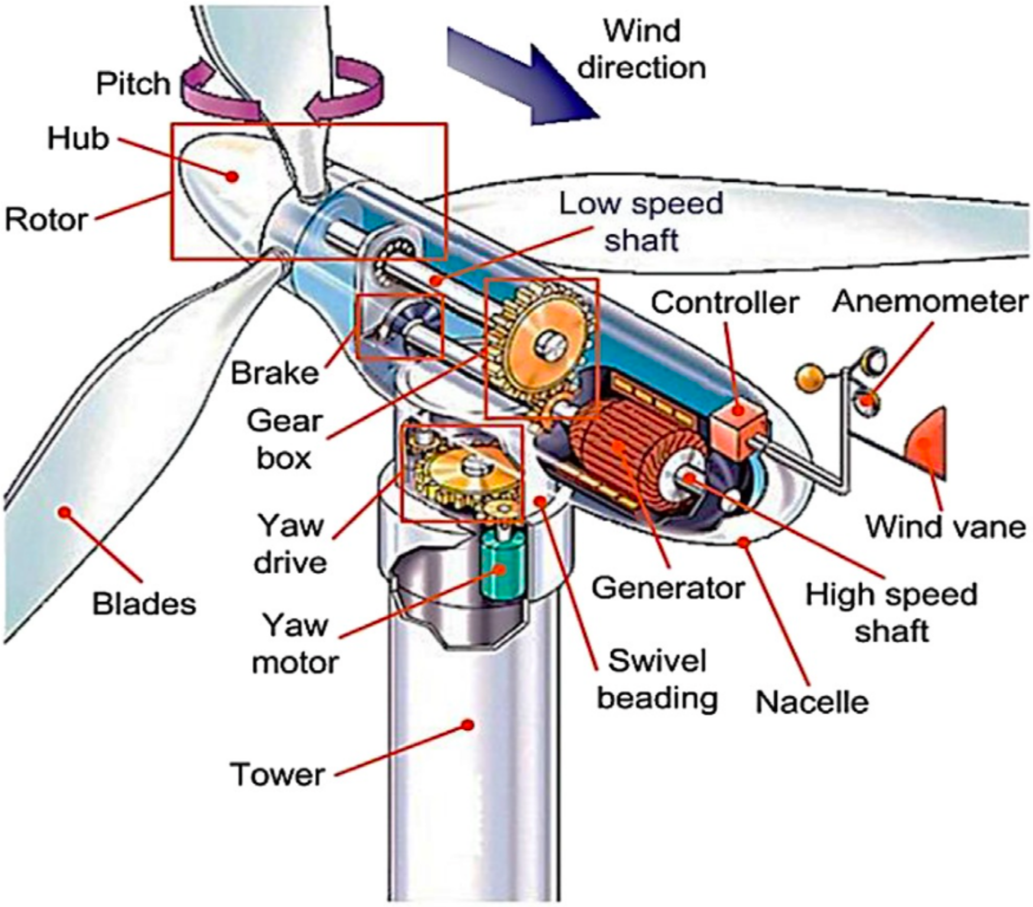

Figure 2-9 Inside wind turbine [16]

2.3.2.1 Wind Power Curve

A wind turbine's power production is plotted against the velocity of the wind in what is called the wind power curve. The graph depicts the normal relationship between wind speed and power output from the turbine at different wind speeds. There are three important parameters determining wind turbine mode of operation as following:

- *Cut-in wind speed*

  The term "cut-in speed" refers to the minimum value of wind speed at which the wind turbine is able to function and generate electricity. When wind speed drops below this figure, the wind turbine will go into the parking mode.

- *Cut-out wind speed*

  The maximum value of wind speed at which the wind turbine can continue to function without being damaged is referred to as the cut-out speed. When this threshold is exceeded, the wind turbine is forced to shut down and switch to the parking mode.

- *Rated wind speed*

  The value of wind speed at which the wind turbine is designed to function and generate its nominal power is referred to as the "rated speed." Once this threshold is reached, the output power of a wind turbine remains constant despite any increase in wind speed up to the cut-out speed.

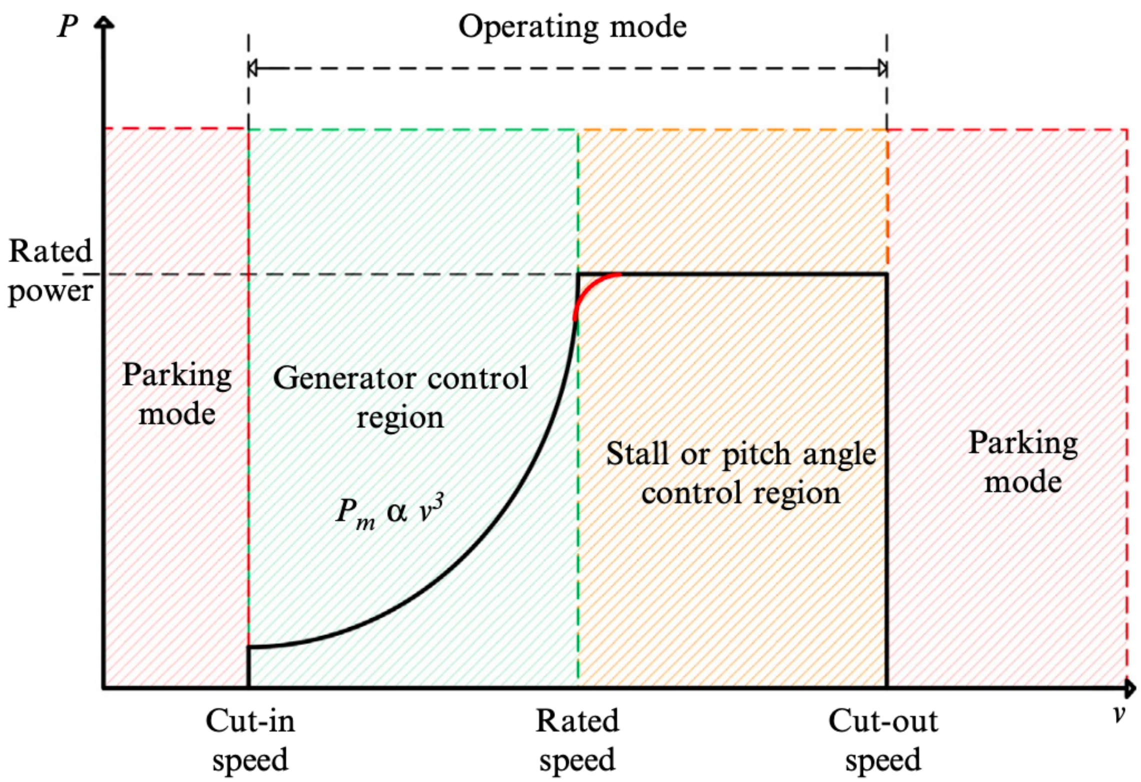

Figure 2-10 The wind turbine power characteristic curve [16]

Additionally, the operating mode is split into two sections known as the generator control region and the stall or pitch angle control region. The generator control region begins at the cut-in wind speed and extends to the rated wind speed. This region's primary benefit is that mechanical power is proportional to the cube of wind speed. In order to protect the wind turbine from any damage, stall or pitch angle control region is defined. Thus, the mechanical power output from the turbine is kept at rated power [16].

2.3.2.2 Wind Farm Power Collection System

A wind farm power collecting system is a collection of infrastructure that absorbs and converts the energy of several wind turbines into electricity that may be utilised to power homes, businesses, and other structures. Typical system components include wind turbines, transformers (690V/33kV and 33kV/132kV or higher), cable and switchgear. The voltage level used for the primary power circuits within a wind turbine is typically less than 1000 V and is selected to be one of the internationally standard voltages, with 690 V between phases being the norm in Europe. Each wind turbine houses one transformer to step up the voltage to 33 kV for the power collection system. Typically, the selection of medium voltage (MV) level for the wind farm power gathering system is dictated by the local distribution utility. Thus, cable and switchgear are conveniently accessible. Thus, in the United Kingdom, the range for wind farm collection circuits is often between 11 kV and 33 kV, whereas in continental Europe, the range is typically 10–30 kV [17]. In order to sync the wind farm into the grid at the point of connection (POC) or the point of common coupling (PCC), a power transformer is necessary to raise the voltage to 132 kV or higher depending on the voltage level of the grid.

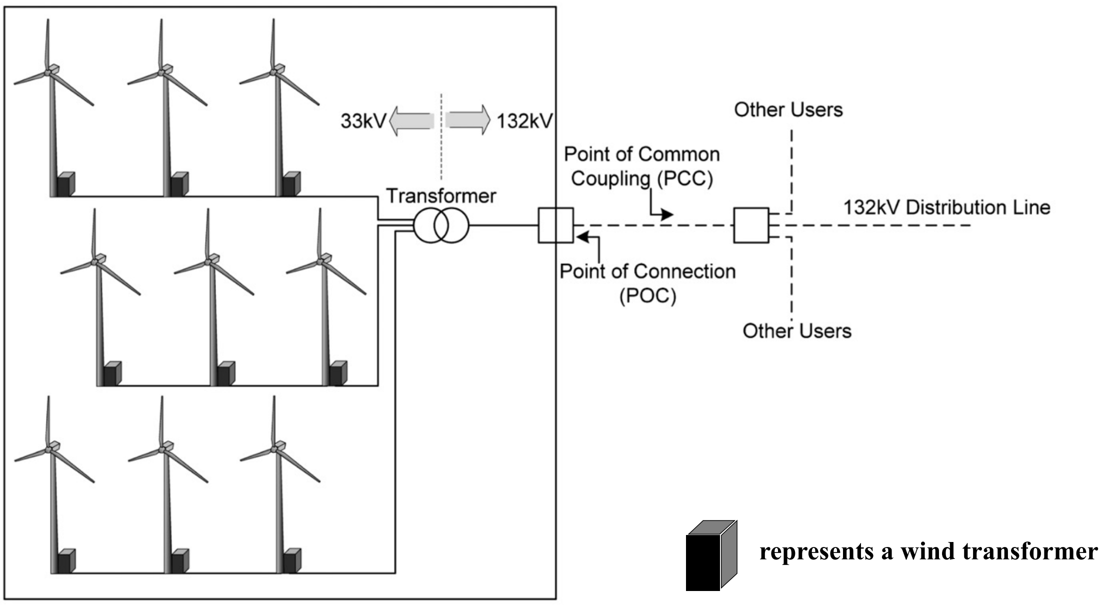

Figure 2-11 Electrical power collection system of a large wind farm [17]

The wind energy resource, the local topography, and the needs of the planning authorities determine the configuration of the wind turbines within the wind farm. The power collection network is then constructed to deliver the collected energy to the local public electricity grid. The Point of Connection is the junction between the wind farm power collection system and the utility distribution network. The Point of Common Coupling is the closest point on the utility network where other customers are (or can be) linked to the wind farm. In numerous situations, these positions may coincide.

2.4 Energy Storage System for Electrified Railway

Energy storage device plays a crucial role in storing excess energy and reusing it when energy demand is high. In some cases, it may provide economic benefits, for instance, absorbing energy during low prices and discharging during peak hours. In this section, the application of energy storage in the railway system and energy storage technologies are reviewed.

2.4.1 Key Parameters of ESS

- Energy Capacity: The amount of energy that can be held in an energy storage system is referred to as its energy storage capacity. It is usually expressed in joules (J) or watt-hours (Wh). The energy capacity of an energy storage system is a critical aspect in determining its suitability for a given application [18].
- Rated Power Capacity: An energy storage system's rated power capacity is the quantity of electricity that the system can deliver at any one time. It is commonly measured in kilowatts (kW) or megawatts (MW).
- State of Charge: State of charge (SOC) refers to the amount of residual charge or energy in a battery or energy storage device at a given time. SOC is often stated as a percentage of the battery or storage system's overall capacity.
- Storage Duration: The duration of storage is the amount of time a storage device can discharge at its power capacity before its energy capacity is depleted.
- Cycle Life: Cycle life is the number of times an energy storage system can be charged and drained before its capacity and performance begin to degrade significantly. The cycle life can vary based on the type of energy storage technology employed, as well as operating conditions, depth of discharge, and charging and discharging rate.

- Depth of Discharge (DOD): Discharge depth affects energy storage system performance and lifespan. Deeper discharges impact batteries and storage devices, reducing lifespan and capacity. DoD reports the percentage of capacity discharged [19].

2.4.2 Energy Storage Technologies

There are several energy storage technologies that are in use in the real world. In this section, the most popular energy storage devices used in railways are reviewed.

- **Battery Energy Storage (BES)**

  Batteries store energy in an electrochemical form in the electrolyte. To produce the necessary electrical characteristic, a set of low-voltage/power battery cells are connected in parallel and series. Arrays of individual battery cells are interconnected to construct larger battery systems [19].There are many types of batteries that are utilised in the railway transportation system, for instance, lead-acid batteries, lithium-ion batteries and nickel-hydride batteries [20].

- **Ultracapacitors (UC)**

  Unlike batteries, which store energy chemically, ultracapacitors store energy electrostatically. They operate similarly to traditional capacitors, but their increased surface area and thinner dielectric materials allow them to store significantly more energy. Even though they have similar advantages of battery storage, the power density of EDLCs is higher than that of batteries, and they can be recharged quickly. In addition, they have a longer lifespan and can tolerate many more charge/discharge cycles than batteries. They are widely used for storing regenerative braking energy in public transportation [20].

- **Flywheel Energy Storage (FES)**

  Flywheels are mass-rotating devices that store energy as kinetic energy. The rotational energy is stored in a huge revolving cylinder-shaped rotor that has been accelerated. During the process of charging, the rotor is accelerated to a very high speed. The energy is stored in the flywheel by maintaining a steady rotational speed. The rotor decelerates and operates the machine like a generator during the discharge [19].

2.4.3 Energy Storage System Components

2.4.3.1 Energy Storage Interface Components

A device or system that permits the connection of an energy storage system (ESS) to a power grid or other electrical system is known as an energy storage interface component (ESIC). The ESIC acts as a link between the ESS and the electrical system, guaranteeing that the ESS can provide power to the system in a safe and efficient manner as required. Some uses of power electronic converters for ESSs in microgrids with a common DC and AC bus are depicted in Figure 2-12. A battery energy storage (BES) requires DC-DC or DC-AC converters to connect to a microgrid, while a flywheel energy storage (FES) requires a back-to-back converter to perform AC-AC conversion; or a rectifier can be used to convert AC output power from FESS to DC in order to connect to a DC link in a microgrid [21].

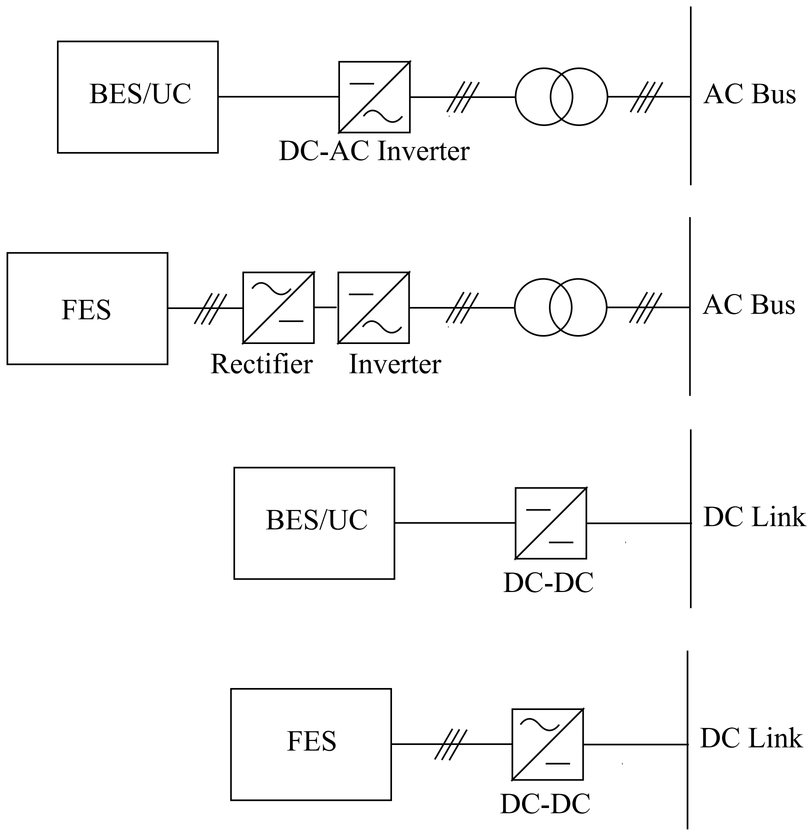

Figure 2-12 Application of converters as energy storage interface component [21]

2.4.3.2 Characteristics of a Generic Storage System

Although different types of energy storage have different working principles, they have some common characteristics. Figure 2-13 presents a simplified model of an energy storage system. Generally, ESSs comprised of an energy storage medium, energy conversion device (or interface component) and controller. The maximum amount of energy that can be stored in an ESS is determined by its storage medium. Furthermore, the energy storage device may acquire energy from the environment and release energy to the environment [22]. The energy conversion device can interchange energy in both directions with a power system, absorbing electrical energy while charging and injecting electrical energy while discharging. Charging and discharging are not 100 per cent efficient; there are some energy losses.

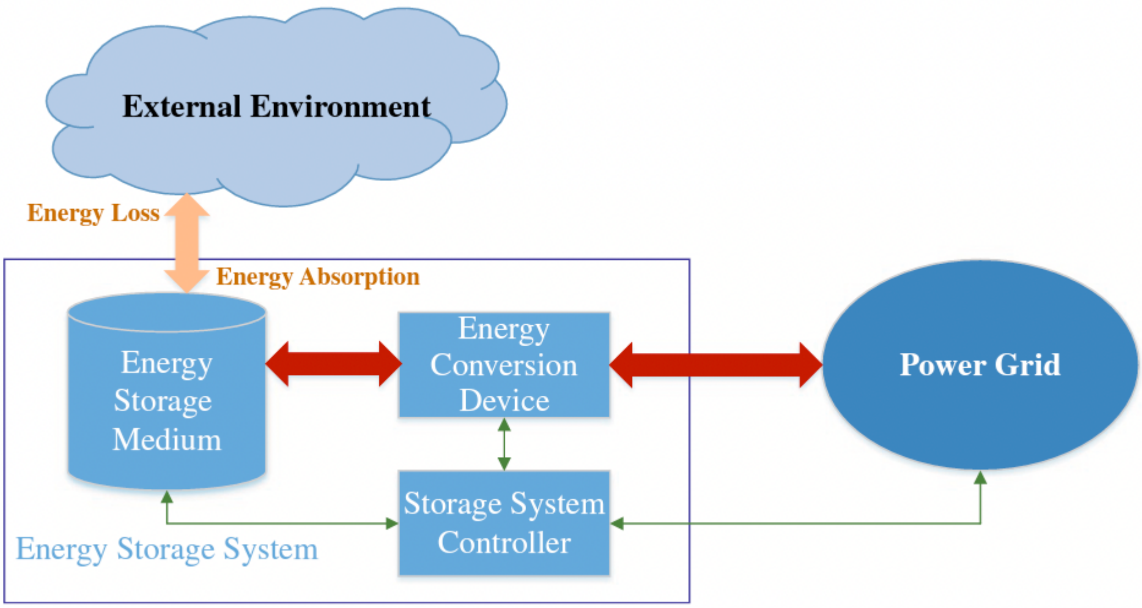

Figure 2-13 Simplified model of a generic energy storage system [22]

2.5 Recent Research of Renewable Integration into Railways

Renewable resources, such as solar, wind, and hydroelectric power, produce negligible or no carbon dioxide emissions during operation. Carbon dioxide (CO2) and other greenhouse gases are released into the atmosphere in large amounts whenever fossil fuels like coal, oil, and natural gas are used to produce electricity. Air quality and human health are negatively impacted by these pollutants, which also contribute to global warming. With the aim to reduce the carbon emissions in the transport sector, especially, rail transport, many researchers have paid attention to energy saving techniques by recuperating regenerative energy from braking trains. For instance, Sebastian et al. [23] propose a methodology to optimize energy storage sizing for utilising regenerative braking energy in electric railway systems. Similarly, Tang S et al. [24] studied SC and VRB energy storages for co-phase traction substation applications and the optimisation was carried out with the aim to maximise the net present value (NPV). The results showed that integrating both energy storage types yielded the highest NPV. Even though, the regenerative braking energy can be reused effectively, its contribution to carbon reduction is still very small. In order to further reduce the carbon footprints, the academic literature review regarding the integration of renewable energy sources and energy storage system into railway power network is studied and summarised in Table 2-1.

Table 2-1 Recent literature on ESS and RES integration in railway power system

Publications	Regen	PV	Wind	ESS	Cost	Large RES	Power losses	Remark
[25]		✓						Studied PV on rooftop of railway station
[26]		✓		✓		✓		Focused on economic aspect
[27]		✓				✓		Evaluated potential of PV along rail route
[28]	✓	✓		✓	✓			Optimal dispatch/DC rail
[29]	✓	✓	✓	✓	✓			Optimal dispatch
[30]	✓	✓	✓	✓				DC rail
[31]	✓	✓	✓	✓	✓	✓		Optimal dispatch
[32]	✓	✓	✓	✓	✓	✓		Require RPC/short time scale
[33]	✓	✓	✓	✓	✓			Optimal dispatch
[34]	✓	✓		✓	✓	✓		Co-phase TS
[35]	✓	✓		✓	✓			Optimal operation
[36]	✓	✓		✓	✓	✓		Optimal dispatch/new type of TS
[37]	✓	✓		✓	✓	✓		Optimal sizing of ESS
[38]	✓	✓		✓				Transient analysis
[39]	✓	✓		✓	✓	✓		Optimal dispatch
[40]	✓	✓		✓	✓			Optimal dispatch/new type of TS

Note: RPC denotes Railway Power Conditioner

2.6 Hypothesis Development

There is abundant research on the railway power supply with the integration of renewable energy sources and energy storage system. However, there are still a few research gaps that are needed to be fulfilled. Hypothesis and research gaps are presented as follows:

1. In the majority of literature, megawatt-scale renewable plants are rarely considered. The low capacity of renewable energy plants has a minor impact on decarbonization. In some cases, structural changes in the traction power supply system or new type of traction substation are needed to accommodate the integration of renewable sources. This research gap is explored in Chapter 4 of this thesis. The renewable integration schemes that can retrofit to the conventional scheme without major changes to the power network structure have been proposed and various aspects are compared.
2. The application of energy storage systems and renewable energy sources together for traction power networks was not fully evaluated in terms of performance and energy flow. Some work focused on transient analysis with a very short time horizon (seconds) to assess the system in terms of power quality. In order to fill the gap, Chapter 5 of this thesis evaluates the traction system with energy storage and solar PV farm. A 24-hr time horizon is used to simulate the proposed model.
3. Due to the resistance of the overhead contact wire, line loss (i.e., contact wire loss) cannot be neglected. Where no research article has taken into account this kind of power loss, this thesis includes it. Choosing the suitable capacity of renewable energy sources and energy storage is a critical topic in the electrified railway system. Considering contact wire loss and sizing renewable energy sources and energy storage together, this thesis solves the optimisation problem to find the optimal sizes and installed locations of renewables and energy storage.

2.7 Summary

The overview of the AC railway power system has been presented in this chapter. Transformer connection and feeding arrangement are one of the most crucial aspects of rail power network design. Additionally, overview of solar PV farm and wind farm are depicted. The literature about renewable energy sources in the railway traction network including the application of energy storage is also reviewed. The gap in the research is found and the hypothesis is proposed.

Chapter 3 AC Railway Power System and Renewable System Modelling

3.1 Introduction

AC railway systems power trains with alternating current (AC). In some instances, a third rail or overhead wires provide AC power to the trains. Compared to DC power, AC power can be transferred across greater distances with less losses. It also permits the use of transformers to increase or decrease the voltage, which is helpful for powering trains that may require different voltages. To examine the AC railway power supply system with the integration of renewable energy sources, all components in the system are modelled and simulated in computer-based software. This chapter presents the theory and methodology for creating simulation models.

3.2 Train Movement Modelling

Train movement modelling refers to the simulation of train movement on a railway network. Modelling the physical properties of the trains and the track, as well as the operating regulations and procedures governing train movement. Train movement modelling can be used for a number of objectives, including evaluating the operation of the railway network under various operating scenarios, and assessing energy consumption and power losses.

3.2.1 Physics of Train Movement

The movement of a train along the railway track follows the motion equation of Newton as shown in Figure 3-1. For a train to move, the traction effort must overcome the resistive forces, which comprise gradient force, train motion resistance, and curvature resistance [41].

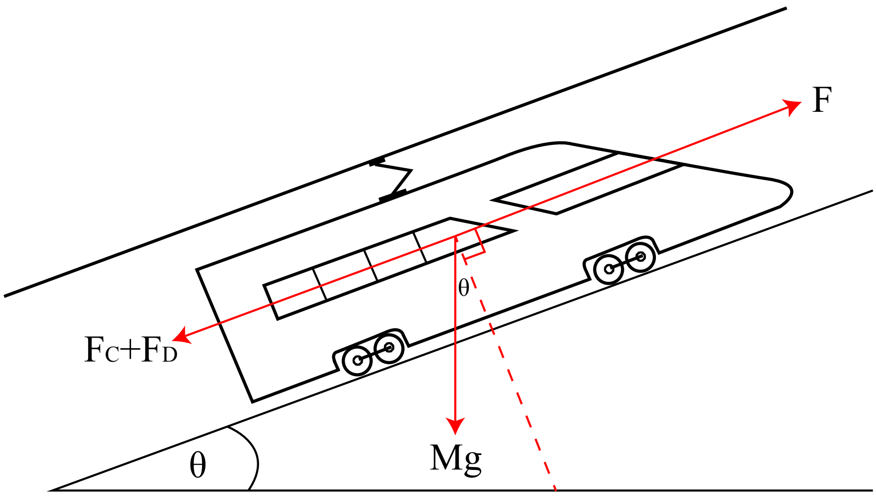

Figure 3-1 Motion of train

$$M_e \cdot a = F - M \cdot g \cdot sin(\theta) - F_C - F_D \qquad (3\text{-}1)$$

where:

M is the total train mass [kg];

M_e is the effective train mass [kg];

a is the train acceleration [m/s^2];

F is the tractive effort [N];

g is the gravity acceleration [m/s^2];

θ is the angle of gradient [rad];

F_D is Davis motion resistance [N];

F_C is the curvature resistance [N].

The sum of the tare mass and the load mass is considered the total train mass as seen in (3-2). Because of the rotating parts such as the wheelsets, gears and motors, the effect of rotational inertia is considered, and it is called the "rotary allowance". The train mass considered the rotational inertia is called effective mass [42] and can be calculated using (3-3).

$$M = M_t + M_l \qquad (3\text{-}2)$$

$$M_e = M_t \cdot (1 + \lambda) + M_l \qquad (3\text{-}3)$$

where:
M_t is the tare mass [kg];
M_l is the load mass [kg];
λ is the rotary allowance.

The curvature resistance happens when the train travels through the railway tracks which have a curved shape. Equation (3-4) is employed to estimate the curvature resistance. As the train moves, there is another friction called "aerodynamic resistance" or "Davis motion resistance". This resistance mainly depends on the train speed, and it can be estimated by (3-5).

$$F_C = \frac{D}{r} \quad (3\text{-}4)$$

$$F_D = A + B \cdot v + C \cdot v^2 \quad (3\text{-}5)$$

where:
A is Davis equation constant [N];
B is Davis equation linear term constant [N/(m/s)]
C is Davis equation quadratic term constant [N/$(\mathrm{m/s})^2$]
D is an experimentally determined constant [Nm];
r is the curve radius of the train track [m].

The train mechanical power at the wheel can be computed by multiplying tractive force with train velocity as shown in (3-6) below:

$$P_{tr,mech} = F \cdot v \quad (3\text{-}6)$$

where:
$P_{tr,mech}$ is the train mechanical power at the wheel [W];
F is the tractive force [N];
v is the train velocity [m/s].

3.2.2 Train Movement Simulator

In order to obtain a train power demand, rolling stock data (rated power, maximum traction, maximum speed, etc.) and route information (speed limit, gradient, location of stops and dwell time) are input to Single Train Simulator (STS) which is based on the second law of Newton and equations in Physics of Train Movement. Train mechanical power requirement, train position and train speed profile are generated including the train elapsed time. Figure 2-2 illustrates the structure of the Single Train Simulator.

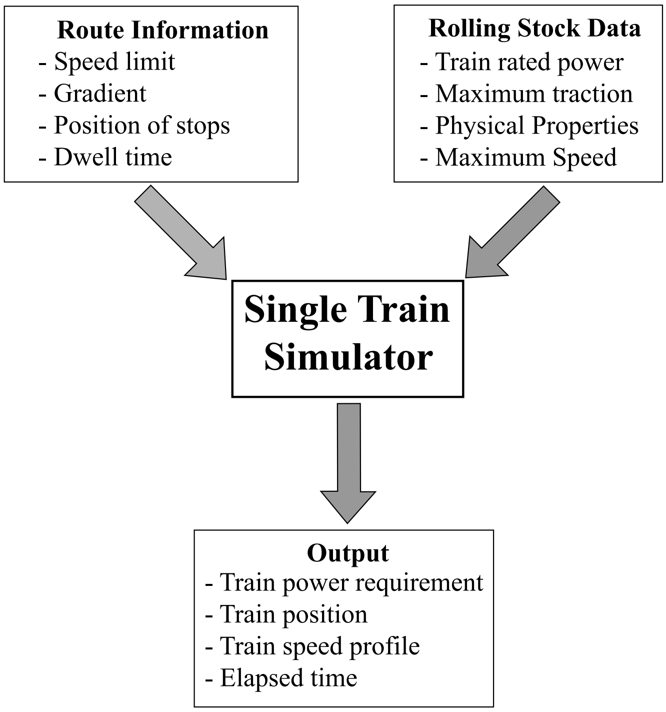

Figure 3-2 Structure of the single train simulator

Figure 3-3 shows an example of the output from the Single Train Simulator. Train driving modes are normally classified into four styles: motoring, cruising, coasting, and braking. The motoring mode starts at time t_0 when the train accelerates from a standstill until reaches its base speed v1 at time t_1. This zone is also called constant torque operation. Afterwards, train continues to increase speed until reaching v2 with constant power. The cruising mode in which the train travels at a constant speed and constant power starts from t_2 and end at t_3. Furthermore, as the stop is not far, the coasting mode is adopted at t_3 in which the train travels by inertia and no power is taken. Finally, the train starts braking at t_4 until stop as seen as the negative power.

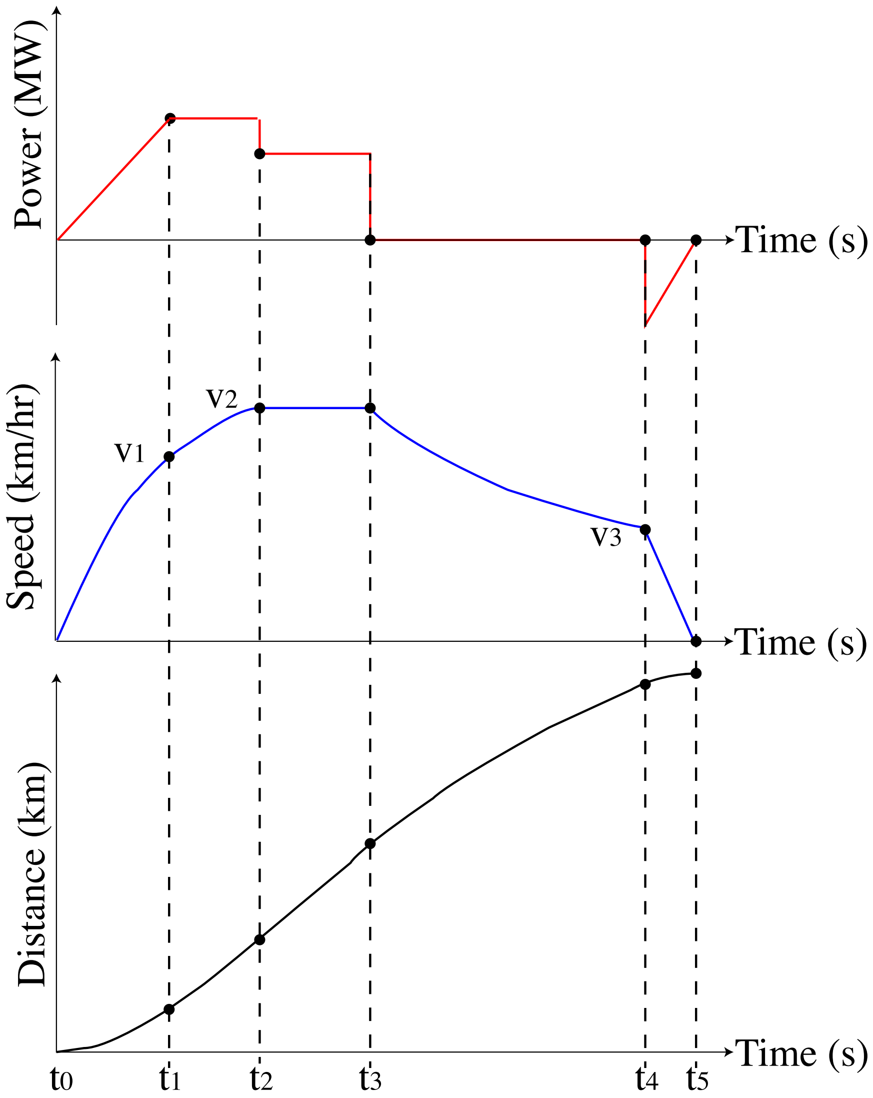

Figure 3-3 Example of single train simulator output

For an electric train equipped with a regenerative brake, there is energy generated during the braking of the train called "regenerative braking energy". This regenerative power is shown as a negative sign in the power demand curve. Therefore, to separate mechanical power requirements for traction and power regenerated from braking, Equations (3-7) and (3-8) are used. It is worth mentioning that these are the mechanical power at the wheel of the vehicle.

$$P_{traction,mech}^{t} = \begin{cases} P_{tr,mech}^{t}, & P_{tr,mech}^{t} > 0 \\ 0, & P_{tr,mech}^{t} \leq 0 \end{cases} \tag{3-7}$$

$$P_{regen,mech}^{t} = \begin{cases} \left|P_{tr,mech}^{t}\right|, & P_{tr,mech}^{t} < 0 \\ 0, & P_{tr,mech}^{t} \geq 0 \end{cases} \tag{3-8}$$

where:

$P_{traction,mech}^{t}$ is mechanical tractive power [W];

$P_{regen,mech}^{t}$ is mechanical regenerative braking power in W at time t.

During the conversion from electrical power to mechanical power at the wheel, there is a conversion loss. Thus, motor efficiency, which includes the whole traction chain, is adopted in the conversion process for traction and regenerative modes [43]. Equations (3-9) and (3-10) presented the electrical tractive and regenerative power, respectively. The net electrical power is given by (3-11).

$$P_{traction}^{t} = \frac{P_{traction,mech}^{t}}{\eta_{motor}} \tag{3-9}$$

$$P_{regen}^{t} = P_{regen,mech}^{t} \cdot \eta_{motor} \tag{3-10}$$

$$P_{tr}^{t} = P_{traction}^{t} + P_{regen}^{t} \tag{3-11}$$

where:

η_{motor} is the efficiency of motor (PU), which is set to 0.9;

$P_{traction}^{t}$ is the electrical tractive power;

P_{regen}^{t} is the electrical regenerative braking power;

P_{tr}^{t} is the net electrical power of trains. All are at time t and in W.

3.2.3 Train Power Profile and Location

Due to the interruption from the neutral section to separate different phases of electricity, the train power profile from the single-train motion simulation needs to be divided into several parts according to the number of feeding sections and length. Figure 3-4 illustrates the traction substation with two feeding areas on the left-hand and right-hand sides. Assuming that the train starts at 0 km and ends at D2, there is one neutral section at location D1. With train location and time output from the single train simulator, the train power profile is divided into two sections: feeding section 1 and feeding section 2 at this point (D1).

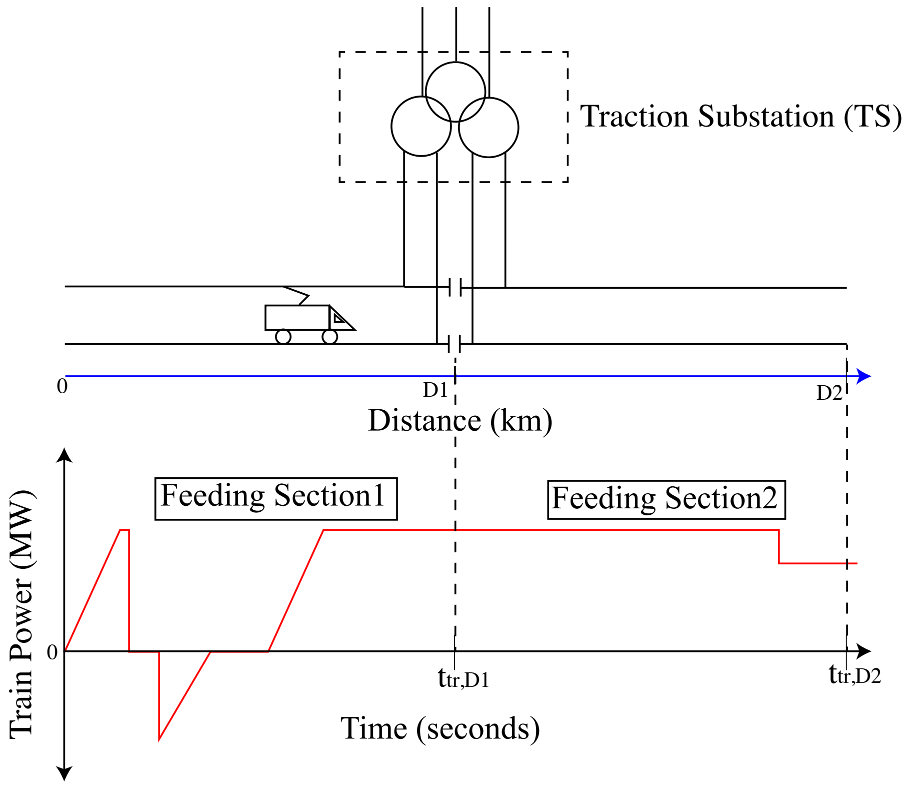

Figure 3-4 Single train power profile and train position for one traction substation

3.2.4 Multiple Train Power Profile

In real operations, there are several trains operated according to timetables. The power profile is more complex than before. In this section, the power profile and location for multiple train services will be generated for different feeding sections. The train power (P in MW), location (d in km) and time (t in second), obtained from the single-train motion simulation, are employed and tabulated in Figure 3-5 (a). By assuming that the first train of the day departed from the first station at time T1 (5 A.M. or 18000 seconds in this study) and location d is equal to zero, it can be seen that the power, location and time are divided by neutral section into two parts; feeding section 1 (FS1) from 0 km to location D1 and feeding section 2 (FS2) from location D1 to D2. The second train started service at time T2, which is time T1 plus headway (T_{HW1}). Similarly, the third train and the fourth train departed from the origin at times T3 and T4, respectively. However, for illustration purposes, there are two values of headway: T_{HW1}

and T_{HW2}. The headway between the third and fourth train is (T_{HW2}) in which in this case T_{HW1} is higher than T_{HW2}. Each train profile was separated into two parts the same way as the first train. It is worth noting that all trains are identical in terms of rolling stock specification, driving style and route.

In order to obtain the train profile for the entire day of multiple train services for simulation purposes, the power profile and location of each train in the same feeding section are combined into one single profile versus the time of the day as illustrated in Figure 3-5 (b). However, for cases with a short headway, the train power profile and location may overlap, causing a more complicated model. Train profiles in the same feeding section are separated into subsections: a and b. For example, the FS1 is split into FS1a and FS1b. As seen in Figure 3-5 (b), the power profile and location in the feeding section 1 of train 1 and train 3 are grouped into FS1a, and FS1b for train 2 and train 4, so that they are not overlapped. This is the same for FS2.

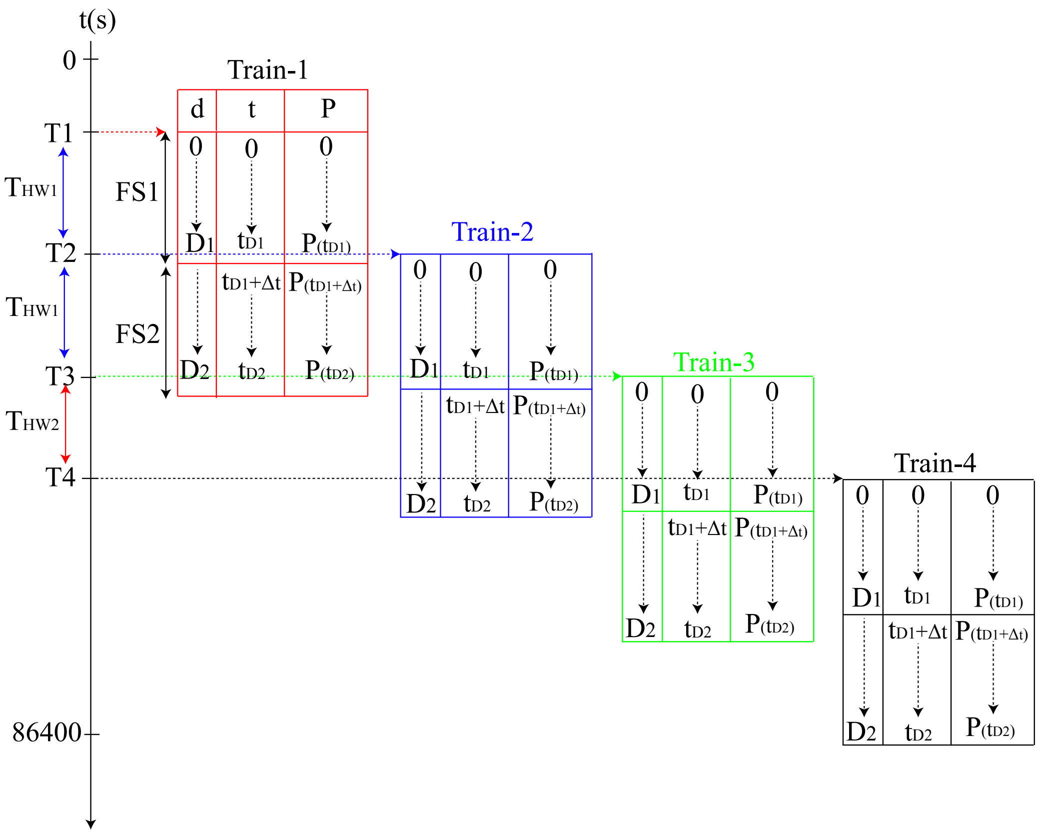

(a)

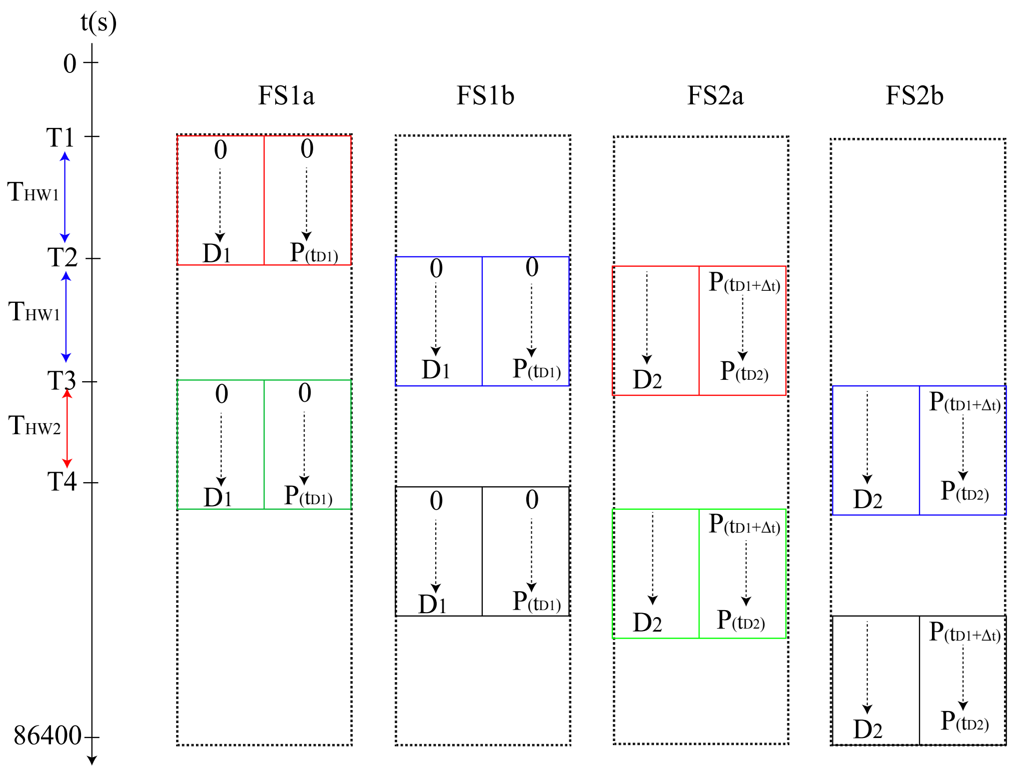

(b)

Figure 3-5 Illustration of multiple-train power profile and location generation

3.3 AC Railway Power Network Modelling

There are several types of power supply arrangements around the globe. They are designed differently to suit specific rail projects. In this research, the AC railway power supply scheme for a high-speed train project under construction in the UK is adopted as shown in Figure 3-6. This section will explain a method to model the main components of the AC railway power system, i.e., national grid, transmission line, traction substation, overhead contact line and rolling stock.

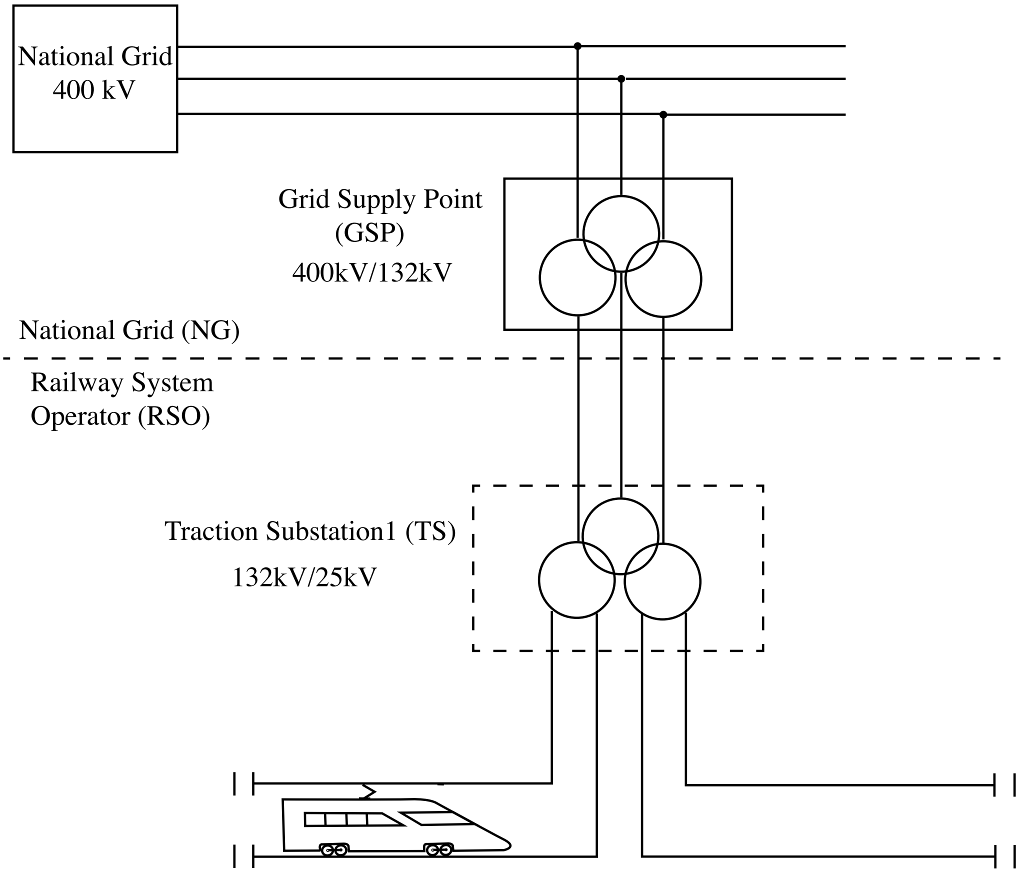

Figure 3-6 AC railway power supply system for High Speed 2 project [44]

3.3.1 Power Grid

Power grid is a primary source of energy that supplies the railway system. Three-phase electric power with a voltage of 25 kV is mainly generated from synchronous generators in power stations. Then, it is raised up to higher voltage levels (132 kV, 275 kV or 400 kV) to lessen the transmission losses and sent through the transmission lines to the grid supply point (GSP) to step down the voltage to a suitable level before entering the traction substation. The grid is modelled in Simulink using a Three-Phase Source block and assigned as a swing bus. As seen in Figure 3-7, the 400-kVrms phase-to-phase voltage ($V_{ab} = V_{bc} = V_{ca}$ with 120-degree phase difference) at 50 Hz is adopted to reduce the voltage imbalance due to power fluctuation from the high-speed train.

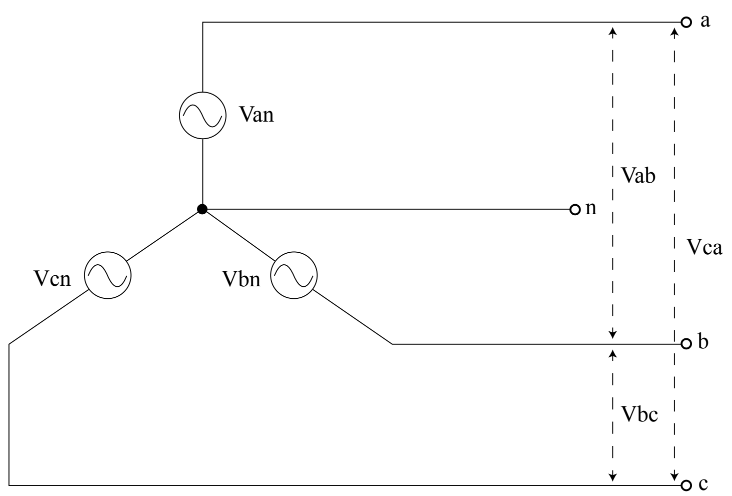

Figure 3-7 Three-phase AC power source

3.3.2 Transmission line

Three-phase current from the power station is transmitted through high-voltage AC transmission lines to the distribution substation. One of the transmission circuit's main components is the conductor which exhibits the electrical properties of resistance, inductance, conductance and capacitance. However, as leakage current flows across the insulator and in the air is very low, the conductance is generally neglected. In order to model the transmission line, those three parameters are needed. The electrical resistance is adopted from the manufacturers' data sheet. To calculate the capacitance and inductance, the conductor's physical properties and the transmission tower's dimension are required.

3.3.2.1 Line Inductance

Equation (3-12) is utilised to compute the inductance per phase of the transmission lines [45].

$$L = 0.2 \ln \frac{GMD}{GMR_L} \tag{3-12}$$

As the transposed three-phase double circuit is considered and two conductors are bundled to carry electric current in each phase of each circuit, equation (3-13) and equation (3-14) to (3-16) are used to calculate geometric mean radius (GMR) for the two-subconductor bundle and GMR of each phase group, respectively. The equivalent geometric mean radius can be determined using (3-17). Figure 3-8 shows details of double circuit transmission line with bundled conductors.

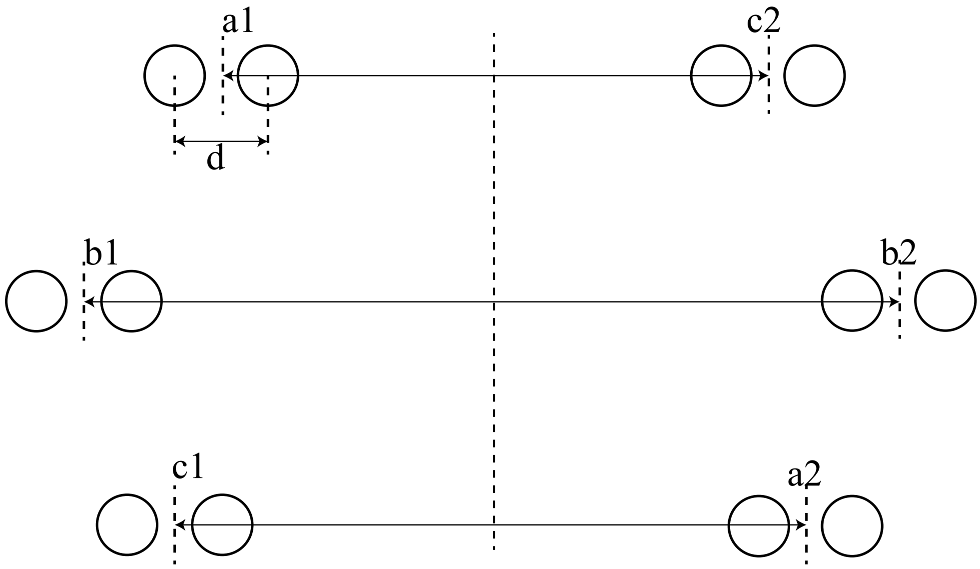

Figure 3-8 Double circuit transmission line

$$D_s^b = \sqrt{D_s \cdot d} \qquad (3\text{-}13)$$

$$D_{SA} = \sqrt{D_s^b \cdot D_{a1a2}} \qquad (3\text{-}14)$$

$$D_{SB} = \sqrt{D_s^b \cdot D_{b1b2}} \qquad (3\text{-}15)$$

$$D_{SC} = \sqrt{D_s^b \cdot D_{c1c2}} \qquad (3\text{-}16)$$

$$GMR_L = \sqrt[3]{D_{SA} \cdot D_{SB} \cdot D_{SC}} \qquad (3\text{-}17)$$

In order to find the value of equivalent geometric mean distance (GMD), the geometric mean distance between each phase group must be first calculated by using (3-18) to (3-20). Finally, the GMD is computed by (3-21).

$$D_{AB} = \sqrt[4]{D_{a1b1} \cdot D_{a1b2} \cdot D_{a2b1} \cdot D_{a2b2}} \quad (3\text{-}18)$$

$$D_{BC} = \sqrt[4]{D_{b1c1} \cdot D_{b1c2} \cdot D_{b2c1} \cdot D_{b2c2}} \quad (3\text{-}19)$$

$$D_{AC} = \sqrt[4]{D_{a1c1} \cdot D_{a1c2} \cdot D_{a2c1} \cdot D_{a2c2}} \quad (3\text{-}20)$$

$$GMD = \sqrt[3]{D_{AB} \cdot D_{BC} \cdot D_{AC}} \quad (3\text{-}21)$$

where:

L is the inductance per phase [mH/km];

GMD is the geometric mean distance [m];

GMR_L is the geometric mean radius for inductance calculation [m];

d is the bundle spacing [m];

D_s is the geometric mean radius of each sub conductor [m];

D_s^b is the geometric mean radius of the two-sub conductor bundle [m];

D_{a1a2}, D_{b1b2}, D_{c1c2} is the spacing between the bundled conductor of the same phase for phase A, B and C [m];

D_{SA}, D_{SB}, D_{SC} is the geometric mean radius for phase group A, B and C [m];

D_{AB} is the geometric mean distance between phase group A and B [m];

D_{BC} is the geometric mean distance between phase group B and C [m];

D_{AC} is the geometric mean distance between phase group A and C [m].

3.3.2.2 Line capacitance

When there is a potential difference between the conductors, capacitance exists on them with respect to each other. In order to compute the capacitance for a double circuit transmission line with two-bundled conductors, equation (3-22) is used. It is worth noting that GMD can be determined using the same procedure as line inductance calculation from (3-18) to (3-21) [45].

$$C = \frac{0.0556}{\ln \frac{GMD}{GMR_C}} \quad (3\text{-}22)$$

Equation (3-23) is employed to find an equivalent radius for a two-strand bundle. Furthermore, as there are two bundled conductors per phase for a double circuit line, the GMR calculation of each phase group is necessary and it can be accomplished by using (3-24) to (3-26).

$$r^b = \sqrt{r \cdot d} \quad (3\text{-}23)$$

$$r_A = \sqrt{r^b \cdot D_{a1a2}} \quad (3\text{-}24)$$

$$r_B = \sqrt{r^b \cdot D_{b1b2}} \quad (3\text{-}25)$$

$$r_C = \sqrt{r^b \cdot D_{c1c2}} \quad (3\text{-}26)$$

Finally, the equivalent geometric mean radius for calculating the per-phase capacitance to neutral is shown in (3-27)

$$GMR_C = \sqrt[3]{r_A \cdot r_B \cdot r_C} \quad (3\text{-}27)$$

where:

C is the capacitance of three-phase double circuit line [mF/km];

GMR_C is geometric mean radius for calculating the capacitance per phase [m];

r is radius of each subconductor [m];

r^b is geometric mean radius for the two-subconductor bundle [m];

r_A, r_B, r_C is geometric mean radius of phase group A, B and C [m].

3.3.2.3 Line model

In this research, a medium line model as illustrated in Figure 3-9 which is commonly used for line lengths between 80 km and 250 km is considered to represent the effect of electrical parameters. Although, most sections of the transmission line in this study are below 80 km in length, using the medium line model will give more accurate results in case of transmission voltage higher than 69 kV [45].

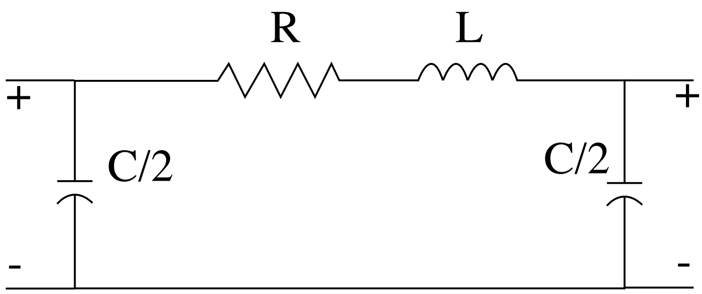

Figure 3-9 Medium line model

The calculated values of line inductance and capacitance together with the conductor resistance from the manufacturers' data are input to the medium line model block (or pi-model) in the Simulink based on MATLAB environment.

3.3.3 Transformer

Both single-phase and three-phase transformers are utilized in different parts of the AC railway power network. Each grid supply point houses one three-phase transformer to step down voltage. Then, the traction transformer which consists of two single-phase transformers connected in V/V forms further drops the voltage to feed the rolling stocks. Linear transformer blocks (for single-phase) and three-phase transformer blocks in Simulink are used to simulate the transformer. These simulation blocks need several input parameters such as nominal power, winding resistance, primary and secondary voltage, etc. Figure 3-10 illustrates a single-phase transformer diagram. The detail of input parameter calculation is presented in Chapter 4.

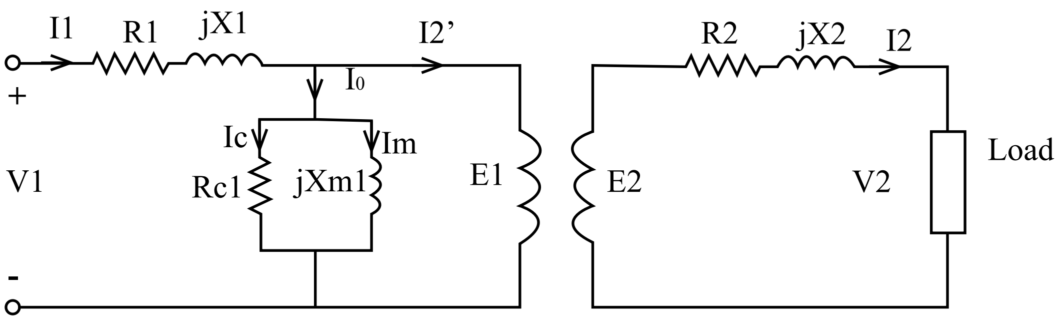

Figure 3-10 Diagram of a single-phase transformer [45]

where:

$E1$ is voltage across the primary of ideal transformer;

$E2$ is voltage across the secondary of ideal transformer;

$V1$ is supply voltage;

$V2$ is load voltage;

I_0 is no-load current;

$I1$ is supply current;

$I2'$ is current to neutralize the secondary MMF;

$I2$ is secondary current;

Ic is current in the core (supplies eddy current and hysteresis losses);

Im is magnetizing current;

$R1$, $R2$ is winding resistance on primary and secondary;

$Rc1$ is core resistance;

$jXm1$ is magnetizing reactance;

$jX1$, $JX2$ is leakage reactance on primary and secondary.

3.3.4 Traction load

From the relationship between the power demand which is calculated in section 3.2 and voltage for a single-phase AC system, the traction load current can be calculated from (3-28). In order to represent electric current in the Simulink, a controlled current source is used to convert the traction load current which can be called input signal to an equivalent current source in the simulation circuit. As demonstrated in Figure 3-11, the positive current will flow according to the direction of the arrow icon.

$$I_{tr} = \frac{P_{tr}}{V_{cw} \cdot \cos \emptyset} \qquad (3\text{-}28)$$

where:

I_{tr} is the electrical current required by train;

P_{tr} is the net electrical power of the train;

V_{cw} is the voltage of the contact wire;

$\cos \emptyset$ is the power factor (equal to 1 in this thesis).

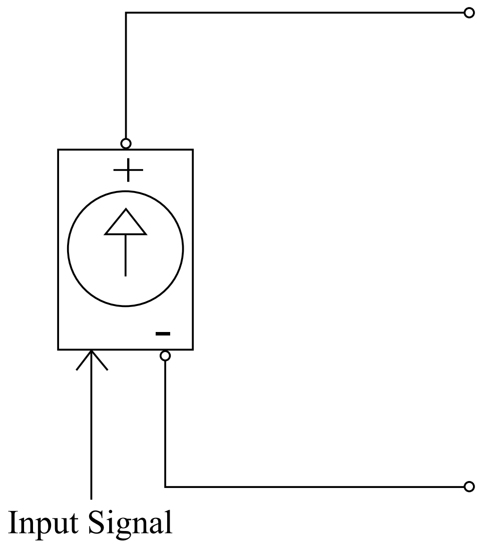

Figure 3-11 Controlled current source

3.4 Modelling of Renewable Energy Sources

3.4.1 Solar PV Farm

The installed capacity of solar PV farms is continuously growing around the world. One of the main reasons is that the capital cost of the PV farm is decreasing significantly over the last few years. In this study, the PV farm in the MW range is used. Several PV arrays, frequently 2 MW each, are formed to obtain a PV farm. Due to the DC power output of the PV array, the inverter is employed to convert the DC to three-phase AC power. Before connecting the PV array to the combiner which combines AC power from all PV arrays, the step-up transformer is used to raise the low voltage from the inverter to high voltage. A solar PV farm is integrated into each feeding section in this research.

Due to the nature of the simulation type (steady-state model), the effect of temperature is ignored. Therefore, solar irradiance is the only input of the PV model. The capacity of the PV farm is determined by the PV surface area multiplied by solar irradiance at standard test conditions (1000 W/m^2). For example, a PV farm with a surface area of 1000 m^2 can output up to 1 MW of power. The amount of electrical power from the PV farm is calculated as given in (3-29). A PV model is created in Simulink with a controlled-current source block and the workflow for modelling solar PV farm is demonstrated in Figure 3-12. After the power calculation step, the generated power is multiplied by the efficiency of the PV inverter and transformer, respectively to account for losses. Finally, before entering the controlled-current source, the power is divided by the voltage at the connection point to convert to electric current.

$$P_{pv}(s) = s \cdot A \qquad (3\text{-}29)$$

where:

$P_{pv}(s)$ is the power produced by the PV farm [W];

E_{pv} is the energy of the PV farm [Wh];

s is the solar irradiance [W/m2];

A is the surface area of the PV farm [m2];

t is time [s].

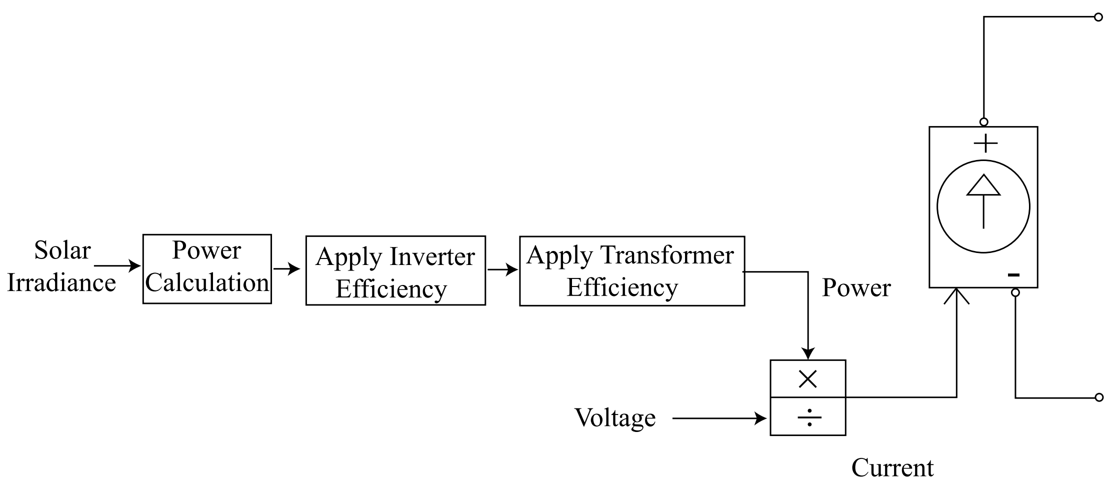

Figure 3-12 Solar PV farm modelling representation

In addition to the aforementioned single-phase current conversion utilised to connect an energy source to a single-phase power system, three-phase current conversion is also necessary. A concept of symmetrical components is adopted to calculate the phasor current in each phase [46]. Equation (3-30) shows the derivation of the positive sequence voltage of phase a. Furthermore, with the positive sequence voltage and the power generated from the PV farm (assume power factor is equal to 1), the positive sequence current in phase a can be computed using (3-31). It is worth noting that the current and voltage presented are peak values and in the form of the phasor.

$$V_a^1 = \frac{1}{3} \cdot (V_{ab} - a^2 \cdot V_{bc}) \tag{3-30}$$

$$P = 3 \cdot \left(\frac{V_a^1}{\sqrt{2}} \cdot \frac{I_a^1}{\sqrt{2}} \right) \tag{3-31}$$

According to the symmetrical component concept, the current in each phase is the sum of zero sequence, positive sequence, and negative sequence current as depicted in (3-32). Based on the assumption that the power source is balanced three-phase power, negative sequence current can be neglected. Similarly, for a three-phase ungrounded neutral, zero sequence current is equal to zero. Thus, the current in phase a is equal to the positive sequence current. In a balanced system, the magnitude of current in phases a,b and c is equal but with 120 degrees displaced in phases. Therefore, the current in phase b and phase c can be presented in (3-33) and (3-34), respectively. The identical methodology is applied for constructing a three-phase wind farm and three-phase energy storage system.

$$I_a = I_a^0 + I_a^1 + I_a^2 \tag{3-32}$$

$$I_b = a^2 \cdot I_a \tag{3-33}$$

$$I_c = a \cdot I_a \tag{3-34}$$

where:

a is equal to $1\angle 120^{\circ}$;

I_a, I_b, I_c is phasor current in phases a, b, and c, respectively [A];

I_a^0, I_a^1, I_a^2 is zero sequence current, positive sequence current, negative sequence current in phase a [A];

P is power generated from energy source [W];

V_{ab} is a line-to-line voltage between phases a and b [V];

V_{bc} is a line-to-line voltage between phases b and c [V];

V_a^1 is positive sequence phase to ground voltage of phase a [V].

3.4.2 Wind Farm

A wind farm consists of several wind turbines. Each wind turbine has its own transformer inside the nacelle. This transformer is used to increase the 690 Vac power generated by the asynchronous generator to 33 kV. Then, the conductor carries this 33-kV power to the collection system which combines all three-phase AC power from several wind turbines.

The electrical power output of a wind turbine is dependent mainly upon wind speed. The turbine will start generating power when the wind speed exceeds the cut-in speed. When the wind speed reaches the cut-out speed, the turbine will shut down to prevent structural damage. To calculate the wind speed at a specific hub height, the reference height of 10 meters is used, at which most data sources of wind speed profile are recorded. The relationship between height and wind speed is shown in (3-35) [16].

$$v_h = v_0 \cdot \left(\frac{h}{h_0}\right)^{\alpha} \tag{3-35}$$

where:

v_h is the wind speed at height h[m/s];

v_0 is the average wind speed at height h_0 [m/s];

h is the hub height of the wind turbine [m];

h_0 is the referenced height (10 m);

α is the Hellman height exponent.

The value of the Hellman height exponent is assumed to be 0.159, which is used in a location with a small number of wind obstacles [47]. The electrical power produced by a wind turbine is given in [48] as follows:

$$P_w(v) = \begin{cases} 0, & v < v_{ci} \\ P_r \cdot \dfrac{v^a - v_{ci}^a}{v_r^a - v_{ci}^a}, & v_{ci} \le v \le v_r \\ P_r, & v_r < v < v_{co} \\ 0, & v > v_{co} \end{cases} \tag{3-36}$$

where:

P_w is the power output (W) of the turbine [W];

E_w is the energy (Wh) from a wind farm [Wh];

P_r is the rated power or turbine capacity [W];

V is the wind speed [m/s];

V_{ci} is the cut-in wind speed [m/s];

V_{co} is the cut-out wind speed [m/s];

V_r is the rated wind speed [m/s];

a is the Weibull shape parameter (a = 2 in this study).

The workflow to connect the wind farm to the power system is presented in Figure 3-13. After the wind speed conversion and power calculation steps mentioned above, the transformer efficiency is adopted and multiplied by wind power. Similar to the PV farm, the generated power is then divided by the voltage to obtain the current which is input to the controlled-current source.

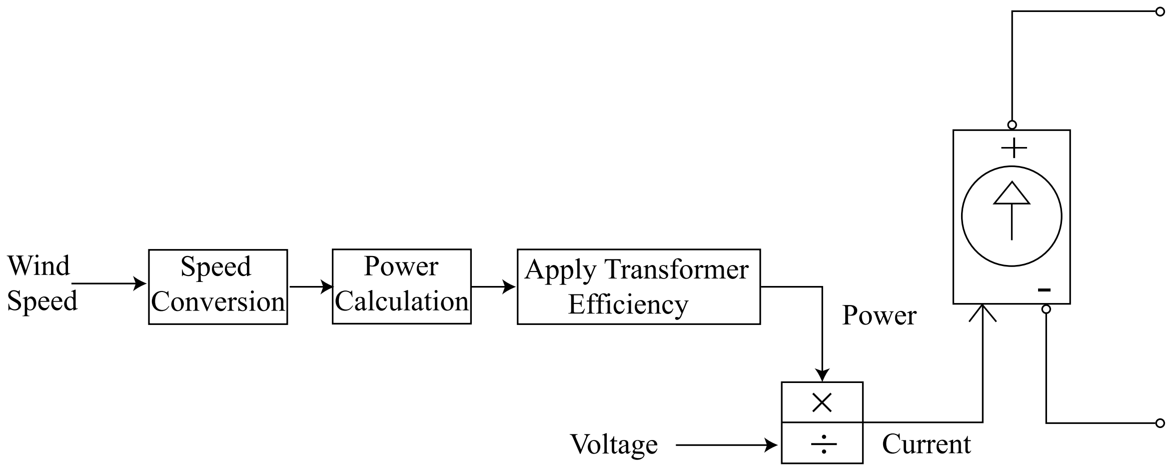

Figure 3-13 Wind farm modelling representation

3.5 Energy Storage System

Energy storage offers numerous benefits to the electrical power system, especially in terms of economic and technical aspects. Similar to the solar PV farm and wind farm, the main element of the energy storage system model is the controlled-current source. The modelling workflow is described in Figure 3-14. The model requires input parameters, for example, train power demand, power generated from renewable energy sources, etc. Each ESS model needs different input parameters depending on its control strategy. After that, the ESS control block will determine the output power from the ESS to the connected system. The efficiencies of the converter and transformer are applied to the output power to account for losses. Diving the power by the voltage at the point of common coupling, the current is obtained and injected into the controlled-current source.

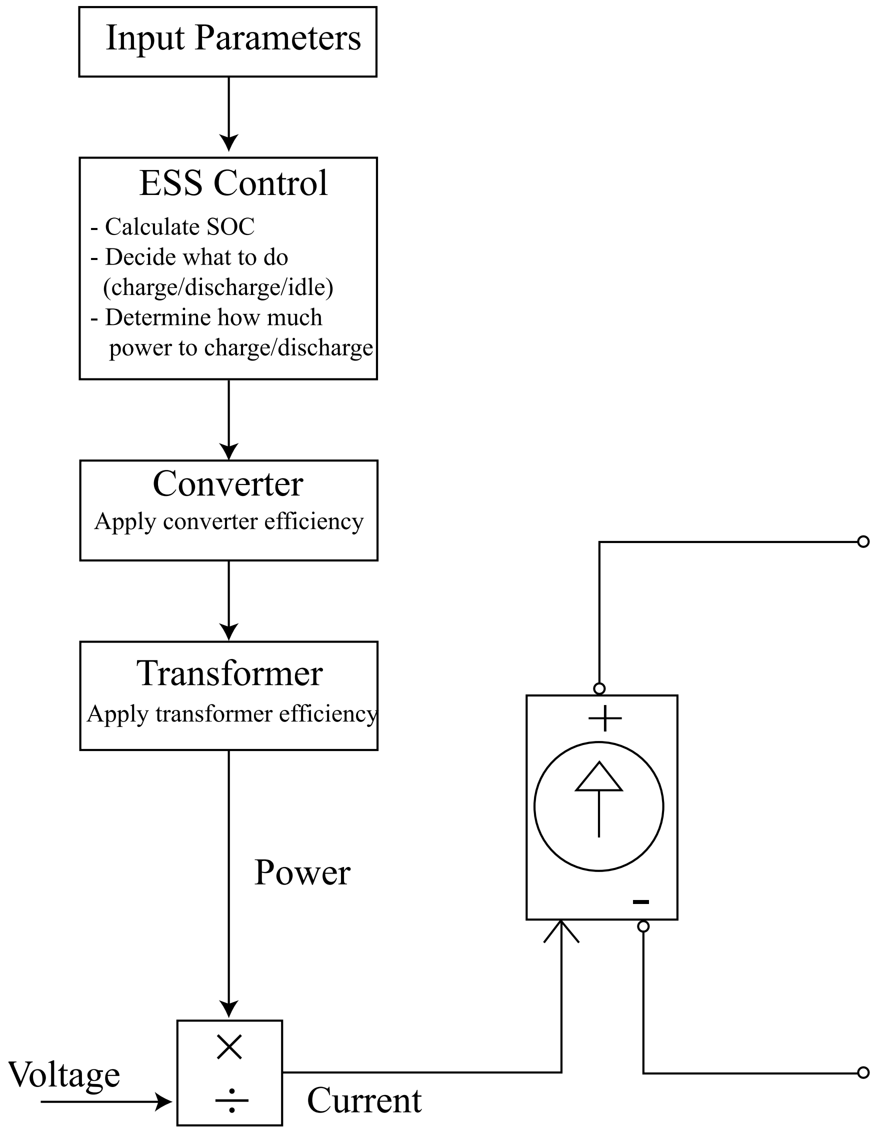

Figure 3-14 Energy storage system modelling workflow

3.6 Summary

This chapter presented the AC railway traction power network modelling. In order to obtain a train power profile, single train simulator is employed based on rolling stock data. Furthermore, with train service timetable, multiple train power profile can be attained according to train movement modelling. Afterwards, the methodology to develop each main component of the AC railway power supply system was presented. The controlled current source in Simulink is used for building the simulation block of solar PV farm and wind farm. These renewable energy block can be customised by changing parameters e.g., generation capacity, inverter efficiency and etc. Finally, the steps to create the energy storage model are illustrated. In the next chapter, simulation blocks created using the methods in this chapter will be connected to form railway traction power system with renewable integration except for the energy storage model which will be utilised in chapter 5.

Chapter 4 Connection Schemes to Integrate Renewables Into AC Railway Power Supply System

4.1 Introduction

With the concern about climate change, renewable energy sources (RESs) play a vital role in the field of electricity production, being clean and sustainable. Several countries have set policies to support the use of renewable energy, especially in Europe and the USA. In 2019, the UK government set an ambitious goal to reach net-zero emissions by 2050 [49]. Many sectors, especially the energy supply sector, have started planning to reduce CO2 emissions. The UK installed capacity of RESs has risen continuously since 2000. According to [50], the cost of adding new onshore wind farms and solar PV farms is lower than that of other types of new generation units. It was reported that the share of electricity produced from solar power and wind went up from 23.6% in 2019 to 28.3% in 2020, with 88.5 TWh generated [51]. The estimate from the UK's Department for Business, Energy and Industrial Strategy (BEIS) shows a 10.7% reduction in CO2 emissions in 2020 [51]. The largest contributor to CO2 emissions is the transport sector with 27%, followed by the energy supply sector, which accounts for 21%. Road transport is the main source of emissions, with a share of over 90%. In contrast, railway transport only accounts for 1.4% of the transport sector or 0.5% of the UK's total emissions [52]. Although electrified trains emit nearly zero emissions at the point of use, the CO2 emissions come from the power generation process. Integration of RESs into the railway power network may alleviate various issues, especially carbon emissions and the reliance on energy from the national grid. Nevertheless, there are only a few projects implemented in the real world.

There is some interesting research regarding the RES integration for railway traction power supply. D'Arco et al. [26] proposed PV integration schemes for AC railways and compared them in terms of cost and power losses. The train energy demand and the solar irradiance in

Italy were used in a case study. The study revealed that the PV farm power rating is the critical factor determining the system's cost. Nonetheless, wind farms were not included in the study. A multi-period AC railway optimal power flow problem formulated by considering PV plants and wind turbines was introduced by Aguado et al. [29]. The authors also included the utilisation of a hybrid energy storage system (HESS) to capture excess energy from the RES and train regenerative braking energy. To analyse the uncertainties of the energy from the RES, a scenario tree approach was employed in the case study, resulting in cost and energy savings of 33.22% and 9.63%, respectively. A Railway Station Energy Management (RSEM) system was proposed by Şengör et al. [28]. The main goal of the RSEM was to effectively reuse the regenerative braking energy from electric trains by using an energy storage system (ESS). Additionally, the PV generator was integrated into the railway power supply system. Mixed-integer linear programming (MILP) was formulated to solve the optimisation problem. The case study showed that a cost reduction of about 35% was observed when the PV, ESS, and regenerative braking energy were utilised. The abovementioned studies are based on RES integration into the conventional traction substation.

A few scholars presented other approaches for integrating the RESs into a new type of traction substations. Liu et al. [34] proposed a co-phase traction substation (CTSS) energy management system to minimize operating costs, considering the power flow controller and the PV generator and HESS. The study also considered the three-phase unbalance constraint. A two-stage robust optimisation problem was modelled to deal with the PV and train load uncertainties. The goals of the first stage were to find the operating point of the HESS and energy transactions with the grid. The CTSS optimal power dispatch was determined in the second stage. Compared to the conventional traction substation, a cost saving of 4.99% was attained through the proposed methodology. Besides that, the voltage unbalance was well controlled below the maximum admissible constraint of 2% in China. A flexible traction power supply system (FTPSS) was proposed by Chen et al. [36]. A back-to-back converter, HESS, and solar PV plant were integrated into the scheme. Moreover, the authors also presented flexible railway energy management (FREM) for multi-scale optimal dispatch to compensate for the demand and supply imbalance. It was shown in the case study that PV and HESS integration helped reduce the total operational cost of FTPSS by 32.7%.

The existing work has mainly focussed on cost-saving and energy reduction, but details regarding power losses in each component are still not presented. Therefore, this chapter presents three schemes for integrating RESs into the railway power network and considers the lifetime cost and power losses of each component relating to RESs. Simulink, based on the MATLAB environment, is used to model and simulate the energy flow for each proposed scheme. The contributions of this chapter are as follows:

1) Renewable integration schemes for the 25 kV AC railway power system are proposed. Various sizes of PV farms and wind farms are simulated.
2) The electrical losses, that is, transformer losses, transmission line losses, and inverter losses (including losses in the static converter) of each scheme, are compared comprehensively.
3) The effect of RES integration on the grid is explored, and the voltage unbalance factor (VUF) is calculated for each proposed scheme.
4) The lifetime cost of each proposed scheme with various RES installed capacities is also compared.

4.2 System Description

The 25 kV, 50 Hz AC railway power supply system was designed to support the need for the high traction power of high-speed trains. With the issue of poor power quality due to power unbalance, for example, negative-phase current and harmonic distortion, the railway power supply system needs to be connected to a high-voltage power supply point that possesses a high short-circuit capacity.

In this chapter, the three-phase 400 kV power system from the national grid is used as the main power supply. The Grid Supply Point (GSP), a substation owned by the national grid, steps down the transmission line voltage to 132 kV before entering the railway traction substation, where traction transformers are located [44]. It is assumed that the electrical power system after the GSP is owned by the railway system operator, seen as the dashed line in Figure 4-1(a), which indicates a responsibility boundary between the national grid and the railway system operator. A V/V transformer connection is employed to convert three-phase 132 kV power to two single-phase 25 kV (2 × 25 kV) at the traction substation in this research.

A solar PV farm and a wind farm are integrated into the existing power supply system, with different proposed schemes to reduce dependence on power from the national grid, which is mainly generated from fossil fuels. Three renewable energy integration schemes are proposed in this study:

4.2.1 RES Connected to the Three-phase Railway Power Network (Scheme-1)

For this scheme, a three-phase solar PV farm and wind farm are installed and connected to a three-phase 132 kV distribution line at the point between the GSP and the traction substation, as seen in Figure 4-1(a). The PV farm and wind farm locations are assumed to be close enough to share the transmission line and are in the proximity of three-phase railway distribution lines. Therefore, the transmission losses due to the connection of RESs are ignored in this study.

Figure 4-1(b) shows a single-line diagram of a solar PV farm implemented in this configuration. The electricity produced from each PV module is a low-voltage direct current. To obtain the required voltage level and power, the PV modules are connected in series and parallel; an arrangement called a PV array. The PV arrays are assumed to always operate at their maximum power point. Generally, for large-scale PV farms, several PV arrays are used to generate the required power, and central inverter topology is used to convert DC power to AC for each array. In this research, the PV farm comprises several sets of PV arrays, each with a 2 MW power capacity. The 1100 VDC output from each PV array is inverted to three-phase 460 VAC power via 2.2 MVA inverters [53]. Then, 2.5 MVA transformers are operated to step up the voltage from 460 VAC to 33 kVAC. The output of all PV arrays is then combined and raised to 132 kV by a 33 kV/132 kV power transformer to connect to the distribution network. Similarly, the wind farm is made up of several 2 MW wind turbines. The asynchronous generator with a wound rotor in the turbine generates a three-phase voltage of 690 VAC. For each wind turbine, the voltage is stepped up to 33 kV by a 2.1 MVA transformer located inside the nacelle of the wind turbine [54]. The electricity from each wind turbine then gathers at the collection system and is raised again to 132 kV to connect to the grid system, as seen in Figure 4-1(c).

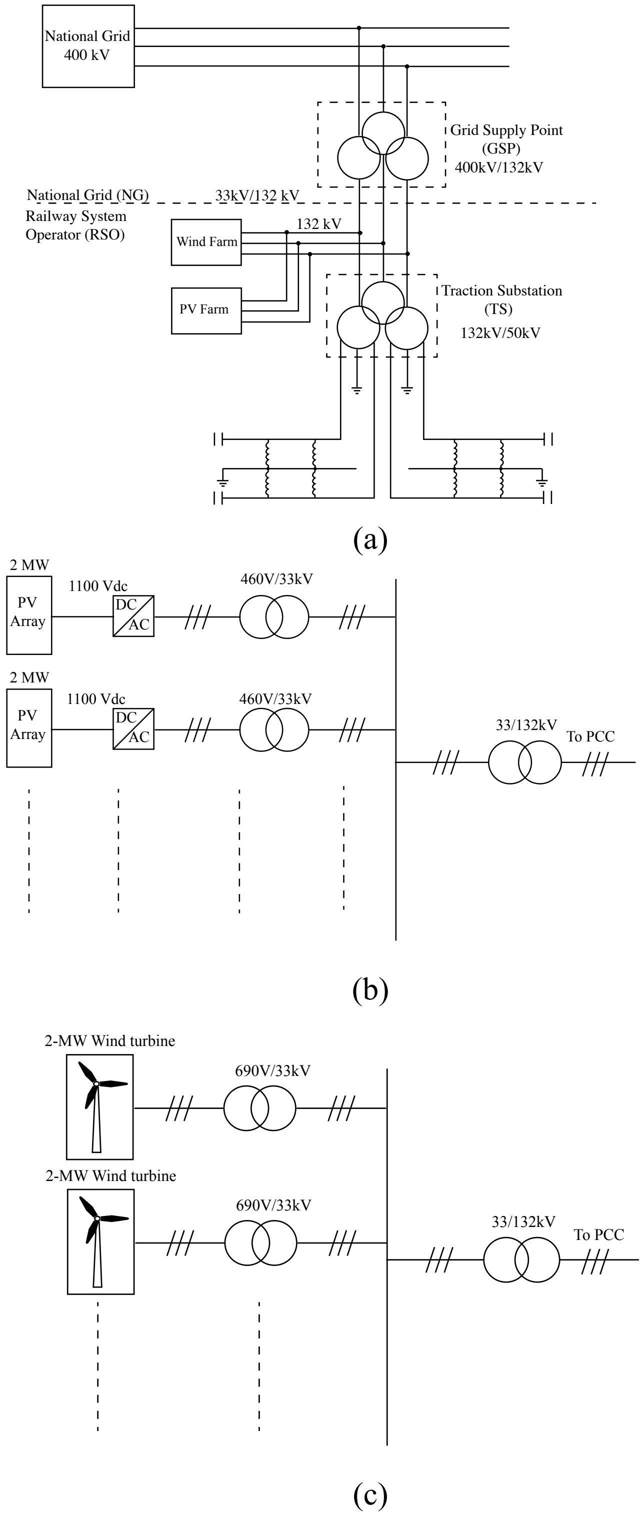

Figure 4-1 (a) scheme of RESs connected to the three-phase railway power network, (b) single-line diagram of a solar PV farm, (c) single-line diagram of a connected wind farm (PCC is a point of common coupling). (b) and (c) are used for scheme-1 and scheme-2.

4.2.2 RES Connected to Railway Power Supply System via V/V Transformer (Scheme-2)

In this scheme, the details of the PV and wind farms are identical to the first scheme, excluding the connection point and methods. Both RESs are connected to the V/V transformer (V/V TF), as shown in Figure 2-2. The primary purpose of this transformer is to convert the three-phase power from both PV and wind farms to a pair of single-phase 25 kV power lines. These 25 kV lines are integrated into the railway at the secondary side of the traction transformer. The PV and wind farms are identical to the previous scheme, as seen in Figure 4-1(b) and Figure 4-1(c).

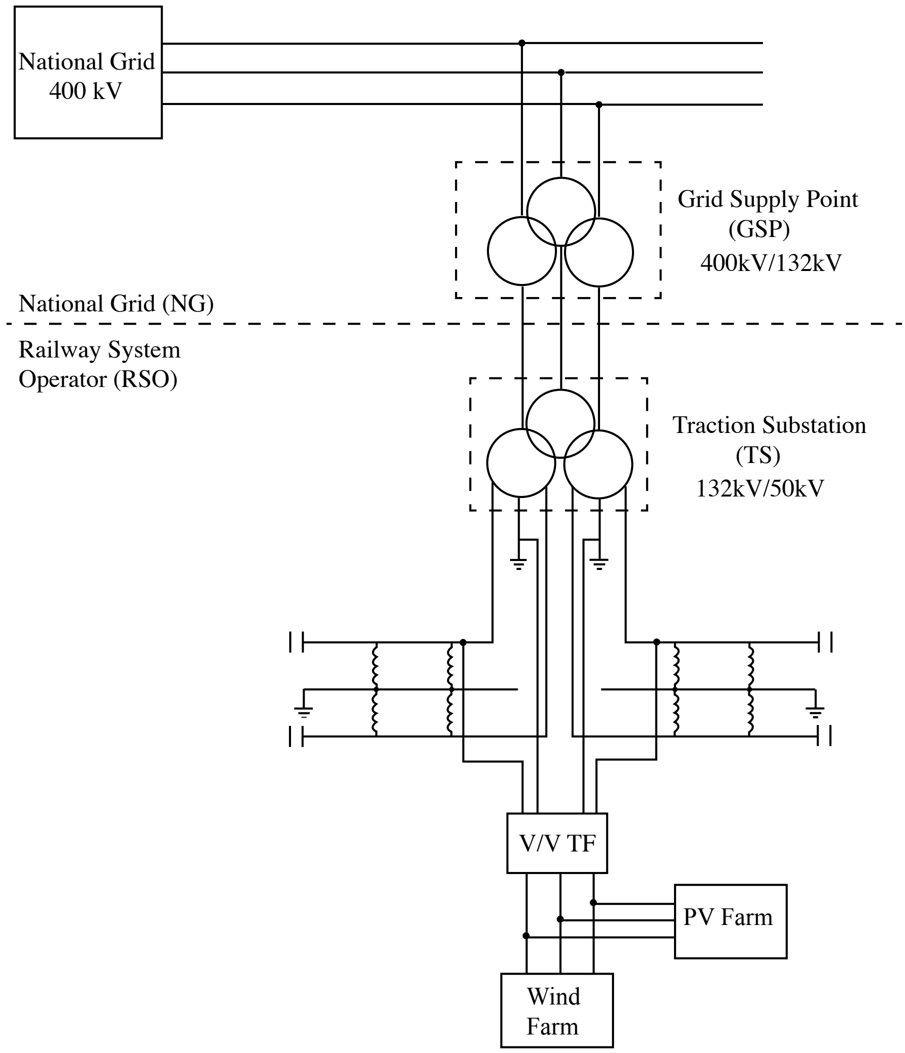

Figure 4-2 Scheme of RESs connected to railway power supply system via V/V transformer.

4.2.3 RES Connected to Railway Power Supply System via Static Converter (Scheme-3)

This scheme is different from the first two schemes. A smaller RES is connected to the low-voltage side of the traction transformer via a Static Frequency Converter (SFC), as shown in Figure 3-4(a).

The capacity of each PV and wind farm is half that of the first two schemes. However, another set of both is installed and connected at the opposite feeding section. Additionally, it is assumed that there are no transmission losses (PV and wind farms are installed nearby the traction substations). It should be noted that, usually, a megawatt-scale PV farm is transmitted as a three-phase power system. Thus, a special converter, such as a static converter, is required to convert a three-phase 33 kV power system to a single-phase 25 kV power system.

The single-line diagram of the distributed solar PV farm and wind farm is illustrated in Figure 3-4(b). For instance, a 10 MW PV farm consists of five 2 MW PV arrays. The 10 MW wind farm consists of five 2 MW wind turbines. Instead of using power transformers to step up the three-phase voltage of the PV farm and wind farm from 33 kV to 132 kV in the first two schemes, the SFC is utilized to convert three-phase 33 kV to single-phase 25 kV.

SFCs are widely used in many European countries, e.g., Germany, Switzerland and Austria, to convert the frequency from 50/60 Hz to 16.7 Hz for railway power supply systems [55]. However, according to [56], an SFC can operate as a three-phase to single-phase converter without converting frequency. For instance, on the Doncaster East Coast Main Line (ECML) in the UK, ABB's SFC will be used to convert three-phase 33 kV, 50 Hz to single-phase 25 kV, 50 Hz to feed the traction load [57][58].

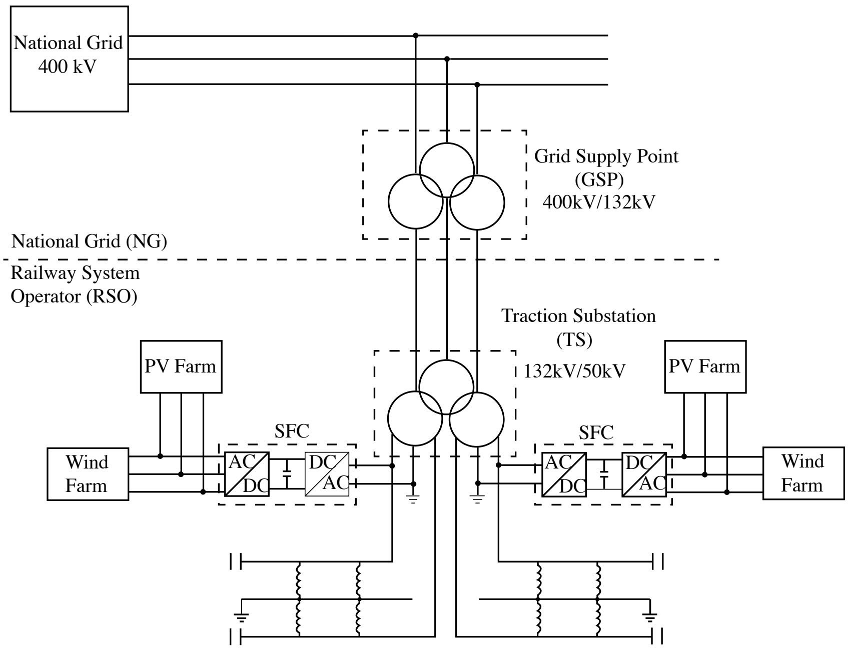

(a)

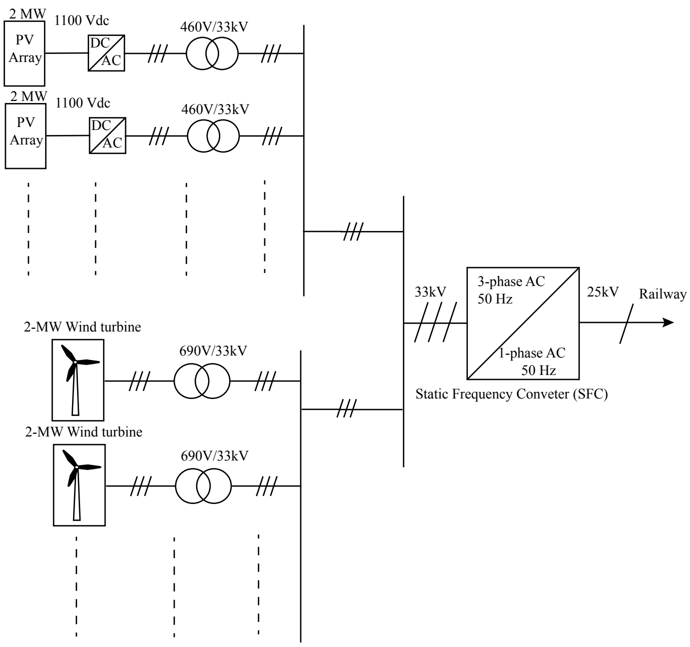

(b)

Figure 4-3 (a) Scheme of RES connected to railway power supply system via SFC, (b) single-line diagram of solar PV farm and wind farm connected to railway overhead line via SFC.

4.3 Methodology

4.3.1 Train Energy Consumption

To calculate train energy demand, the rolling stock specification (train power, maximum traction, physical properties) and route information (speed limit, gradient) are needed. The movement of the train follows the motion law of Newton as explained in Chapter 3.

For electric trains equipped with a regenerative brake, electric power is generated during train braking. If there is a train in traction mode in the same feeding section without interruption of the neutral zone, this regenerative energy will be consumed by that train. Otherwise, it will flow back to the national grid in the case of an AC railway power system.

4.3.2 Renewable Energy Sources

4.3.2.1 Solar PV Farm

The natural light from the sun is the most abundant source of energy. In this chapter, the megawatt-scale PV farms are connected to the system in different ways according to the proposed schemes.

A PV model is created in Simulink with a controlled-current source block. Due to the nature of the simulation type (steady-state model), the effect of temperature is ignored. Therefore, solar irradiance is the only input of the PV model. The amount of electrical energy generated from the PV farm is computed by:

$$E_{pv} = \int_0^t P_{pv} dt \qquad (4\text{-}1)$$

where:
$P_{pv}(s)$ is the power produced by the PV farm [W];
E_{pv} is the energy of the PV farm [Wh];
t is time [s].

4.3.2.2 Wind Farm

According to [59], energy generated from wind in 2019 accounted for nearly one-fifth of the UK's total supply and became the second biggest energy source, only behind gas combined-cycle generation.

Energy from the wind turbine is calculated by:

$$E_w = \int_0^t P_w dt \tag{4-2}$$

where:
P_w is the power output (W) of the turbine [W];
E_w is the energy (Wh) from a wind farm [Wh].

4.3.2.3 Transformer

Power transformers play a crucial role in a power system. They are operated to step down/up the voltage level to a suitable level according to the end-user. Usually, the efficiency of a transformer is already high. Nevertheless, as the global trend for energy reduction and energy efficiency keeps increasing, the European Union (EU) has set a minimum requirement for transformer efficiency by defining a performance indicator for transformers called Peak Efficiency Index (PEI).

In order to simulate the transformer losses, the transformer capacity (S_r), magnetization resistance (R_m), equivalent resistance (R_{eq}), and equivalent reactance (X_{eq}) must be known. The transformer capacity (S_r) was determined by the authors to meet the system requirements and match the sizes available in [60]. The PEI is used to compute R_{eq} and X_{eq} at specified transformer sizes. The value of magnetization resistance is assumed to be 1000 pu. The transformer equivalent resistance (R_{eq}) and equivalent reactance (X_{eq}) are calculated in the following steps:

1) acquire the PEI value from [60] according to the transformer power rating,

2) assign the short-circuit impedance (Z) according to the size of the transformer: for 3.151 to 6.30 MVA, Z = 0.0715 pu; for 6.301 to 12.5 MVA, Z = 0.0835 pu; for 12.5 to 25 MVA, Z = 0.10 pu; for 25 to 250 MVA, Z = 0.125 pu [61],

3) find the no-load loss (P_0) at the rated primary voltage using (4-3),

4) find the copper loss (P_k) at the rated current using (4-4),

5) find the equivalent resistance (R_{eq}) from the copper loss using (4-5),

6) find the equivalent reactance (X_{eq}) using (4-6).

The equivalent resistance and reactance from the calculation will be filled in the transformer model in Simulink. Table 4-1 lists the parameters that are used in the simulation.

$$P_0 = \frac{V_{rated}^2}{R_m} \tag{4-3}$$

$$PEI = 1 - \frac{2 \cdot (P_0 + P_{c0} + P_{ckPEI})}{S_r \cdot \sqrt{\frac{P_0 + P_{ckPEI} + P_{c0}}{P_k}}} \tag{4-4}$$

$$P_k = I_{rated}^2 \cdot R_{eq} \tag{4-5}$$

$$X_{eq} = \sqrt{Z^2 - R_{eq}^2} \tag{4-6}$$

where:

PEI is the peak efficiency index [pu];

P_0 is the no-load loss measured at the rated voltage and rated frequency [W];

P_{c0} is the electrical power required by the cooling system for no-load operation (equal to 0 in this study);

P_k is the measured load loss at the rated current and rated frequency [W];

P_{ckPEI} is the additional electrical power required by the cooling system for operation (equal to 0) at *k*pei

S_r is the rated power of the transformer on which P_k is based [MVA];

*k*pei is the load factor at which PEI occurs.

There are several types of transformer losses. Nevertheless, only core loss or no-load loss (P_0) and copper loss or load loss (P_l) are considered in this paper. Thus, the total transformer loss is computed as given in (4-7). Transformer efficiency is calculated using (4-8) [45].

$$P_{loss,tf} = P_0 + P_l \tag{4-7}$$

$$\eta_{tf}(k) = \frac{k \cdot S_{tf}}{k \cdot S_{tf} + k^2 \cdot P_k + P_0} \tag{4-8}$$

where:

$P_{loss,tf}$ is the total transformer loss [W];

P_l is the copper loss or load loss [W];

$\eta_{tf}(k)$ is the transformer efficiency (pu) at load factor k.

The efficiency (η_{tf}) obtained when load loss (P_l) equals core loss (P_0) is PEI.

Table 4-1 Transformer efficiency and parameters

Transformer	**PEI (%)**	P_0 **(W)**	P_k **(W)**	R_m **(Ω)**	Z **(%)**	R_{eq} **(Ω)**	X_{eq} **(Ω)**
2.1 MVA, 690 V/33 kV	99.319	2100	24347	227	6.25	0.002629	0.013924
2.5 MVA, 460 V/33 kV	99.514	2500	14762	85	6.25	0.000500	0.005266
5 MVA, 33 kV/132 kV	99.548	5000	25538	217800	7.15	1.112435	15.532916
10 MVA, 33 kV/132 kV	99.615	10000	37056	108900	8.35	0.403543	9.084191
15 MVA, 33 kV/132 kV	99.656	15000	44376	72600	10.00	0.214780	7.256822
20 MVA, 33 kV/132 kV	99.684	20000	49928	54450	10.00	0.135929	5.443303
25 MVA, 33 kV/132 kV	99.700	25000	56250	43560	10.00	0.098010	4.354897
40 MVA, 132 kV/25 kV	99.724	40000	76176	435600	12.50	0.829557	54.443680
80 MVA, 400 kV/132 kV	99.758	80000	117128	2000000	15.00	2.928200	299.985709

4.3.2.4 PV Inverter and Static Frequency Converter

For a large-scale PV farm, the central inverter topology is commonly employed [15]. The DC power output from the PV panels is combined by string combiners. The recombiners gather the power from each string combiner to feed into the central inverter, where the DC power is converted to three-phase AC power. There is always a loss in electrical equipment, and the inverter is no exception. There are two parts of the inverter losses: the constant part (supply to the control system and the auxiliary devices) and the load-dependent part (conduction losses and switching losses from IGBT). To calculate the inverter efficiency for each input level, (4-9) is used [62].

The main function of the SFC is to convert three-phase power from the RESs to a single-phase power supply to the 25 kV railway overhead line via switchgear at the traction substation. Due to the unavailability of SFC efficiency information, it is assumed that the efficiency curve of the SFC has the same characteristics as that of the inverter. Thus, (4-10), derived from (4-9), is used to determine the SFC efficiency. Equations (4-11) and (4-12) are used to determine the inverter and SFC losses, respectively.

$$\eta_{Inv}\left(P_{dc,pu}\right) = A_{Inv} + B_{Inv} \cdot P_{dc,pu} + \frac{C_{Inv}}{P_{dc,pu}} \tag{4-9}$$

$$\eta_{SFC}\left(P_{3p-AC,pu}\right) = A_{SFC} + B_{SFC} \cdot P_{3p-AC,pu} + \frac{C_{SFC}}{P_{3p-AC,pu}} \tag{4-10}$$

$$P_{loss,Inv} = (1 - \eta_{Inv}) \cdot P_{dc} \tag{4-11}$$

$$P_{loss,SFC} = (1 - \eta_{SFC}) \cdot P_{3p-AC} \tag{4-12}$$

where:

η_{Inv} is the inverter efficiency [%];

η_{SFC} is the static frequency converter efficiency [%]

P_{dc} and $P_{dc,pu}$ are the DC input powers [W, pu];

P_{3p-AC} and $P_{3p-AC,pu}$ are the three-phase AC input powers of SFC [W, pu];

$P_{loss,Inv}$ and $P_{loss,SFC}$ are the total losses in the inverter and SFC, respectively [W];

A_{Inv}, A_{SFC}, B_{Inv}, B_{SFC}, C_{Inv}, and $C_{SFC}$are the parameters computed from the method in [62].

In order to find parameters A, B, and C, three pairs of η_{Inv} and P_{dc} values per unit are required. In this study, inverter efficiencies of 0.1, 0.2, and 1 pu of P_{dc} are used. They are taken from the efficiency curve of the manufacturer's datasheet [63] for a 2.2 MVA inverter with a peak efficiency of 98.6%. The same procedures are applied to determine the SFC efficiency curve. The SFC is a modular system with the assumption of 5 MVA per unit. Thus, the number of units can be customised to obtain the required power rating suitable for the installed RES. The efficiency of 98% at the rated capacity taken from the converter at an equivalent rating [64] is assigned and used in (4-10).

The estimation of A, B, and C for the inverter and the SFC is implemented using the Curve fitting tool in MATLAB. A_{Inv}, A_{SFC}, B_{Inv}, B_{SFC}, C_{Inv}, and $C_{SFC}$are 98.86, 98.82, −0.8611, −0.7222, −0.09722, and −0.09444, respectively. The efficiency curves of the 2.2 MVA PV inverter, 5 MVA SFC, and power transformers are shown in Figure 4-4.

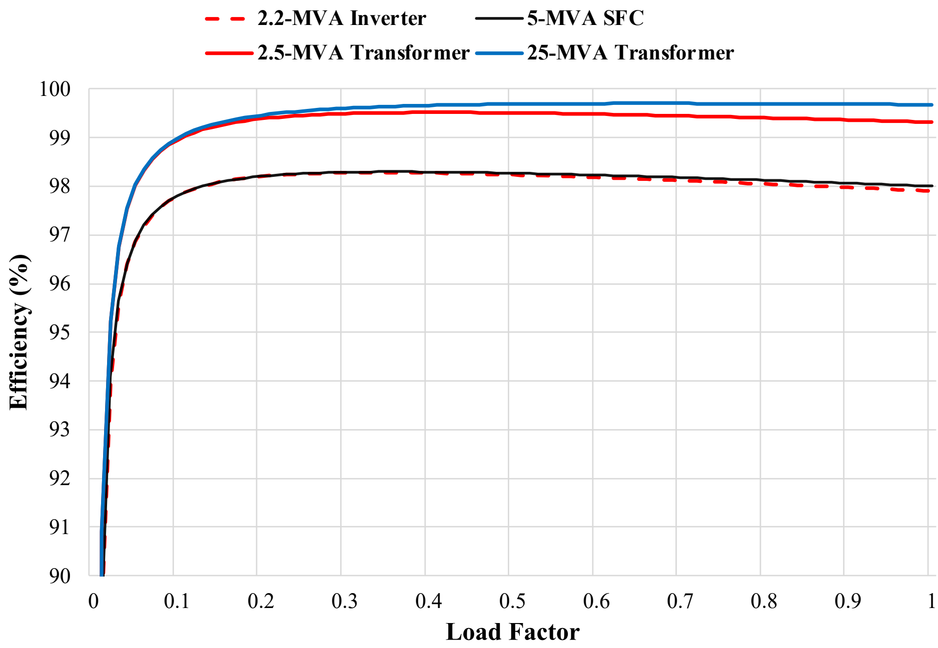

Figure 4-4 The efficiency of the inverter, SFC, and transformers used in this study versus load factor.

4.3.2.5 Transmission Line

Another critical component is the transmission line. The L12 pylon, used in the UK for 275kV and 400 kV transmission systems, is used in this study to find the electrical parameters [65]. To calculate the per-phase capacitance, inductance and resistance per unit length, the All-Aluminum Alloy Conductor (AAAC) with 700 mm^2 nominal area and 37.26 mm diameter with the code name 'Araucaria' is adopted on the pylon to carry the current from the power station to the GSP [66]. The DC resistance of this conductor is 0.04047 Ω/km [67].The capacitance and inductance from the calculation using the equations from [45] are 0.024 µF per phase per km, and 0.466 mH per phase per km, respectively. Equation (4-13) shows the losses in transmission line calculation.

$$P_{loss,TL} = |I_{cond}|^2 \cdot R_{cond} \quad (4\text{-}13)$$

where:

I_{cond} is the current flow in the conductor [A];

R_{cond} is the conductor resistance [Ω];

$P_{loss,TL}$ is the transmission line losses [W].

4.3.2.6 Voltage Unbalance Factor (VUF)

Due to a single-phase traction load, load imbalance occurs, and it causes negative-phase sequence currents and voltages in the upstream power system. Rotating machines are susceptible to these negative-phase sequence components and may malfunction. The VUF, commonly used to measure the imbalance of a power system, is the ratio of negative-phase sequence voltage to positive-phase sequence voltage [68],as seen in (4-14).

$$VUF\ (\%) = \frac{|V_{Neg}|}{|V_{Pos}|} \times 100 \quad (4\text{-}14)$$

where:

V_{Neg} is the negative-phase sequence voltage [V];

V_{Pos} is the positive-phase sequence voltage [V].

According to the UK grid code [69], the VUF for England and Wales transmission systems should not exceed 1.5% for voltage levels above 150 kV and 2% for 132 kV

4.3.2.7 Cost Calculation

The cost of renewable energy generation plants is comprised of several components. In this study, six main elements of cost are considered to estimate the lifetime cost of solar PV and wind farms. The first one is the pre-development costs, which are the cost of licensing and technical design. The second one is the construction costs, which include the infrastructure cost, grid connection cost, transformer cost, substation cost, inverter cost, and balance of system cost. The operation and maintenance (O&M) costs, consisting of fixed O&M and variable O&M, are considered as the third and fourth components, respectively. The amount of energy generated (MWh) determines the variable O&M costs [70]. Additionally, the insurance cost is included to cover the risk of unforeseen events. Lastly, the cost of using the transmission network is considered as the Network Use of System (UoS) charges [71]. Equations (4-15) and (4-16) are used to calculate the lifetime costs of PV and wind farms. Their abbreviations and values are shown in Table 4-2.

$$\begin{aligned} C_{LF,PV} = {} & c_{PD,PV} \cdot P_{PV,rated} + c_{CN,PV} \cdot P_{PV,rated} + c_{IN,PV} \cdot P_{PV,rat} \\ & + c_{UoS,PV} \cdot P_{PV,rated} + c_{OMfix,PV} \cdot P_{PV,rated} \cdot T_{LF,I} \\ & + c_{OMvar,PV} \cdot E_{PV,LT} \end{aligned} \quad (4\text{-}15)$$

$$\begin{aligned} C_{LF,Wind} = {} & c_{PD,Wind} \cdot P_{Wind,rated} + c_{CN,Wind} \cdot P_{Wind,rated} \\ & + c_{IN,Wind} \cdot P_{Wind,rated} + c_{UoS,Wind} \cdot P_{Wind,rated} \\ & + c_{OMfix,Wind} \cdot P_{Wind,rated} \cdot T_{LF,Wind} + c_{OMvar,Wi} \\ & \cdot E_{Wind,LT} \end{aligned} \quad (4\text{-}16)$$

Table 4-2 Abbreviation list for (4-15) and (4-16)

Parameter	Units	Definition
$C_{LF,PV}$ $C_{LF,Wind}$	£	Lifetime costs of PV and wind farms
$c_{PD,PV}$ $c_{PD,Wind}$	£50/kW £120/kW	Pre-development costs of PV and wind farms [70]
$c_{CN,PV}$ $c_{CN,Wind}$	£400/kW £1000/kW	Construction costs of PV and wind farms
$c_{OMfix,PV}$ $c_{OMfix,Wind}$	£6700/MW/year £23500/MW/year	Fixed operation and maintenance cost for PV and wind farms
$c_{OMvar,PV}$ $c_{OMvar,Wind}$	£0/MWh £6/MWh	Variable operation and maintenance cost for PV and wind farms
$c_{IN,PV}$ $c_{IN,Wind}$	£1824/MW £1376/MW	Insurance cost for PV and wind farms

$c_{UoS,PV}$ $c_{UoS,Wind}$	£1513/MW £3109/MW	Use of System charges (transmission system) for PV and wind farms [71]
$P_{PV,rated}$ $P_{Wind,rated}$	MW	Power rating of PV and wind farms
$E_{PV,LT}$ $E_{Wind,LT}$	MWh	Amount of electricity generated from PV and wind farms during their lifetime
$T_{LF,PV}$ $T_{LF,Wind}$	Years	Lifetime of PV and wind farms

The lifetime costs of the V/V transformer, SFC, and 33 kV/132 kV transformer are calculated by (4-17), (4-18), and (4-19), respectively. These costs are comprised of two parts: the capital cost and the O&M cost. The O&M costs for the three pieces of equipment are assumed to be 10% of the capital cost.

$$C_{VV,TF} = C_{Cap,VV} + C_{OM,VV} \quad (4\text{-}17)$$

$$C_{SFC} = C_{cap,SFC} + C_{OM,SFC} \quad (4\text{-}18)$$

$$C_{TF} = C_{cap,TF} + C_{OM,TF} \quad (4\text{-}19)$$

where:

$C_{VV,TF}$, $C_{cap,VV}$, and $C_{OM,VV}$ are the lifetime cost, capital cost, and O&M cost of V/V transformer in scheme-2;

C_{SFC}, $C_{cap,SFC}$, and $C_{OM,SFC}$ are the lifetime cost, capital cost, and O&M cost of the SFC in scheme-3;

C_{TF}, $C_{cap,TF}$, and $C_{OM,TF}$ are the lifetime cost, capital cost, and O&M cost of the power transformer (33 kV/132 kV) in scheme-1.

Equation (4-20) shows the lifetime cost of scheme-1. Due to the extra transformer (V/V transformer) in scheme-2, the lifetime cost of the V/V transformer is added to (4-20) and becomes (4-21). To compute the cost of scheme-3, the 33 kV/132 kV power transformer lifetime cost is subtracted from that of scheme-1 and the lifetime cost of SFC is added instead as presented in (4-22). It should be noted that (4-20) to (4-22) show the lifetime cost for one traction substation only.

$$C_{RES,S1} = C_{LF,PV} + C_{LF,Wind} \quad (4\text{-}20)$$

$$C_{RES,S2} = C_{LF,PV} + C_{LF,Wind} + C_{VV,TF} \quad (4\text{-}21)$$

$$C_{RES,S3} = C_{LF,PV} + C_{LF,Wind} + 2 \cdot C_{SFC} - 2 \cdot C_{TF} \quad (4\text{-}22)$$

where:

$C_{RES,S1}$, $C_{RES,S2}$, and $C_{RES,S3}$ are the lifetime cost of RESs in scheme-1, scheme-2, and scheme-3, respectively.

Table 4-3 summarizes the SFC and transformer costs used in this chapter. The capital cost of transformers and SFCs is modified from [72], where SFCs are assumed to cost 1.5 times the converter due to the unavailability of SFC data.

The railway system operator normally buys electricity from the national grid. Equation (4-23) shows the amount that needs to be paid by the railway system operator. This study also considers the carbon cost or carbon tax as seen in the second term. Furthermore, it is assumed that the regenerative braking energy that has not been utilised is fed back to the grid, and the railway gets paid for this depending on the amount of energy (E_{sell}). In the case of the integrated RES, the excess energy is also sold to the grid at the same price as the regenerative energy.

Table 4-3 Transformers and static converter cost

33 kV/132 kV Transformer		**V/V Transformer**		**Static Converter (SFC)**	
Size (MVA)	**Cost (£m)**	**Size (MVA)**	**Cost (£m)**	**Size (MVA)**	**Cost (£m)**
5	0.08	10	0.15	5	0.86
10	0.15	20	0.3	10	1.73
15	0.23	30	0.45	15	2.59
20	0.31	40	0.6	20	3.45
25	0.39	50	0.75	25	4.31

$$C_{Electricity} = c_{buy} \cdot E_{buy} + c_{cbn} \cdot M_{cbn} - c_{sell} \cdot E_{sell} \quad (4\text{-}23)$$

where:

$C_{Electricity}$ is the net cost of electricity (including carbon cost) that the railway system operator needs to pay in one year [£];

c_{buy} is the electricity price [£140/MWh [73]];

c_{cbn} is the carbon tax [£18/ton CO_2 [70]];

c_{sell} is the price of energy sold to the grid [£70/MWh];

E_{buy} is the amount of energy purchased [MWh];

E_{sell} is the amount of energy sold to the grid [MWh];

M_{cbn} is the amount of carbon emissions for generating electricity to supply the railway.

4.4 Case Study

In order to compare the energy flow of each renewable energy integration scheme, a part of the UK High-Speed Two (HS-2) project from London to Birmingham, which is in the development phase [74] is used as a benchmark scheme in this case study. This route is around 176 km [75] with 4 stations: London Euston, Old Oak Common, Birmingham International and Birmingham Curzon Street. Three 400/132 kV GSP substations are located at Ickenham, Quainton and Burton Green, as seen in Figure 4-5.

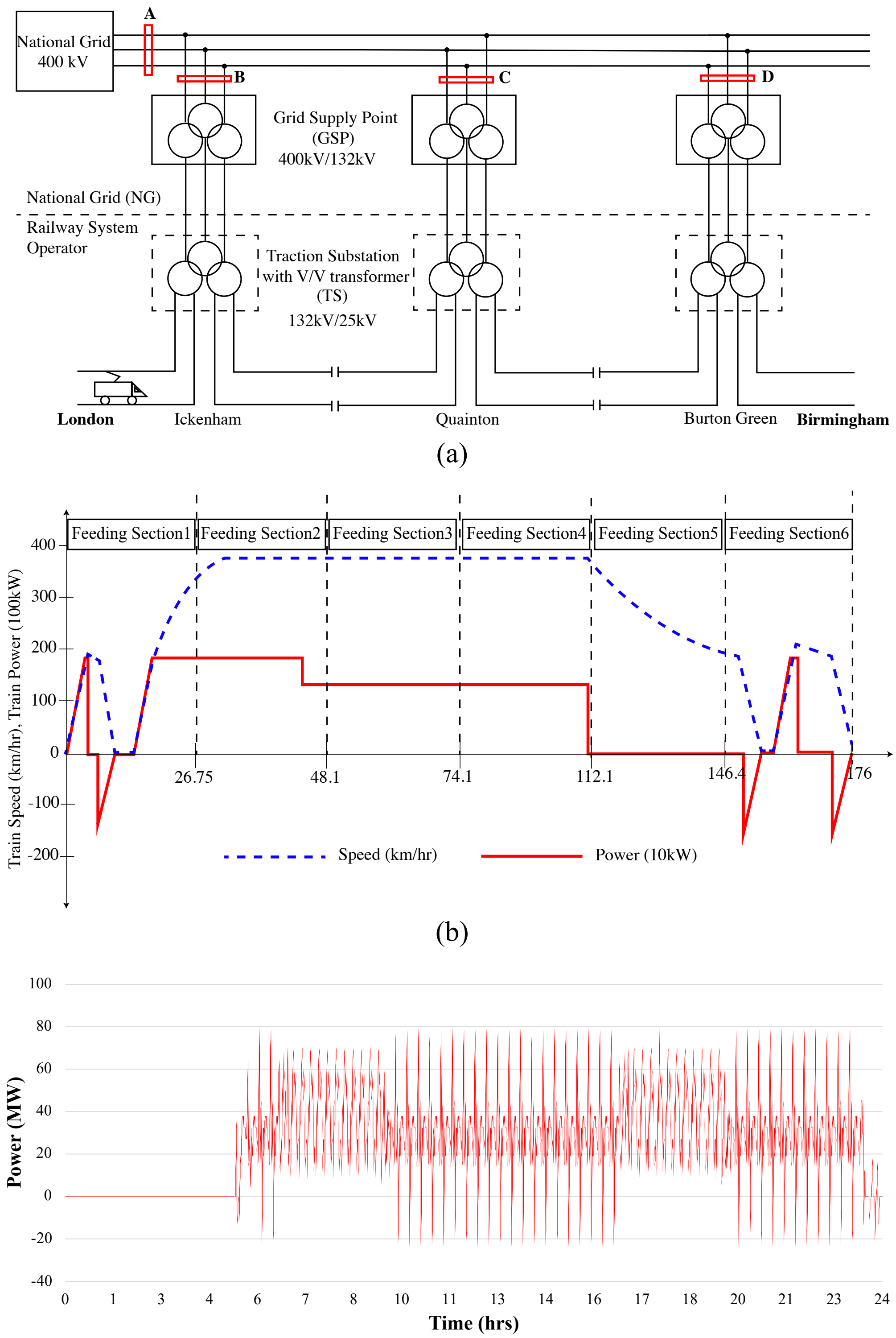

Figure 4-5 (a) Conventional connection scheme (benchmark), showing the entire power system connection of the case study, (b) train energy profile of a single train trip from London Euston to Birmingham Curzon Street from Single Train Simulator, (c) train power demand for 24-hour operation.

4.4.1 Simulation Description

The energy profile of multiple train servicing for an entire day is created using MATLAB with the train timetable in Table 4-4. It can be observed in Figure 4-5(a) that each traction substation supplies power to two feeding sections at its left and right. Thus, there is a total of six feeding sections for this system. Each feeding section is separated by a neutral section (NS). In this paper, the location of the neutral section is known from the HS2 project data [75]. Figure 4-5(b) illustrates the power profile and speed profile with the train elapsed time of a train journey from London Euston to the destination at Birmingham Curzon Street. The power profile is sampled at 20-second intervals to ensure that it will not miss the regenerative braking data. The train starts to travel from the first station and stops at Old Oak Common after 4 minutes (9.5 km). Then, 12 minutes after departing, the train passes the first traction substation (27 km see Figure 4-5(a)). During the first 12 minutes, the train is supplied power by the feeding section 1. Therefore, the train will eventually be supplied by all six feeding sections during one trip. As the relationship between train elapsed time and position is perceived, multi-train services for the entire day can be implemented based on the assumption that the driving style of each train is the same. This is to ensure that the relation between the elapsed time and position can be applied to all trains.

The total power demand of multiple trains operated for 24 hours is shown in Figure 4-5(c). This power demand is the results of combining the power demand of multiple trains together according to the timetable and headway in Table 4-4. As can be seen in Figure 4-5(c), the first train departs at 5 a.m. and the next trains departs 20 minutes later than the train before. However, during peak time, the headway is reduced to 15 minutes. This can be noticed from 6 a.m. to 9 a.m. and 4 p.m. to 7 p.m. Moreover, the regenerative braking energy is utilized by trains in the same feeding section during peak time. Overall, there are 61 train trips in each direction or 122 trips for both directions. The impedance of the feeding line (contact wire and messenger wire) is given as $0.15 + j0.45\ \Omega/\text{km}$ to simulate the losses during current flows in contact wire. Table 4-5 displays the train station locations and maximum speed.

Table 4-4 HS2 train service timetable [76]

First train departs	05:00
Last train departs	23:00
Peak time	06:00 to 09:00 and 16:00 to 19:00
Headway for off-peak time	20 minutes
Headway for peak time	15 minutes

Table 4-5 Train station and maximum speed information [75]

Stations	**Location (km)**	**Max speed (km/h)**
Euston	0	230
Old Oak Common	9.5	360
Birmingham Interchange	156.7	230
Birmingham Curzon Street	176	0

The capacity of the PV and wind farm at each traction substation for scheme-1 and scheme-2 is varied, at 4, 8, 12, 16, and 20 MW. Thus, the total installed capacity of the RES for each traction substation is 8, 16, 24, 32, and 40 MW. For scheme-3, each side of the feeding section is connected with a PV farm and wind farm each rated at 2, 4, 6, 8, and 10 MW. The total capacity per traction substation is identical to that of scheme-1 and scheme-2.

The solar irradiance and wind speed data for each day from 2015 to 2019 were acquired from [77]. Owing to the huge amount of data, the simulation would take a tremendous time; thus, they are averaged and represented by months. For example, the solar irradiance and wind speed of every day in a month are averaged and represented for that month. Furthermore, since the data available are sampled at a one-hour interval, they are interpolated into 20-second intervals to match the train energy profile. The simulation of each scheme is carried out for 60 months in 5 years.

Additionally, as it is assumed that PV farms and wind farms are situated close to the traction substations, the solar irradiance and wind speed data are taken from the location of each traction substation or GSP (both are very close to each other).

4.4.2 Power Losses

The simulations were run on MATLAB Simulink with 20-second intervals starting from the 0^{th} to the $86{,}400^{th}$ seconds, which is the time from 00:00 to 24:00 hrs. Since this chapter focuses on the losses of the steady-state model of each scheme, the results are separated into three parts: 1) the conversion losses (transformer loss and inverter loss including SFC), 2) the transmission line losses, and 3) the total losses. It is worth mentioning that the transmission line losses in this study only exist on the power grid side which is outside railway system operator's responsibility boundary. Moreover, it is assumed that no transmission line losses between grip supply point, traction substation. Therefore, the transmission losses presented is for comparison purpose only.

The bar chart in Figure 4-6(a) shows the conversion losses, which combine energy losses in transformers and inverters (also in the SFC), using the average meteorological data between January 2019 and December 2019. Overall, scheme-2 gives the highest conversion losses, except in March and August, in which it is surpassed by scheme-3. The lowest conversion losses for the proposed RES integration scheme happen with scheme-1. The conventional scheme (without RES) has the least loss among all schemes because it does not need additional equipment to accommodate the RESs. Furthermore, it is noticeable that the conversion losses of scheme-3 follow the trend of the percentage of renewable energy penetration, shown as the black dashed line. This can be explained in Figure 4-6(b). When the amount of renewable energy rises, the power loss in the inverter and the SFC also increases. The inverter loss in scheme-3 is significantly higher than in the other schemes, and it determines the trend of the conversion loss. From observing all the simulation results from every single month from 2015 to 2019, it is found that when the RES energy penetration exceeds 90%, scheme-3 produces the largest conversion losses as seen in March and August in Figure 4-6(a). Considering the transformer loss, Figure 4-6(c) illustrates that scheme-2 generates the biggest transformer losses due to having an extra transformer (V/V transformer), followed by scheme-1, scheme-3, and lastly, the conventional scheme.

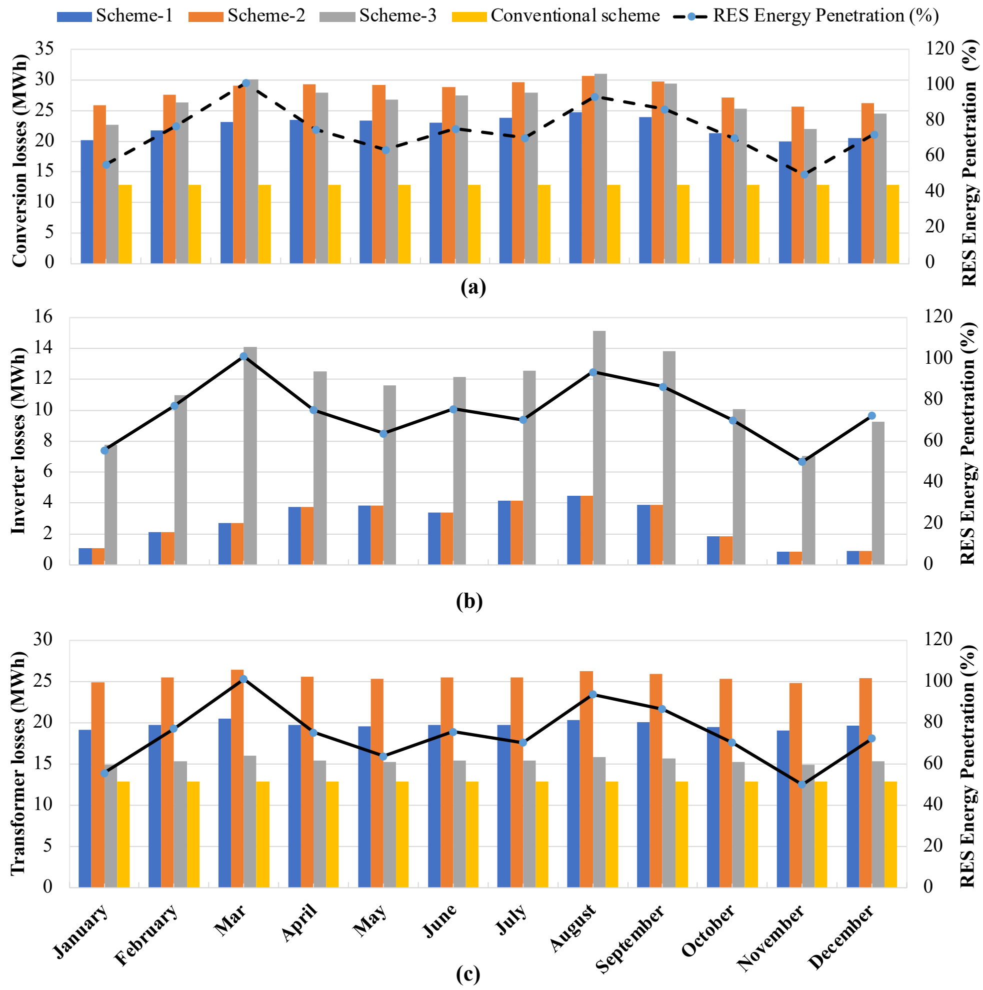

Figure 4-6 Conversion losses for different schemes and the renewable energy penetration percentage using meteorological data for the year 2019: (a) conversion losses, (b) inverter losses (including the SFC losses for the scheme-3), and (c) transformer losses.

In contrast to the conversion losses, as the grid is the only supply, the conventional scheme generates the maximum transmission line losses as presented in Figure 4-7(a). In this case, the energy source is far from the load center. As a result, the current flows through the long-distance conductor to the load and a small part of the energy is dissipated as heat. In comparison, the difference in transmission line losses is marginal for each scheme since the resistance of the conductor is very small. To see the losses in the conductor more clearly, Figure 4-7(b) shows the transmission line losses that occur during the flow of electricity from the grid to the load and vice versa. It can be seen that loss is similar though the amount of RES is different. In addition, it is obviously seen that the transmission line loss caused by the excess renewable energy flowing to the grid has the same trend as the percentage of renewable energy penetration. Because the transmission line losses for all schemes are marginally different, the total losses follow the trend of the conversion losses, as shown in Figure 4-8.

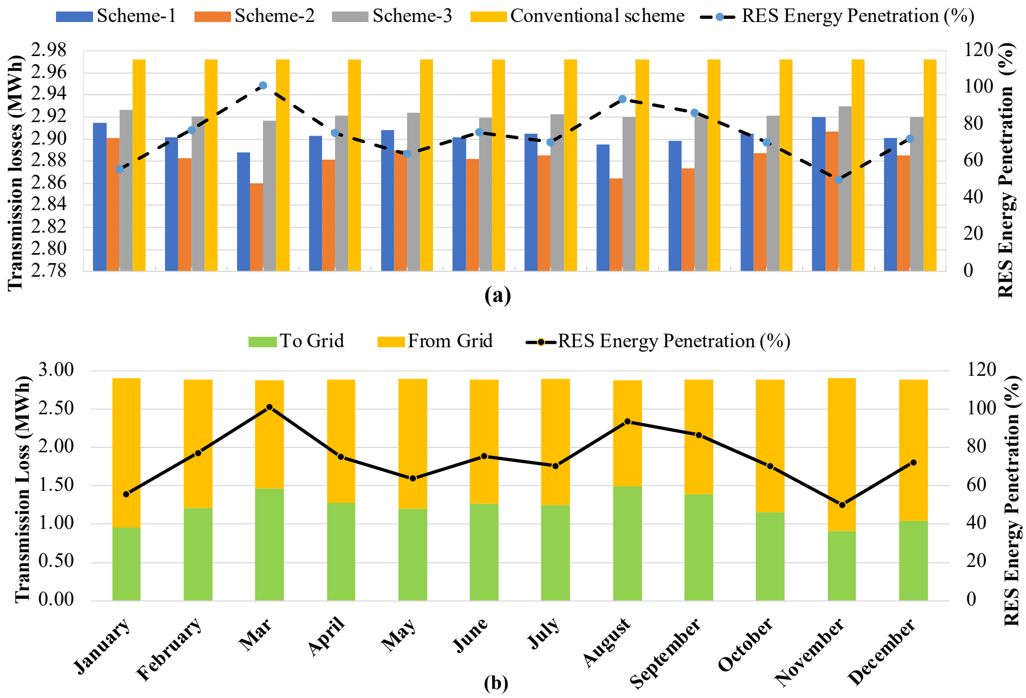

Figure 4-7 (a) Transmission line losses and (b) transmission line losses from scheme-1 (2019) due to the flow of electricity to and from the grid to supply the railway load, using meteorological data from 2019.

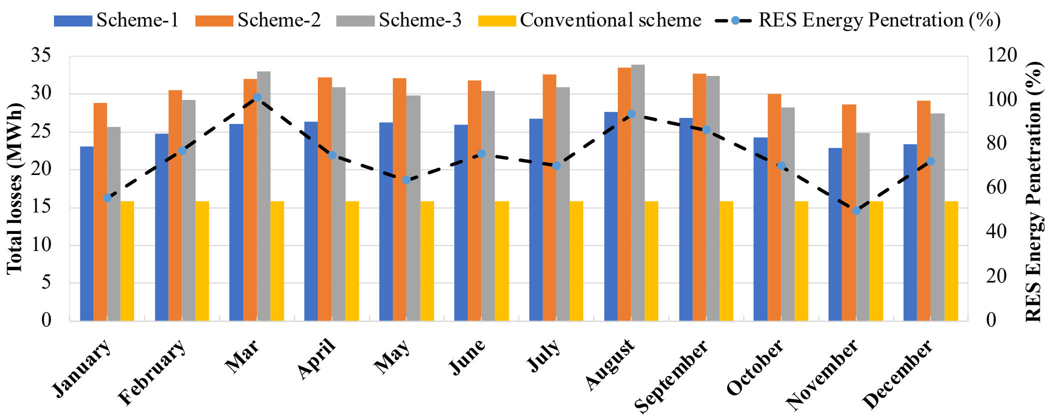

Figure 4-8 Total losses (combination of conversion losses in Figure 4-6(a) and transmission line losses in Figure 4-7(a)).

4.4.3 Voltage Unbalance Factor

The VUF is determined at four locations, from A to D (see Figure 4-5(a)); the results are tabulated in Table 4-6. At the 400 kV level which is used as the transmission system for this study, the VUFs for all locations and all schemes are below the defined limit at 1.5%.

Table 4-6 Voltage unbalance factor results

Transmission Voltage	**Scheme**	**Voltage Unbalance Factor (VUF, %)**			
		Location A	**Location B**	**Location C**	**Location D**
132 kV	Benchmark	2.75	2.93	4.24	7.12
	Scheme-1	2.74	2.92	4.22	7.07
	Scheme-2	2.74	2.92	4.19	7.00
	Scheme-3	2.71	2.88	4.06	6.83
275 kV	Benchmark	0.72	0.76	1.00	1.58
	Scheme-1	0.72	0.76	1.00	1.58
	Scheme-2	0.72	0.76	0.90	1.57
	Scheme-3	0.72	0.76	1.01	1.54
400 kV	Benchmark	0.32	0.34	0.46	0.73
	Scheme-1	0.32	0.34	0.46	0.73
	Scheme-2	0.32	0.34	0.45	0.73
	Scheme-3	0.32	0.34	0.46	0.71

The results are identical or slightly different at the same measured locations. This indicates that the integration of the RES has not worsened the system imbalance. The reason is that the 400 kV transmission system has a significantly high short-circuit capacity. The design limit of the fault level for a 400 kV system in the UK is 34,500 MVA or 50 kA [78]. Consequently, the effect of imbalance caused by the railway load and the connection of the RES is insignificant. In addition, 132 kV and 275 kV voltage levels are also commonly employed in the UK. Thus, the VUF of these voltage levels is calculated as well. For the 275 kV system, the VUF for most locations stays below the limit, except for location D in which the VUFs marginally exceed 1.5%. On the other hand, all the VUFs for the 132 kV system are beyond the maximum permissible level of 2%. Hence, without a compensation device, such as a load balancer, a railway power system with a high traction load should not be connected to the 132 kV and 275 kV transmission systems. It is worth mentioning that Static Var Compensator (SVC), Static Synchronous Compensator (STATCOM) and Railway Power Conditioner (RPC) can be utilized as load balancers [6].

From the VUF results in Table 4-6 if the 132 kV transmission system supplies the traction loads, the load balancers will be required for all three traction substations to suppress the unbalance so that the VUFs at spots A, B, C and D are reduced below the tolerance. On the other hand, only one traction substation at Burton Green will require a load balancer to deduct the VUF at spot D if the traction loads are connected to a 275 kV transmission system. Nevertheless, a feasibility study and cost assessment must be done to choose which transmission level the traction substations will be connected to. For instance, the lifetime cost of using 400 kV may be less than that of 132 kV and 275 kV with load balancers due to maintenance costs.

4.4.4 Cost Evaluation

In order to compare the lifetime cost of the system, the project lifetime of the PV and wind farms is assumed to be 25 years, from 2026 to 2050. According to [73], the average electricity price of £140 per MWh is applied for the UK. It is assumed by the authors that the electricity can be sold to the grid for half the buying price. Moreover, since the UK has a target to reduce carbon emissions, the amount of equivalent carbon is calculated, and the carbon tax is applied. The forecast carbon intensity data [79] illustrated in Figure 4-9 are used to compute the amount of carbon emitted from the power generation.

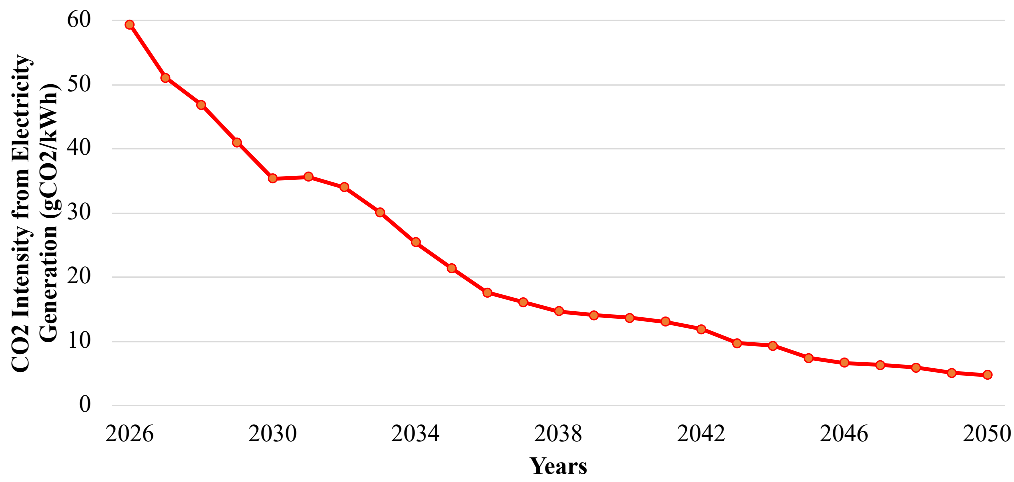

Figure 4-9 Estimated carbon intensity from power generation sector in the UK [79].

The cost calculation results are illustrated in Figure 4-10 for different sizes of RES (PV farm and wind farm), varying from 24 MW to 120 MW for the whole project. It should be noted that the RES installed capacity shown is for the entire project (three locations of RES). The first three bars (blue, orange, and grey) show the electricity cost saving for each proposed scheme compared to the conventional scheme. In other words, the total electricity cost of the conventional scheme minus the total electricity cost of the RES integration schemes in 25 years of operation, the cost saving increases with the size of the RES installed. For the RES with installed capacity of 24 MW, the energy cost is around £115m lower than that of the conventional scheme during the 25-year project, and about £550m lower for the 120 MW RES. The lifetime cost of the RES is shown in the last three bars (yellow, light blue, and green) for each RES installed capacity. It can be seen that the lifetime cost of scheme-1 is the lowest for all RES installed capacities, followed by that of scheme-2, and lastly scheme-3. Due to the extra transformer required, scheme-2 costs more than scheme-1. With the SFC in scheme-3, this scheme has the highest lifetime cost as the SFC cost is exceptionally high. Overall, the electricity cost saving is much higher than the RES lifetime cost for all proposed schemes and installed capacities. This indicates that it is worth the railway system operator investing in integrating the RESs into the railway power system.

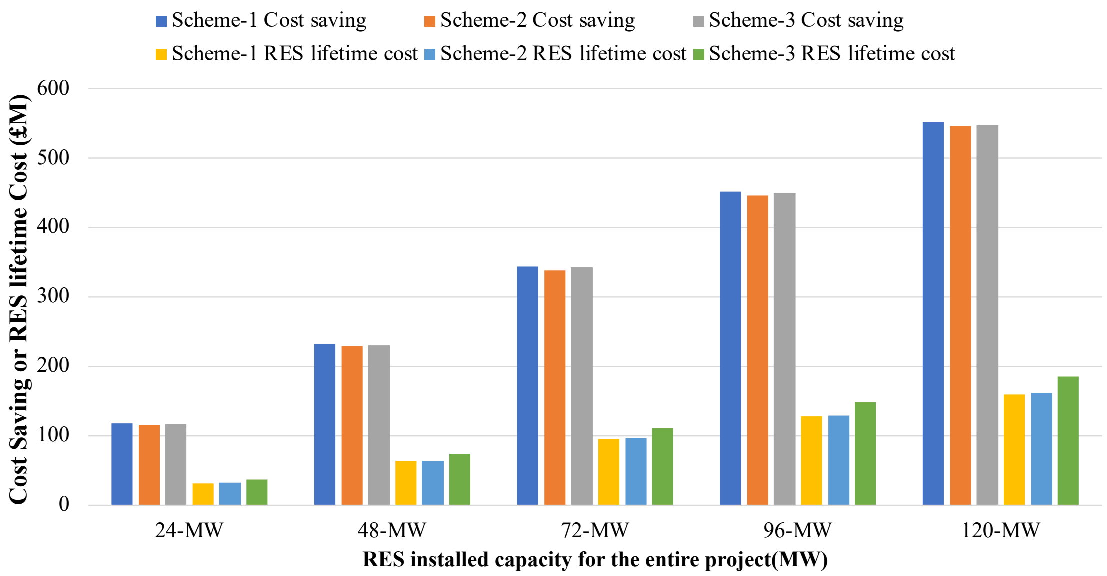

Figure 4-10 Total cost saving compared to the conventional scheme, and lifetime cost of RES for each proposed scheme.

Figure 4-11 depicts the payback time for the 120 MW RES in scheme-1 when the cost of the PV farm and wind farm (including the O&M cost) is matched by the electricity cost saving. The RES cost is paid off at around 5 years as seen as the breakeven point.

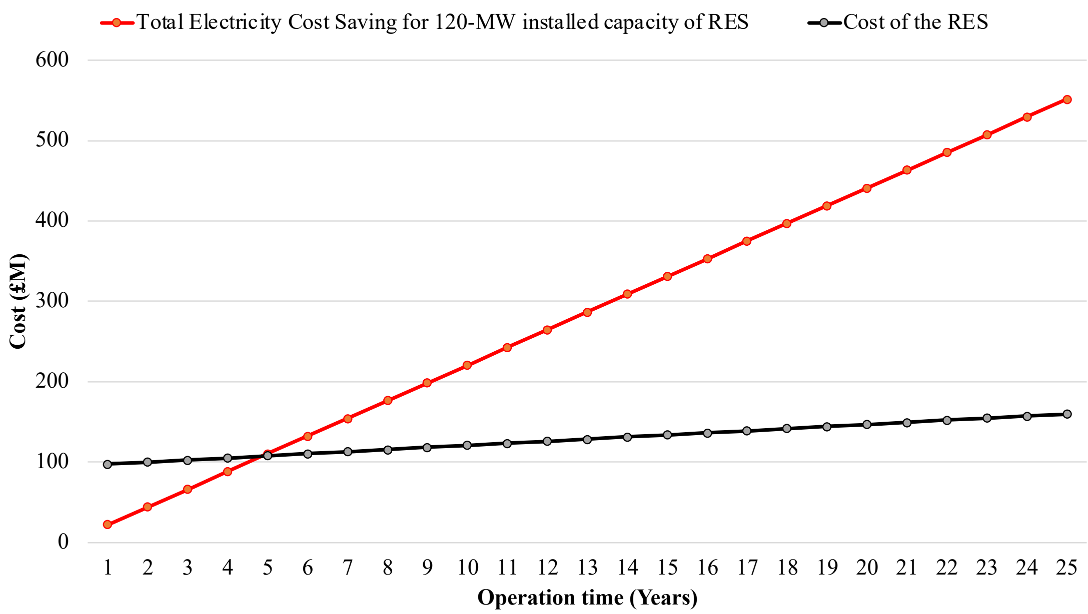

Figure 4-11 Total electricity cost saving of scheme-1 and cost of 120 MW RES (60 MW PV farm and 60 MW Wind farm) over time.

Table 4-7 displays the amount of energy flow of each scheme with various RES sizes and the amount of carbon emissions and costs for 25 years. The amount of carbon emissions can be reduced by half, from 130,200 tonnes with the benchmark scheme to 58,400 tonnes for the schemes with RES.

Table 4-7 Amount of energy and carbon for 25 Years

Type	**RES Size**	**Transaction**	**Scheme-1**	**Scheme-2**	**Scheme-3**	**Benchmark**
Energy (GWh)	24 MW	Buy from grid	5285.6	5295.4	5291.5	6062.2
		Sell to grid	187.0	183.5	186.4	63.8
	48 MW	Buy from grid	4546.4	4565.6	4559.4	6062.2
		Sell to grid	348.8	341.6	346.8	63.8
	72 MW	Buy from grid	3845.9	3882.5	3855.8	6062.2
		Sell to grid	537.0	520.7	535.5	63.8
	96 MW	Buy from grid	3215.6	3248.6	3232.4	6062.2
		Sell to grid	814.1	794.0	804.3	63.8
	120 MW	Buy from grid	2701.3	2730.2	2721.2	6062.2
		Sell to grid	1206.8	1182.1	1185.1	63.8
Carbon	24 MW	Amount (1000 t)	113.92	114.77	113.64	130.20
		Tax (Million-£)	2.05	2.07	2.05	2.34
	48 MW	Amount (1000 t)	97.93	98.76	97.92	130.20
		Tax (£m)	1.76	1.78	1.76	2.34
	72 MW	Amount (1000 t)	82.59	83.38	82.81	130.20
		Tax (£m)	1.49	1.50	1.49	2.34
	96 MW	Amount (1000 t)	69.06	69.77	69.42	130.20
		Tax (£m)	1.24	1.26	1.25	2.34
	120 MW	Amount (1000 t)	58.00	58.60	58.40	130.20
		Tax (£m)	1.04	1.05	1.05	2.34

4.5 Summary

Renewable energy integration schemes for AC high-speed rail were proposed, and the simulations were implemented to obtain the system's energy flow and power losses. The results show that among the RES integration schemes, scheme-1, in which the PV and wind farms are connected to a three-phase railway power network, provides the smallest total losses. Moreover, it also has the lowest lifetime cost for a 25-year lifetime. The scheme with RES connected to the railway side via a V/V transformer is the worst in terms of total losses as greater losses are produced in the V/V transformer, and this scheme will cost more than scheme-1. The total loss for the scheme with an SFC is slightly lower than that of scheme-2 if the RES energy penetration is less than 90%.

Considering the electricity cost-saving, the lifetime cost of each proposed scheme will be paid off in around five years, and an enormous electricity charge is saved in 25 years. Besides that, the VUF demonstrates that the integration of the RESs does not affect the system imbalance, and the VUF stays within the acceptable limit for the 400 kV transmission system. Nevertheless, a vast land area is required for PV and wind farms with a large generation capacity, such as in scheme-1 and scheme-2, which may be unavailable. The problem can be solved by implementing scheme-3 because the RES size on each side of the feeding sections is halved compared to the first two schemes. Furthermore, it is the most flexible scheme in terms of connection points as the RES can be connected to the railway overhead line along the route.

Due to the fluctuation of traction load, the VUF, when connecting traction load to the grid with low short circuit capacity, exceeds the permissible value. Even though the energy storage system cannot completely reduce the VUF to below the limit, it can still support the short-term power stabilisation by capturing the regenerative braking energy and discharging it to the upcoming trains. This will decrease the power difference between peak and minimum power. Hence, the power profile is less fluctuating.

It can be observed in this chapter that the only way to manage the excess energy from the renewable is to sell it to the grid at a lower price than buying. In order to gain more benefits from the energy generated from the renewable energy sources, energy storage devices can play an important role by capturing the excess energy and reuse it. This will reduce the cost of energy, especially during the peak time. The benefits of energy storage device will be presented in Chapter 5 with the modification of scheme-1 from this chapter. Furthermore, with the flexibility of scheme-3, Chapter 6 will introduce optimisation of renewable source and energy storage capacities and locations in which the minimum global cost is attained.

Chapter 5 Integration of Energy Storage System Into AC Railway Traction Power Network

5.1 Introduction

Rail transit is among the most carbon-efficient and energy-efficient modes of transportation [1]. In addition, it offers safety, dependability, and great capacity across many speed levels. In many nations, electrified trains play a crucial role in passenger transportation since they are swift and silent. As a result of the aforementioned rationale, the global construction of railway networks has accelerated significantly. Hence, enormous amounts of energy will be required. In order to reduce carbon emissions from traditional power plants, renewable energy sources attract attention due to their sustainability and cleanliness. Renewable energy sources (RES) and energy storage systems (ESS) can minimise energy acquired from the external grid, greenhouse gas emissions, and energy costs in a railway power system.

A growing number of researchers are interested in railway energy management and the integration of renewable energy sources with ESS into railway power systems. Researchers in [80] developed an idea for the next generation of railway power systems that integrate renewable energy sources with energy storage technology. The authors of [81] examined the application of regenerative braking energy via ESS and energy storage methods. The authors of [23] and [82] demonstrated significant cost savings and optimal sizing of the energy storage system for high-speed trains. The authors in [20] presented the applications and comparisons of energy storage systems in electrified trains. L.P. Di Noia and R. Rizzo [83] presented the best sizing of a hybrid energy storage system for storing energy from regenerative braking and a photovoltaic power plant. In the study, supercapacitors are employed to store regenerative energy, whereas batteries are used to store energy from photovoltaic (PV) plants because of their high energy density. The outcome of the analysis demonstrates economic and technological viability.

S. Boudoudouh and M. Maaroufi [30] investigated the hybrid substation consisting of a PV plant, wind farm, and ESS. Also, the authors proposed Distributed Energy Management (DEM) to regulate the energy flow between the hybrid substation (HSS) and the electrified trains. The study shows that HSS and DEM can remove the voltage loss and voltage surge caused by train acceleration and deceleration. I. Sengor et al. [28] developed a railway station energy management consisting of ESS, regenerative braking energy, PV, and an external grid in order to decrease the daily operational costs of the railway station. The deployment of ESS, regenerative energy, and PV yielded the greatest cost decrease, according to the findings. Aguado J. et al. [29] developed a strategy for optimal operation for energy and cost savings of railway electric energy systems taking PV plants, wind turbines, regenerative braking energy, and hybrid energy storage system into consideration (HESS). The uncertainty of renewable energy generation was taken into account using the scenario tree method. The results demonstrated that the combination of renewable energy sources with HESS improved cost and energy savings by 33.22 per cent and 9.6 per cent, respectively, compared to the base case (No HESS and RES).

Because a high-speed train consumes a significant quantity of energy, a significant amount of carbon dioxide will be released into the atmosphere if the energy supplied to the train is derived from fossil fuel. Furthermore, the railway operator may be required to pay extremely high electricity expenses. This paper's contribution is to investigate the impact of ESS and renewable energy sources on the railway power system in terms of energy and cost savings. A control technique for lowering the energy storage system's electricity costs is introduced. Energy distribution in each component and power losses are also presented. Furthermore, the amount of carbon emission is estimated and used to calculate the carbon tax.

5.2 System Description

Figure 5-1 illustrates a scheme for integrating a solar PV farm and energy storage system into a three-phase railway power supply system which is proposed for this research. Both are connected to distribution lines at the location between the grid supply point (GSP) and the traction substation. This system will supply power demand for two feeding sections (left and right sides). The energy storage is installed to capture the excess energy generated from the PV farm and residual regenerated braking energy from trains. Furthermore, it is also controlled to charge energy during an off-peak time when the electricity price is low and to discharge when there is demand during peak time.

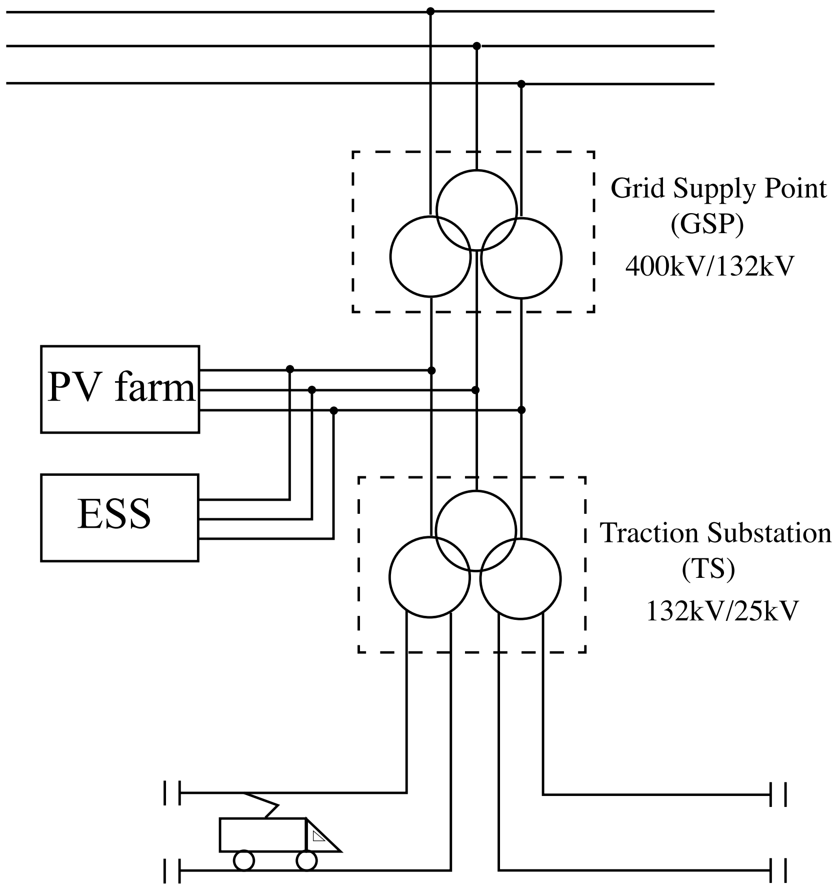

Figure 5-1 A proposed scheme of railway power network with integration of PV farm and energy storage

To reduce the effect of load imbalance from the railway side, the grid supply point is connected to the extra high voltage transmission line, and then the power transformers in the grid supply point are employed to step down the voltage to 132 kV. It is assumed in this study that the components and systems after the grid supply points are belong to railway system operator.

5.3 Methodology

5.3.1 Train Power Profile

With the rolling stock specification, the single-train simulator was used to output the power consumption of the travelling train. Then, the train timetable indicating the headway between the next train is used to determine the power profile for multiple trains. The procedures to obtain the train power are introduced in Chapter 3.

5.3.2 Solar PV Farm

A large-scale solar PV farm is a collection of solar arrays which are groups of solar panels that are built collectively to produce electricity for a specified use, such as supplying power to a utility grid or a community. The power generated from the PV farm in this study is mainly used to supply the electrical demand on the railways. Before being connected to the point of common coupling (PCC), the DC power produced from the PV array is converted to AC power by inverters as shown in Figure 5-2. In order to synchronise the PV farm to the high-voltage transmission line, the power transformer is needed to step up the low-voltage output from the inverter to the same level as the transmission line, i.e., 132 kV.

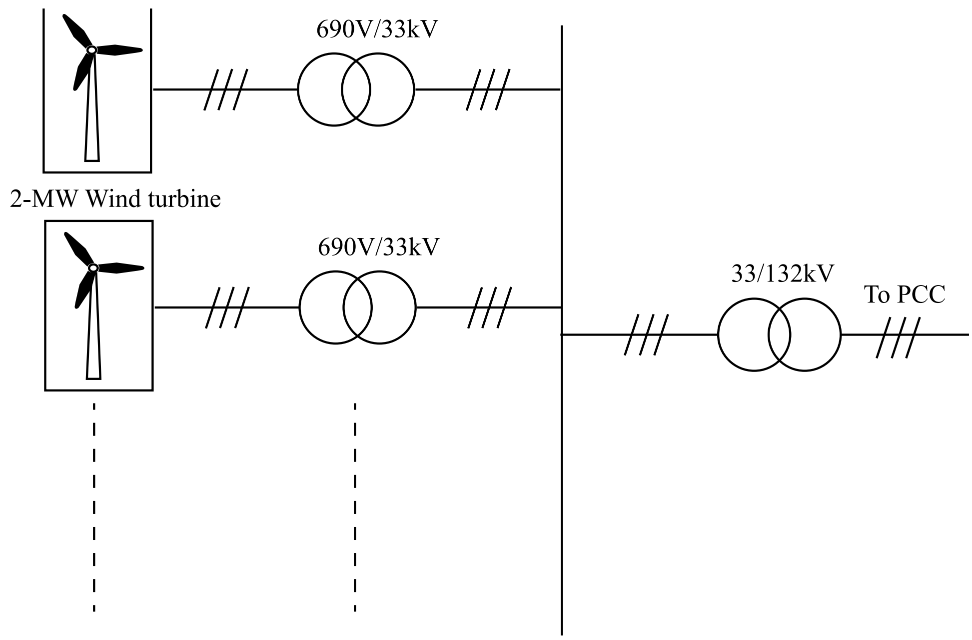

Figure 5-2 Single line diagram of a solar PV farm and a power transformer

5.3.3 Energy Storage System

5.3.3.1 Introduction

A grid-connected energy storage system is one that is used to store excess electricity generated by renewable energy sources such as solar panels or wind turbines. Instead of being sold to the grid at a low price, the stored electricity can be used to meet demand when it is needed. Moreover, it absorbs energy from the grid during the low electricity price period.

The quantity of energy that is available for use and stored within an energy storage system is referred to as the state of charge (SOC). The state of charge is commonly presented as a percentage and can be calculated using (5-1), with a value of 100% indicating that the system is fully charged and a value of 0% indicating that the system is totally discharged. Typically, the lower limit of the SOC is chosen to prevent the energy storage system from being entirely depleted. This is because a fully discharged system is more likely to sustain damage or have a shorter lifespan. Similarly, the top limit of the SOC is set in order to protect the system from being overcharged, which can not only cause the system to become damaged but also shorten its lifespan. Equation (5-2) presents that the working SOC must stay between the lower and upper limit SOC. In the same way, the energy stored in the energy storage must not be less than and greater than the rated energy multiplied by the lower and upper limit of SOC as described in (5-3), respectively.

$$SOC_{ess}^{t} = \frac{E_{ess}^{t}}{E_{ess}^{rated}} \cdot 100 \qquad (5\text{-}1)$$

$$SOC_{ess}^{min} \leq SOC_{ess}^{t} \leq SOC_{ess}^{max} \qquad (5\text{-}2)$$

$$SOC_{ess}^{\min} \cdot E_{ess}^{rated} \leq E_{ess}^{t} \leq SOC_{ess}^{\max} \cdot E_{ess}^{rated} \qquad (5\text{-}3)$$

Another important parameter of energy storage is the power rating. In the context of energy storage, "power rating" indicates the maximum amount of power that the system may either produce or consume at any particular moment. Power is typically expressed in kilowatts (kW) or megawatts (MW) for utility-scale applications. When choosing an energy storage system, the power rating is crucial since it indicates whether or not the system can fulfil the power needs of the load it is charging or supplying. Equations (5-4) and (5-5) depict that the charging power for the energy storage must not exceed the maximum charging power and the highest power that can be discharged is limited by the maximum discharging power. Finally, the maximum charge and discharge power are equal to the rated power of the energy storage as shown in (5-6).

$$0 \leq P_{ess}^{ch,t} \leq P_{ess}^{max,ch} \tag{5-4}$$

$$0 \leq P_{ess}^{dis,t} \leq P_{ess}^{max,dis} \tag{5-5}$$

$$P_{ess}^{max,ch} = P_{ess}^{max,dis} = P_{ess}^{rated} \tag{5-6}$$

where:

E_{ess}^{t} is the stored energy in the energy storage at time t [Wh];

E_{ess}^{rated} is the rated capacity of the ESS [Wh];

$P_{ess}^{ch,t}$ is the charging power at time t [W];

$P_{ess}^{dis,t}$ is the discharging power at time t [W];

$P_{ess}^{max.ch}$ is the maximum charging power of the energy storage [W];

$P_{ess}^{max,dis}$ is the maximum discharging power of the energy storage [W];

P_{ess}^{rated} is the rated power capacity of the energy storage [W];

SOC_{ess}^{t} is the state of charge at time t [%];

SOC_{ess}^{min} is the lower limit of a state of charge [%];

SOC_{ess}^{max} is the upper limit of a state of charge [%].

5.3.3.2 Physical Components

Multiple physical components constitute an energy storage system. Together, these components store and release energy as needed. The precise components of an energy storage system are determined by the energy storage technology employed. Figure 5-3 illustrates the connection of the main components that are considered in this research. Firstly, the energy storage device (ESD) is where energy can be stored and released. The ESD operates on direct current (DC). Therefore, a bi-directional converter is required. A bidirectional converter is used to connect the energy storage medium to the grid or another power source in a reversible energy storage system. The energy storage system's bidirectional converter transforms the grid's alternating current (AC) electricity into direct current (DC) electricity during the charging process. During the discharging phase of an energy storage system, a bidirectional converter converts the DC electricity from the energy storage medium into AC electricity that can be used to power loads or supplied back into the grid. As the energy storage system is designed to be connected to the three-phase power network, the AC side of the bi-directional converter outputs three-phase power. Finally, a step-up transformer is operated to boost the low voltage from the bi-directional converter to the 132-kV level at the point of common coupling.

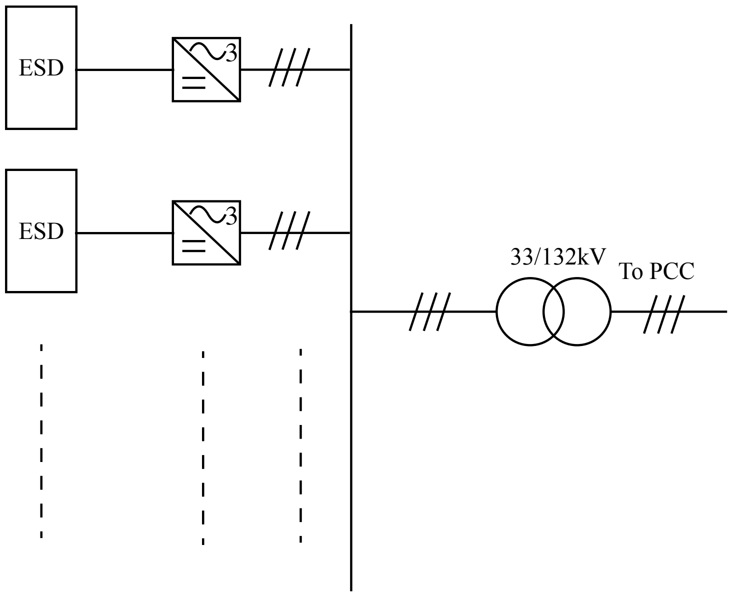

Figure 5-3 A simplified diagram of energy storage system

5.3.3.3 Control Strategy

There are 17 modes of energy storage control strategy with the aim of reducing the electricity cost as seen in Figure 5-4. Amount of power generated from renewable energy i.e., solar PV farm, power profile, electricity price (peak or off-peak time) and SOC define how energy storage will work in each mode. It should be noted that peak and off-peak time are classified based on electricity price.

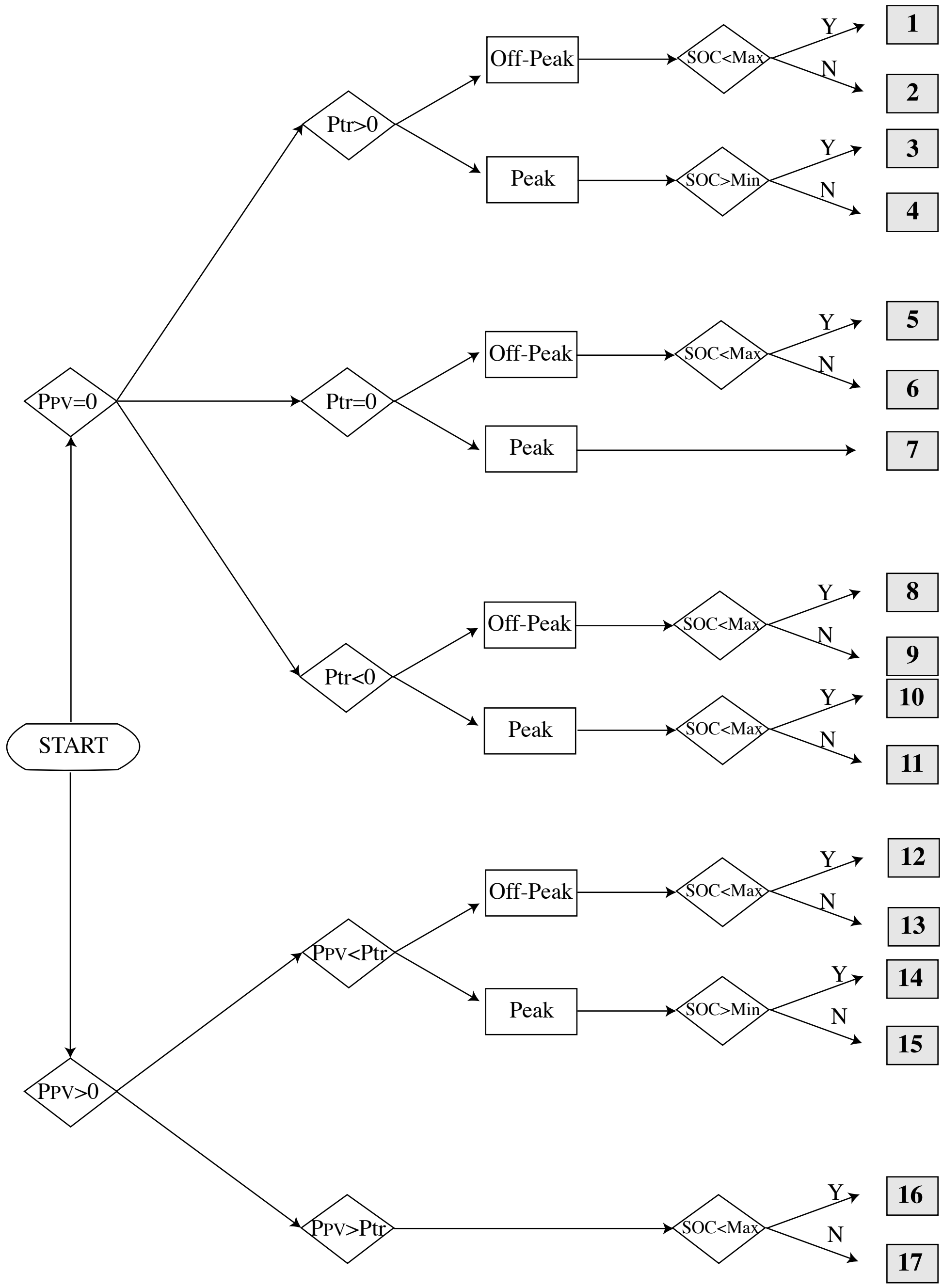

Figure 5-4 Control strategy of the energy storage system

- Mode 1

  Traction substation requires power and no power is produced from renewable. Moreover, it is in the off-peak period when the electricity price is low. Therefore, the demand is met by grid supply and the ESS is charged at the same time.

- Mode 2

  Whereas the grid supplies the demand from the traction substation, it will not charge the ESS as the SOC level is at the upper limit.
- Mode 3

  As it is in peak time and the state of charge of the energy storage is greater than the lower limit, the energy storage supplies energy to the train.
- Mode 4

  The ESS is unable to supply the demand due to low stored energy. Thus, the grid will supply the demand instead.
- Mode 5

  No power demand is required. Thus, the ESS is charged during this off-peak period as it does not reach the upper limit of the SOC.
- Mode 6

  This is similar to mode 5. Nonetheless, as the ESS is fully charged, it stays idle.
- Mode 7

  Regardless of the SOC level, the ESS is in an idle state. The price of electricity in this peak time prevents it from absorbing energy from the grid.
- Mode 8

  There is reverse power flow from the traction substation. The ESS will capture this power. Moreover, as it is in the off-peak time, the ESS will be charged at its rated power.
- Mode 9

  Because the ESS is fully charged, it will not be able to capture the reverse power and will stay idle.
- Mode 10

  The ESS is charged by the reverse power from the traction substation without support from the grid as the electricity price is high.
- Mode 11

  The whole reverse power flows to the grid as the ESS is full.
- Mode 12

Part of the demand is supplied by the grid while power generated from the PV farm is insufficient to support the train power demand. Furthermore, the ESS is also charged by the grid during this low electricity price.

- Mode 13

  The situation is similar to the previous mode, but the ESS is in an idle state.
- Mode 14

  To reduce the amount of energy buying from the grid, part of the demand is supplied by the ESS while power generated from the PV farm is insufficient to support the train power demand.
- Mode 15

  The grid will supply the rest of the demand due to insufficient stored energy in the ESS.
- Mode 16

  An excess power from the PV farm is stored in the ESS. However, part of the energy will flow back to the grid if the peak of the excess power is higher than the rated power of the ESS.
- Mode 17

  Whole excess energy flows to the grid due to fully charged ESS.

The charging and discharging power of the energy storage according to its working mode are provided in Table 5-1. The working states of the energy storage are categorised into three groups as follows:

- Idle – no power is in and out of the energy storage.
- Charging – the energy storage is charged by excess energy and grid power during the off-peak time.
- Discharging – the energy discharges power according to the mode. For mode 3, the energy storage will discharge the magnitude of power at the level of the one with a lower value between P_{tr}^{t} and $P_{ess}^{max,dis}$. A similar condition is applied to mode 14. Equation (5-7) summarises formulas to calculate the stored energy after each mode is operated.

Table 5-1 State of the energy storage and power for each working mode

State	Mode	Power
Idle	2, 4, 6, 7, 9, 13, 15, 17	$P_{ess}^{ch,t} = P_{ess}^{dis,t} = 0$
Charging	1, 5, 12, 8	$P_{ess}^{ch,t} = P_{ess}^{max,ch}$
	10	$P_{ess}^{ch,t} = \lvert P_{tr}^{t} \rvert$
	16	$P_{ess}^{ch,t} = P_{pv}^{t} - P_{tr}^{t}$ or $P_{ess}^{max,ch}$
Discharging	3	$P_{ess}^{dis,t} = \mathrm{Min}[P_{tr}^{t}, P_{ess}^{max,dis}]$
	14	$P_{ess}^{dis,t} = \mathrm{Min}[(P_{tr}^{t} - P_{pv}^{t}), P_{ess}^{max,dis}]$

$$E_{ess}^{t+1} = \begin{cases} E_{ess}^{t} + \dfrac{P_{ess}^{ch,t} \cdot \eta_{ess}^{ch} \cdot \Delta t}{3600}, & \text{charging} \\ E_{ess}^{t}, & \text{idle} \\ E_{ess}^{t} - \dfrac{P_{ess}^{dis,t} \cdot \Delta t}{3600 \cdot \eta_{ess}^{dis}}, & \text{discharging} \end{cases} \quad (5\text{-}7)$$

where:

P_{tr}^{t} is the net power of the load at time t, i.e., the sum of the traction power and regen power [MW];

P_{pv}^{t} is the power generated from the PV farm at time t [MW];

η_{ess}^{ch} is the charging efficiency of the energy storage [p.u.];

η_{ess}^{dis} is the discharging efficiency of the energy storage [p.u.].

5.3.4 Energy Flow Calculation

The power balance equation, which describes the relationship between the power supplied to and consumed by an electrical system, is presented in (5-8). The power supply needs to at least meet the power demand required for trains to operate in traction mode. While the supply is higher than the demand, the excess energy will be absorbed by the energy storage device. Moreover, in case, the energy storage device is fully charged, the excess energy will be sold to the grid by default.

$$P_{traction}^{t} + P_{ess}^{ch,t} + P_{sell}^{t} = P_{regen}^{t} + P_{ess}^{dis,t} + P_{pv}^{t} + P_{buy}^{t} \quad (5\text{-}8)$$

Equation (5-9) shows that the electrical energy from the regenerative braking energy can be consumed by other trains in the same feeding section, charge to the energy storage and sold to the grid. It is worth mentioning that for calculation purposes the regenerative braking energy is prioritised to be consumed by other trains before charging the energy storage and in case of no train in the same section, it will charge the energy storage before flowing to the grid.

$$E_{regen} = E_{regen-train} + E_{regen-ess} + E_{regen-grid} \qquad (5\text{-}9)$$

Similarly, the power generated from the PV farm will be first consumed by the trains. The energy storage will be charged by the excess energy. In some cases, for instance, train is in regenerative mode and the energy storage is full. The grid will accept the PV power. Equation (5-10) presents distribution of the PV energy.

$$E_{pv} = E_{pv-train} + E_{pv-ess} + E_{pv-grid} \qquad (5\text{-}10)$$

There is a wide variety of power sources that can be utilised to charge energy storage systems. In this research, charging power comes from three power sources i.e., regenerative braking energy, PV power and the grid. Thus, total charging energy is the sum of those as seen in (5-11).

$$E_{ess,charge} = E_{regen-ess} + E_{pv-ess} + E_{grid-ess} \qquad (5\text{-}11)$$

While the load gets enough supply, the excess power is sold back to the grid. Furthermore, due to the intermittent nature of renewable energy source, a mismatch between the time of energy demand and supply can occur when there is a disparity between the times when electricity is required and when it is available. If the energy storage is unable to absorb this energy, it will end up being sold to the grid. Equation (5-12) shows that there are two parts of energy that can be sold: regenerative energy and PV energy.

$$E_{sell} = E_{regen-grid} + E_{pv-grid} \qquad (5\text{-}12)$$

The trains can be supplied by four power sources including regenerative power, PV power, discharge power from the energy storage and if these power sources are insufficient, the railway system operator is responsible for procuring the electricity required to operate the trains from the grid, which is commonly derived from fossil fuels and renewable energy. The total energy supplied to the trains is computed according to (5-13).

$$E_{traction} = E_{regen-train} + E_{pv-train} + E_{ess,discharge} + E_{buy} \quad (5\text{-}13)$$

where:

$P^t_{traction}$ is the power required to supply tractive trains [MW];

P^t_{regen} is the regenerative braking power [MW];

P^t_{buy} is the power from the grid to supply the load, which is bought by the railway system operator [MW];

P^t_{sell} is the power sold to the grid [MW];

E_{regen} is the total regenerative braking energy [MWh];

$E_{regen-train}$ is the amount of regenerative braking energy supplied to trains [MWh];

$E_{regen-ess}$ is the amount of regenerative braking energy supplied to energy storage [MWh];

$E_{regen-grid}$ is the amount of regenerative braking energy that flows to the grid [MWh];

E_{pv} is the total solar PV energy [MWh];

$E_{pv-train}$ is the amount of PV energy supplied to trains [MWh];

E_{pv-ess} is the amount of PV energy supplied to energy storage [MWh];

$E_{pv-grid}$ is the amount of PV energy sold to the grid [MWh];

$E_{ess,charge}$ is the amount of energy charged to the energy storage [MWh];

$E_{ess,discharge}$ is the amount of energy discharged from the energy storage [MWh];

$E_{grid-ess}$ is the amount of energy from the grid charged to the energy storage [MWh];

E_{buy} is the total energy bought from the grid [MWh];

E_{sell} is the total energy sold to the grid [MWh];

E_{sell} is the total energy sold to the grid [MWh];

$E_{traction}$ is the total energy consumed by the load [MWh].

5.4 Case Study

5.4.1 Route Profiles

The double-track railway route between London and Birmingham from the High Speed 2 (HS-2) project is taken as a case study. The MATLAB-based single-train simulator is used to acquire the single-train power profile. There are three grid supply points (GSPs) where the voltage from the national grid is stepped down from 400 kV to 132 kV before entering the traction substation (TS). Afterwards, the traction substation will lower the voltage to 25 kV to supply two feeding sections on the left and right sides. Overall, the electrified trains in this route are fed by six feeding sections as seen in Figure 5-5. With the train station locations and the speed limits in Table 5-2, the train power profile and speed profile are generated. Figure 5-6 illustrates the single-train power profile and speed profile for a train departing from London to Birmingham and vice versa.

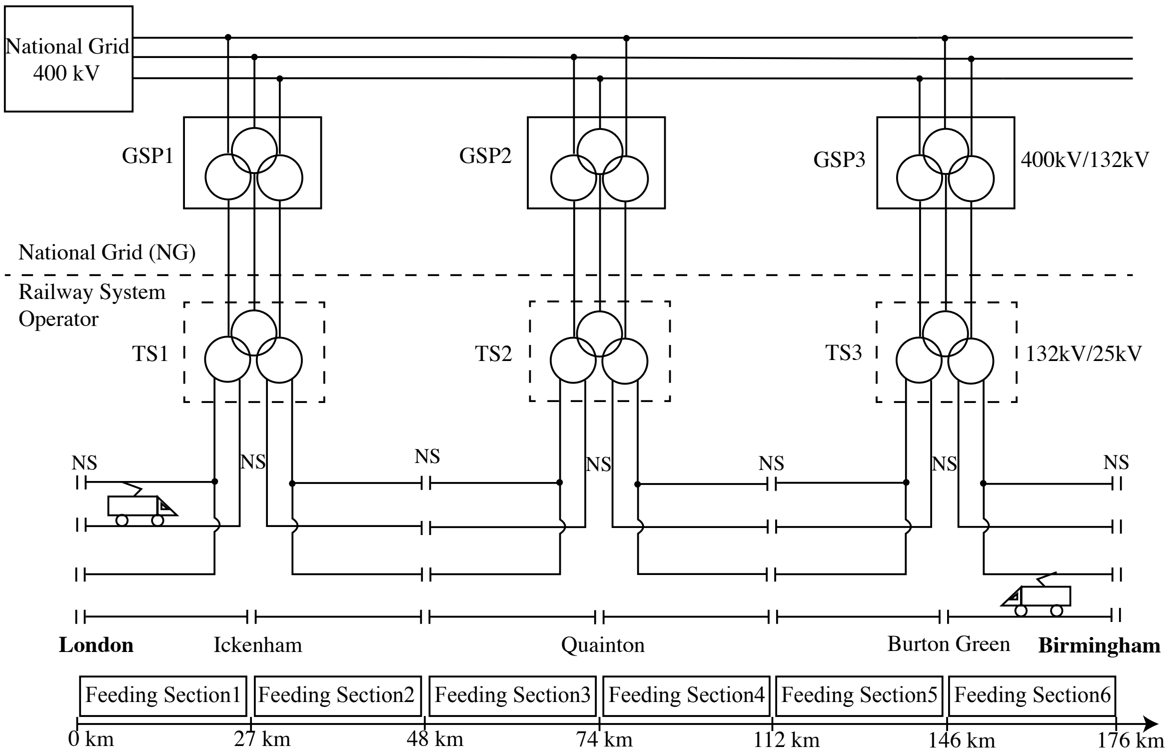

Figure 5-5 HS-2 railway route between London and Birmingham

Table 5-2 Train station and maximum speed information [75]

Stations	Location (km)	Max speed (km/h)
Euston	0	230
Old Oak Common	9.5	360
Birmingham Interchange	156.7	230
Birmingham Curzon Street	176	0

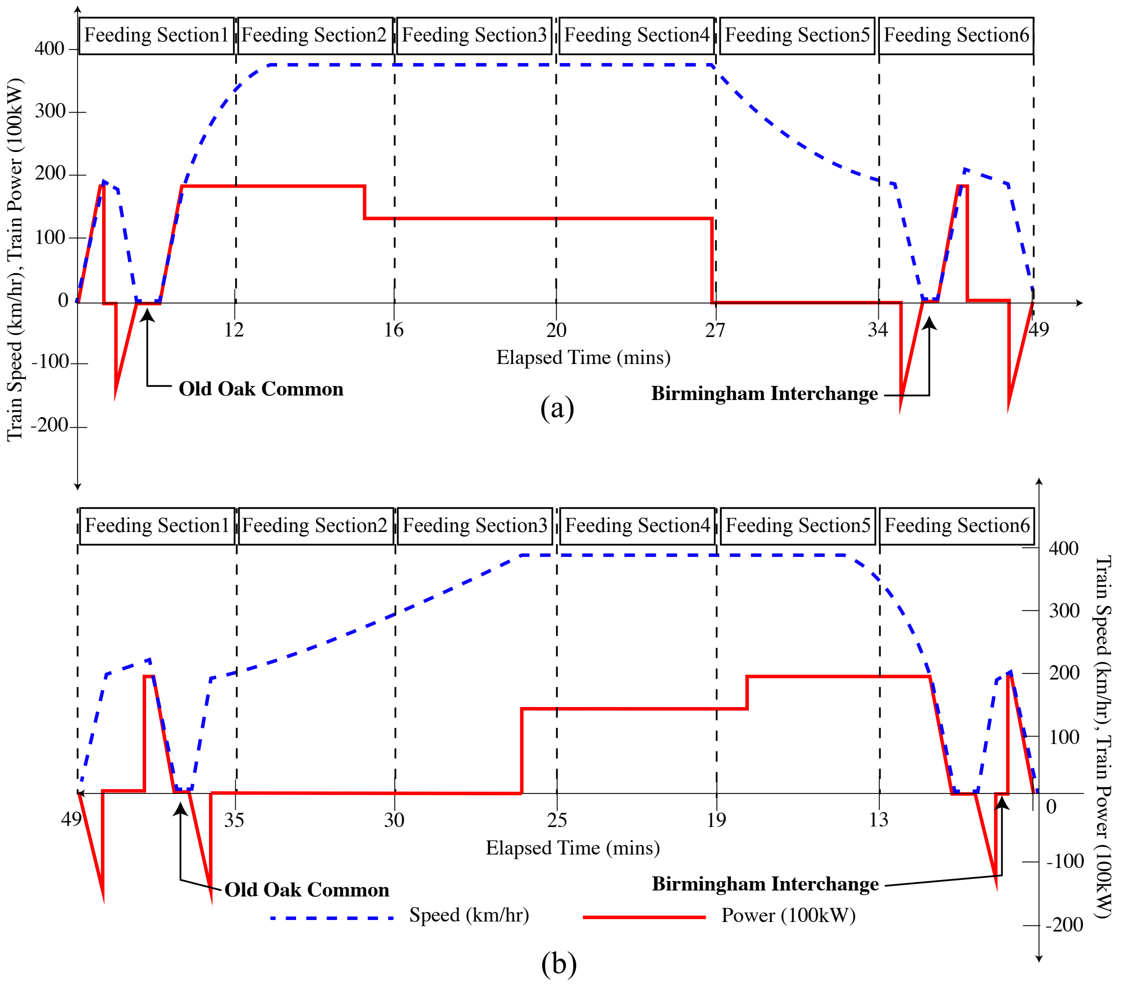

Figure 5-6 Train speed profile and power profile a) London to Birmingham and b) Birmingham to London

5.4.2 Train operation data and power profiles

In order to obtain a multiple-train power profile, the train service timetable is provided in Table 5-3. There are four trains running per hour during peak time operation and three trains during off-peak time operation. The train power profile of the train travelling in the feeding section 1 and feeding section 2 from around 5 AM to 9 AM is illustrated in Figure 5-7. It can be seen from the red line that the trains are braking, and regenerative braking power is observed in feeding section 1 while no regenerative energy is seen in feeding section 2. It is worth mentioning that the regenerative energy seen in each plot is the residual power after being consumed by other trains in the same feeding section. The net power of both feeding sections is displayed as a black line. At 6 AM, the regen power from feeding section 1 supplies the train on another side. The remaining regenerative energy is either charging the energy storage or sold to the grid or both cases.

Table 5-3 HS2 train service timetable [76]

First train departs	05:00
Last train departs	23:00
Peak time	06:00 to 09:00 and 16:00 to 19:00
Headway for off-peak time	20 minutes
Headway for peak time	15 minutes

Figure 5-8 presents the power profile of trains in feeding sections 3 and 4, which is supplied by traction substation 2 (GSP2). It is clearly seen that the trains on both sides consumed positive power, and no regenerative energy was produced. The train power profile of the feeding sections 5 and 6 is shown in Figure 5-9. As the trains terminate and start the journey at this station (and the first station), the power profile is similar to Figure 5-7. All train power profiles are input into the Simulink model to determine the energy flow in other parts of the system.

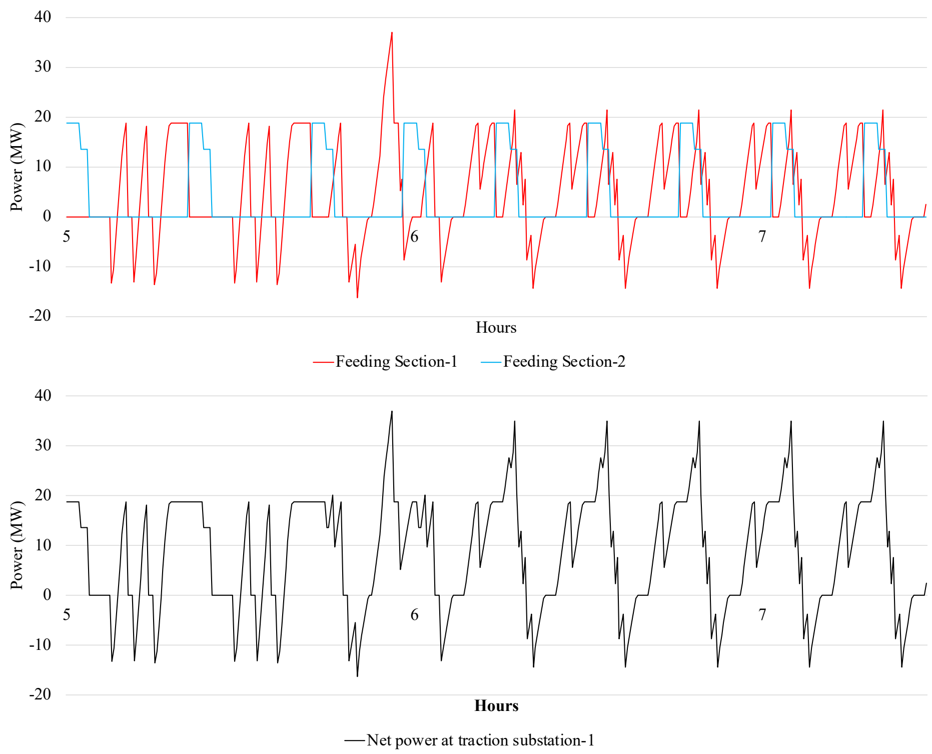

Figure 5-7 Power profile of trains travel in feeding section 1 and 2 and net power demand at traction substation 1.

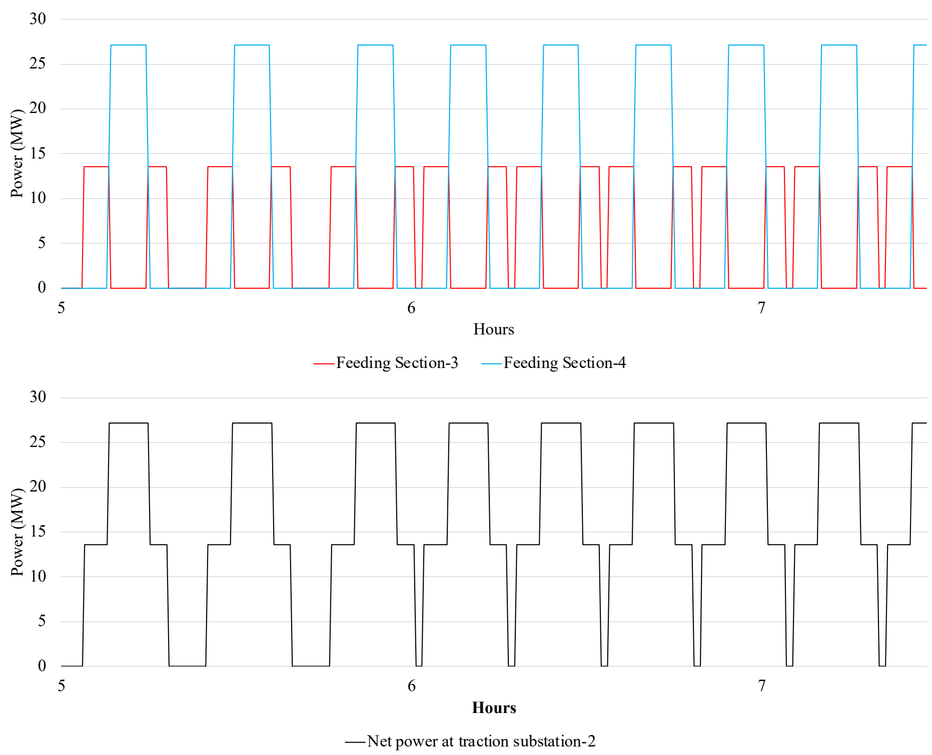

Figure 5-8 Power profile of trains travel in feeding section 3 and 4 and net power demand at traction substation 2.

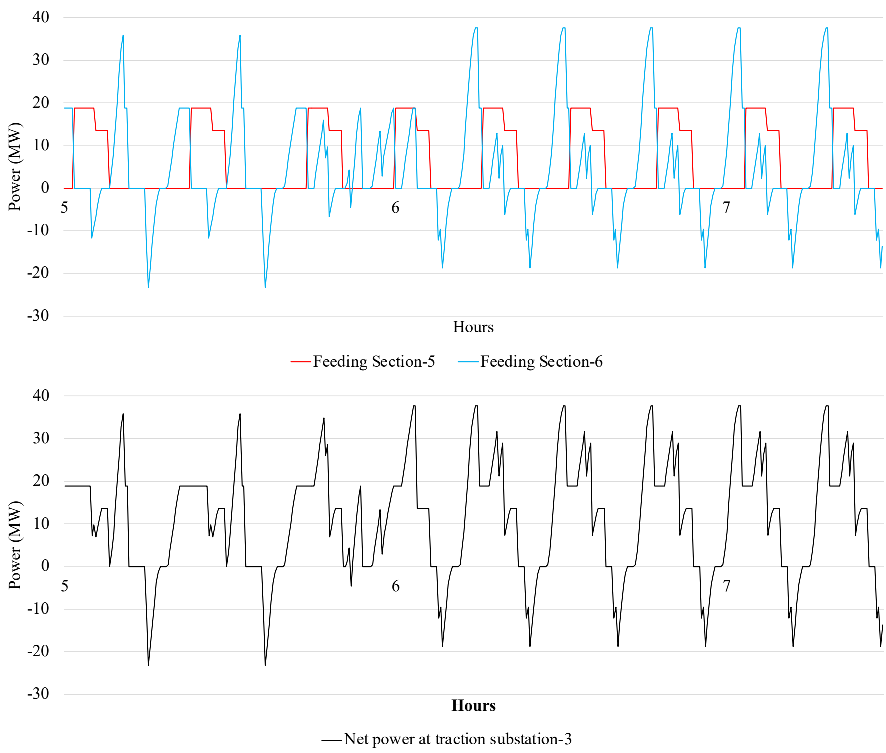

Figure 5-9 Power profile of trains travel in feeding section 5 and 6 and net power demand at traction substation 3.

5.4.3 Feeding Scheme Data

In order to realise the benefits of renewable energy sources and energy storage, the model is separated into four schemes, as illustrated in Figure 5-10.

- Scheme A (Figure 5-10(a)) – this scheme is considered a benchmark scheme. The power demand is met by the power from the utility grid. The residual regenerative energy is sold to the grid.
- Scheme B (Figure 5-10(b)) – the energy storage is added to the system to absorb the regenerative energy and the grid energy during the off-peak period. The load is supplied by the grid, and power is discharged from the energy storage.
- Scheme C (Figure 5-10(c)) – the solar PV farm is connected to the three-phase power network on the railway side to act as a secondary energy source. The excess power from both PV and regenerative braking is fed to the grid.
- Scheme D (Figure 5-10(d)) – this is the proposed scheme in which the PV farm and the ESS are integrated.

It should be noted that all three GSPs are applied with identical parameters according to which scheme being used. For instance, in scheme D, the same PV farm and ESS model and parameters are used for GSP1, GSP2 and GSP3.

The solar irradiance of the three locations in the UK according to the grid supply point location from [77] is adopted. The hourly basis solar irradiance data of every single day for five years based on the location of each GSP is processed to obtain average data by month. Figure 5-11 shows sun irradiance data used for GSP1 according to the real location at Ickenham. Parameters of other components including transformers, inverters, PV farms, energy storage, electricity costs etc., are listed in Table 5-4.

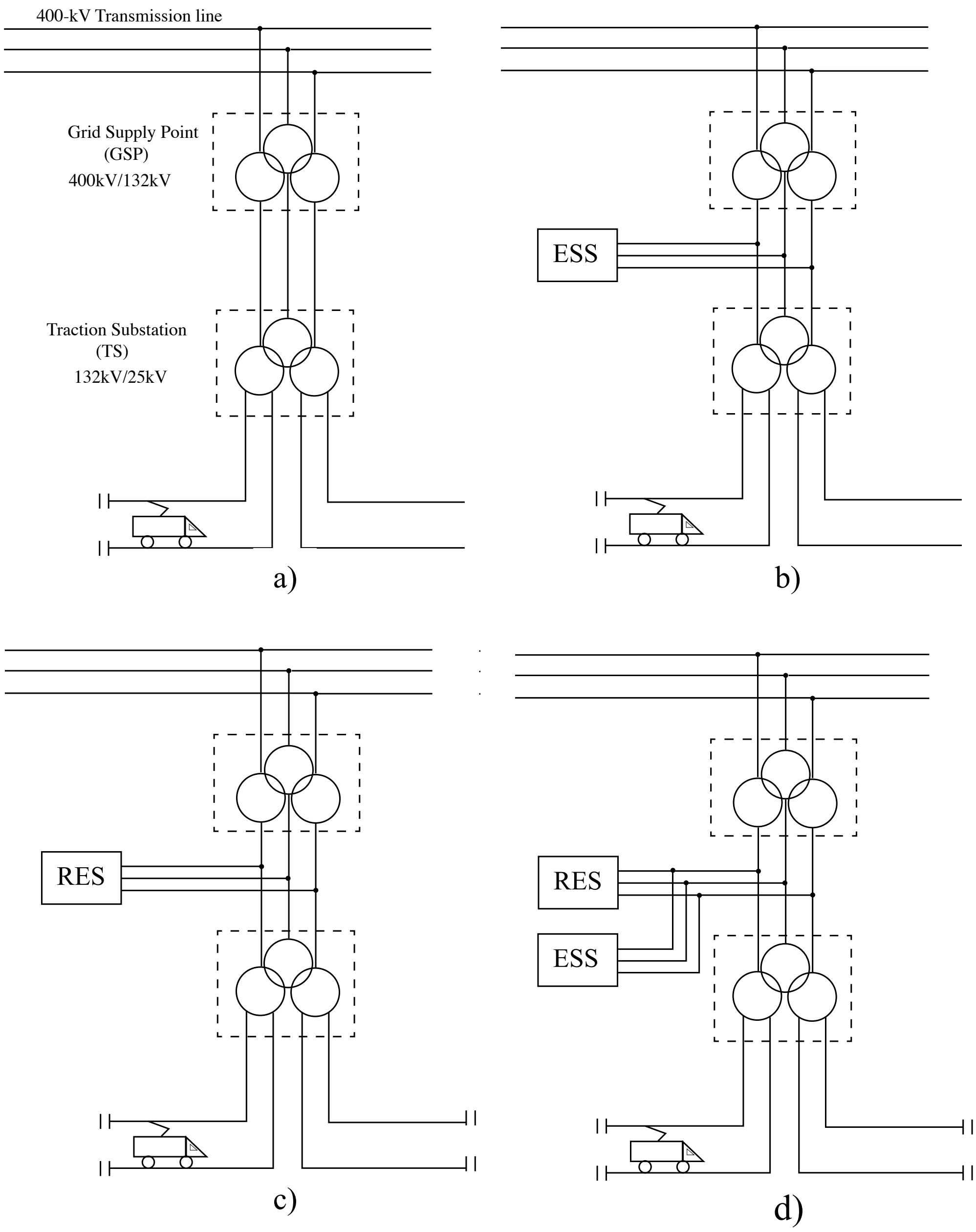

Figure 5-10 schemes used for comparison purposes: a) benchmark, b) with ESS, c) with PV integration and d) with both ESS and PV integration.

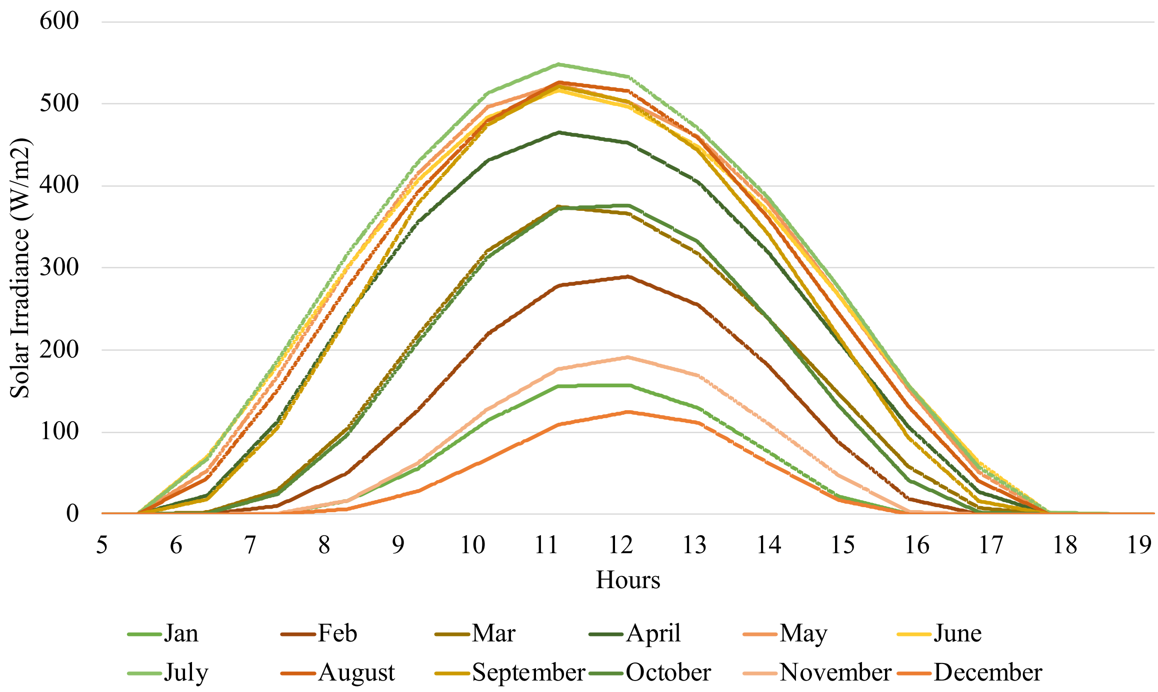

Figure 5-11 Monthly average solar irradiance from the location of GSP1 (Ickenham)

Table 5-4 Parameters for simulation of each grid supply point

Transformer at grid supply points	80 MVA, 400kV/132kV
Transformer at traction substations	40MVA x2, 132kV/25kV
Transformer in PV farm and ESS	40 MVA, 33kV/132kV
Solar PV farm	40 MW (2 MW x 20), 1100 VDC output
Energy Storage System	10 MW, 40 MWh
PV inverter and Bi-directional converter	2 MVA x 20, with 98.6% max, efficiency
Carbon intensity index and carbon tax	Average: 30.8 g per kWh and carbon emissions tax : £18 per ton
Peak time	From 08:00 to 16:00 / electricity price: £140 per MWh
Off-peak time	From 00:00 to 08:00 and 16:00 to 24:00/ electricity price: £70 per MWh
State of Charge	Lower limit: 10%, Upper limit:90%, Initial SOC:10%

5.4.4 Result and discussions

5.4.4.1 Electricity Cost

5.4.4.1.1 GSP1

Table 5-5 displays the energy flow from and to the grid in a year of operation. For schemes with the integration of the PV farm, as a result from the simulation only presents the consumption of the energy for one day; it is then multiplied by the number of days in each month to obtain the total amount of energy in one year. Scheme A, which is considered a benchmark scheme, purchased approximately 64 GWh and sold the energy from the regenerative braking energy of 8.9 GWh to the grid. It should be noted that the selling price is identical to the buying price. The energy storage device decreased the energy bought from the grid and carbon emissions slightly in scheme B as regenerative energy was reused. Moreover, a reduction of around 56 per cent in purchasing power during the peak time compared to Scheme A is observed while there is an increase of around 27 per cent during the off-peak time. Conversely, the amount of energy sold to the grid is reduced by half as a result of installing energy storage device.

With the integration of the PV farm in scheme C, the total purchase of energy is 27 per cent less than in scheme A, with a huge increase in the amount of energy sold to the grid at 190 per cent. The percentage of buying energy from the grid further declined to 36 per cent in scheme D because of the ESS. Nevertheless, as some excess power from the solar farm was stored in the ESS, the amount of energy sold to the grid is less than scheme C. Furthermore, the results reveal that a reduction of carbon emissions is clearly seen with the integration of solar PV farm with around 27 to 36 per cent relative to the benchmark scheme.

Table 5-5 Energy flow and carbon emissions in one year measured at GSP1

		Amount of Energy (MWh)-GSP1			
		Scheme A	Scheme B	Scheme C	Scheme D
From Grid	Peak time	26416	11676 [-55.8%]	10782 [-59.2%]	2971 [-88.8%]
	Off-Peak	37826	48086 [27.2%]	35760 [-5.5%]	37879 [0.1%]
	Total	64241	59761 [-7%]	46542 [-27%]	40850 [-36%]
To Grid	Peak time	3867	380 [-90%]	19772 [411%]	14084 [264%]
	Off-Peak	5081	3670 [-27.8%]	6225 [22.5%]	5813 [14.4%]
	Total	8948	4050 [-54.7%]	25997 [190%]	19898 [122%]
Carbon emissions (tonnes)		1979	1841 [-7%]	1433 [-27%]	1258 [-36%]

Annual electricity cost and revenue from selling energy are presented in Figure 5-12 and Figure 5-13, respectively. Even though scheme B purchased more energy during the off-peak time than scheme A and sold less, the net electricity cost is around 14 per cent lower which results from the integration of the energy storage system. A similar trend to the amount of energy in the above table, the net electricity cost is significantly reduced in schemes C and D. The benefit of the ESS is seen in scheme D as a 2 per cent reduction in the net cost compared to scheme C. It should be noted that the carbon tax is considered in net cost.

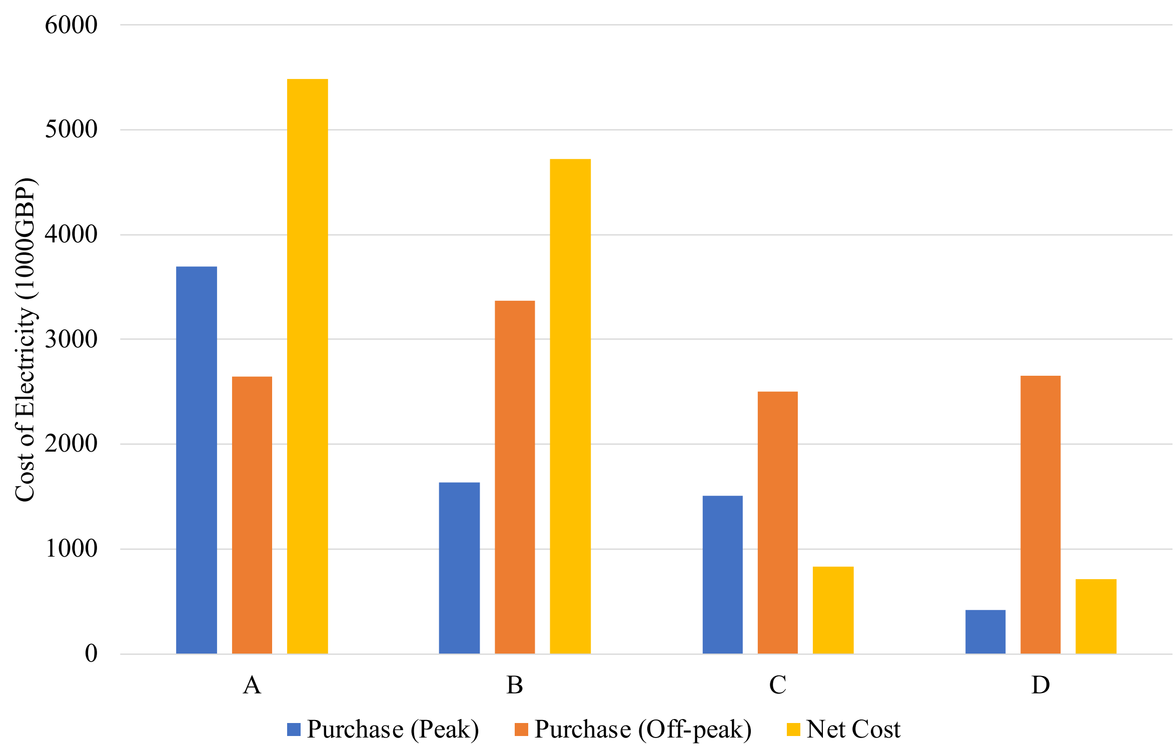

Figure 5-12 Annual electricity cost from purchasing energy from the grid at GSP1

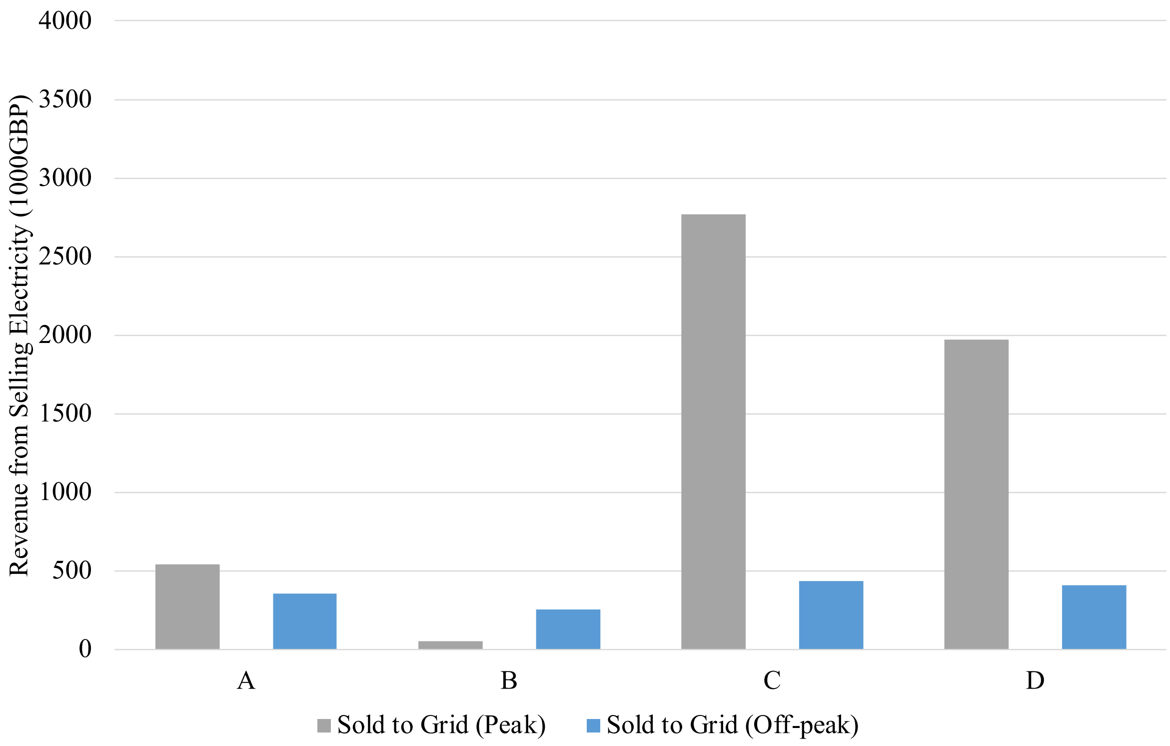

Figure 5-13 Annual electricity revenue from selling energy to the grid at GSP1

5.4.4.1.2 GSP2

This grid supply point steps down the voltage from the national grid and then supplies it to the traction substation 2. It can be seen from the train power profile that the trains travelled in feeding sections 3 and 4 which were supplied by traction substation 2 did not regenerate power as there is no station between both feeding sections. Table 5-6 illustrates the amount of energy flow and carbon emissions at GSP2. Overall, scheme D acquired the lowest energy from the grid at 28 per cent lower compared to scheme A which purchased from the grid the most. It can be noticed that no energy was sold to the grid in schemes A and B. There is a 0.4 per cent rise in purchasing energy from the grid in scheme B because the ESS was charged on the first day of operation from 10% SOC to 90% SOC. In contrast, there is a drop of 22 per cent in scheme C as a benefit of a solar PV farm. Further decrease is seen by scheme D as a result of the ESS. The amount of carbon emissions is proportional to the amount of energy bought from the grid.

In terms of electricity cost and revenue (Figure 5-14 and Figure 5-15), scheme A spent the most and no revenue was made. Even though scheme B required slightly more energy from the grid than scheme A, it spent less money. This was due to the ESS. Total electricity cost dropped significantly in scheme C and the most revenue was made by selling the excess energy during peak time. Besides, with the ESS, a fall in energy bought during the peak time was observed in scheme D. This made scheme D the least expenditure.

Table 5-6 Energy flow and carbon emissions in one year measured at GSP2.

		Amount of Energy (MWh)-GSP2			
		Scheme A	Scheme B	Scheme C	Scheme D
From Grid	Peak time	43773	32492 [-25.8%]	22958 [-47.6%]	10398 [-76.2%]
	Off-Peak	62412	74121 [18.8%]	59694 [-4.4%]	65912 [5.6%]
	Total	106185	106613 [0.4%]	82652 [-22%]	76310 [-28%]
To Grid	Peak time	0	0	9623	2959
	Off-Peak	0	0	350	252
	Total	0	0	9972	3211
Carbon emissions (tonnes)		3270	3284 [0.4%]	2546 [-22%]	2350 [-28%]

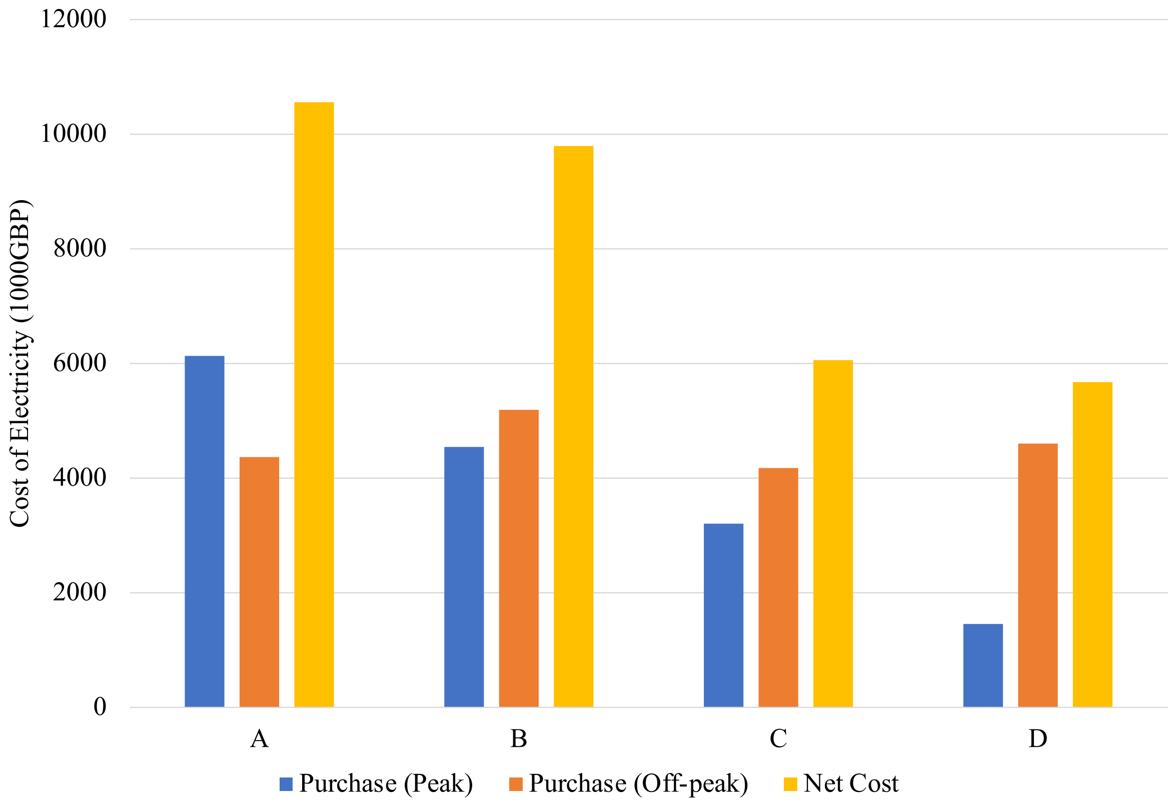

Figure 5-14 Annual electricity cost from purchasing energy from the grid at GSP2

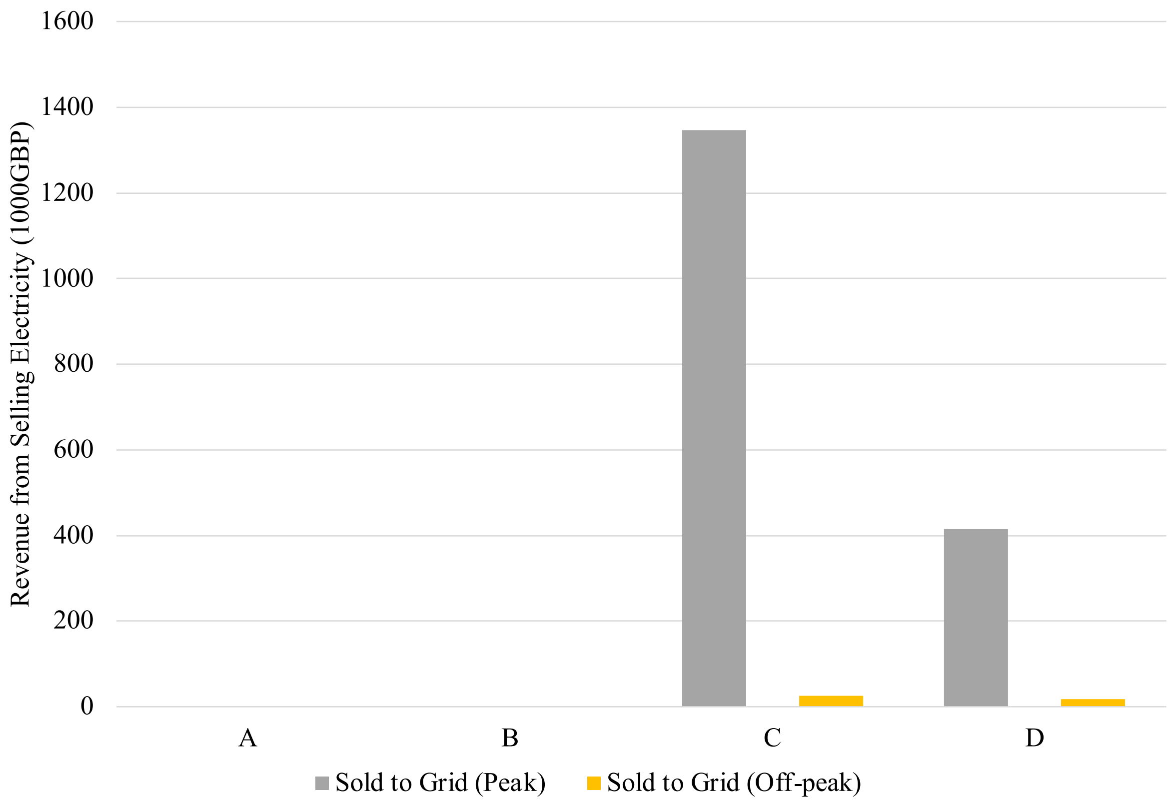

Figure 5-15 Annual electricity revenue from selling energy to the grid at GSP2

5.4.4.1.3 GSP3

A similar trend with the result from GSP1 is observed in this GSP. As a whole, scheme A bought energy from the grid the most, followed by schemes B and C while scheme D purchased the least. The amount of Carbon emissions is also in the same order as tabulated in Table 5-7. In terms of net electricity cost, with the ESS in scheme B, nearly half of the electricity cost was reduced in peak time as opposed to scheme A. Although, purchase during the off-peak time was high, the net cost was dominated by cost at the peak time and enabled the net electricity cost of scheme B is lower as seen in Figure 5-16. Furthermore, with the integration of solar PV farms, net electricity costs in schemes C and D went down by half of scheme B. This reduction also resulted from selling excess energy to the grid as shown in Figure 5-17.

Table 5-7 Energy flow and carbon emissions in one year measured at GSP3

		Amount of Energy (MWh)-GSP3			
		Scheme A	Scheme B	Scheme C	Scheme D
From Grid	Peak time	32281	18425 [-43%]	15485 [-52%]	5566 [-83%]
	Off-Peak	45527	55904 [22.8%]	43629 [-4.2%]	47357 [4%]
	Total	77808	74329 [-4.5%]	59114 [-24%]	52923 [-32%]
To Grid	Peak time	3657	1088 [-70%]	16058 [339%]	10045 [174%]
	Off-Peak	4853	3523 [-27.4%]	5889 [21.3%]	5298 [9.2%]
	Total	8510	4611 [-46%]	21948 [158%]	15343 [80%]
Carbon emissions (tonnes)		2396	2289 [-4.5%]	1821 [-24%]	1630 [-32%]

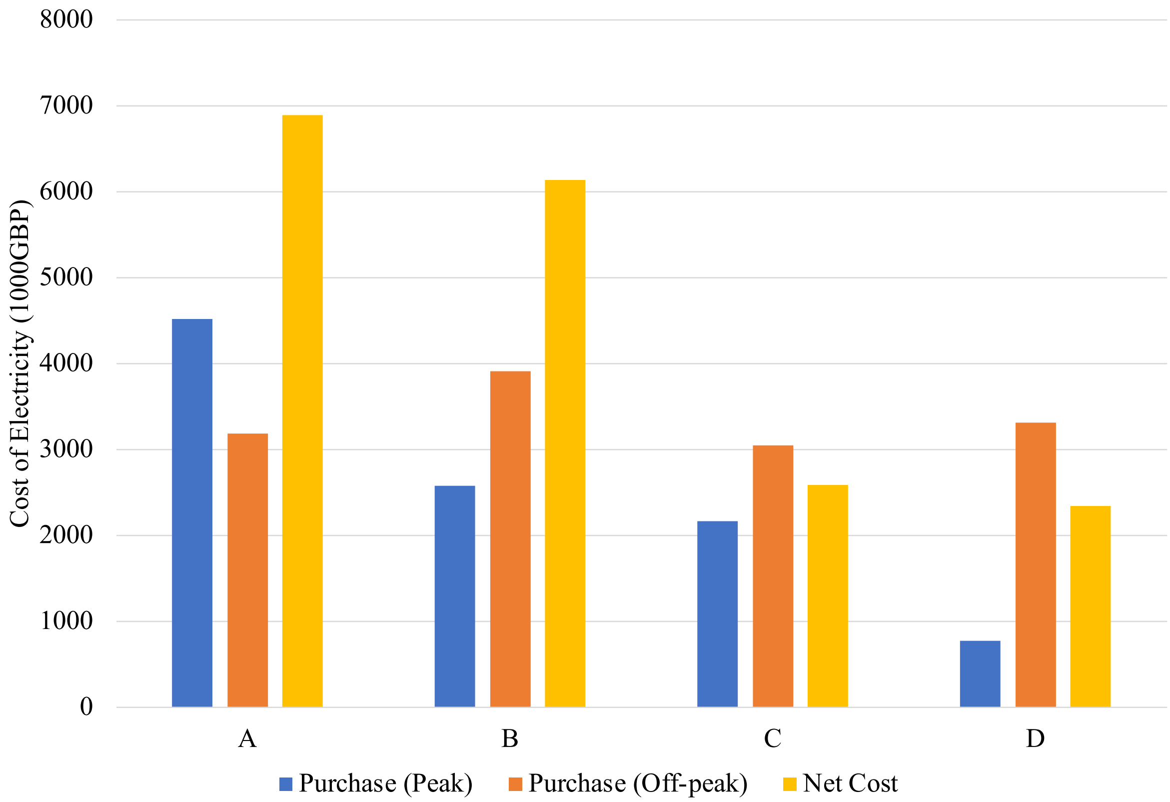

Figure 5-16 Annual electricity cost from purchasing energy from the grid at GSP3

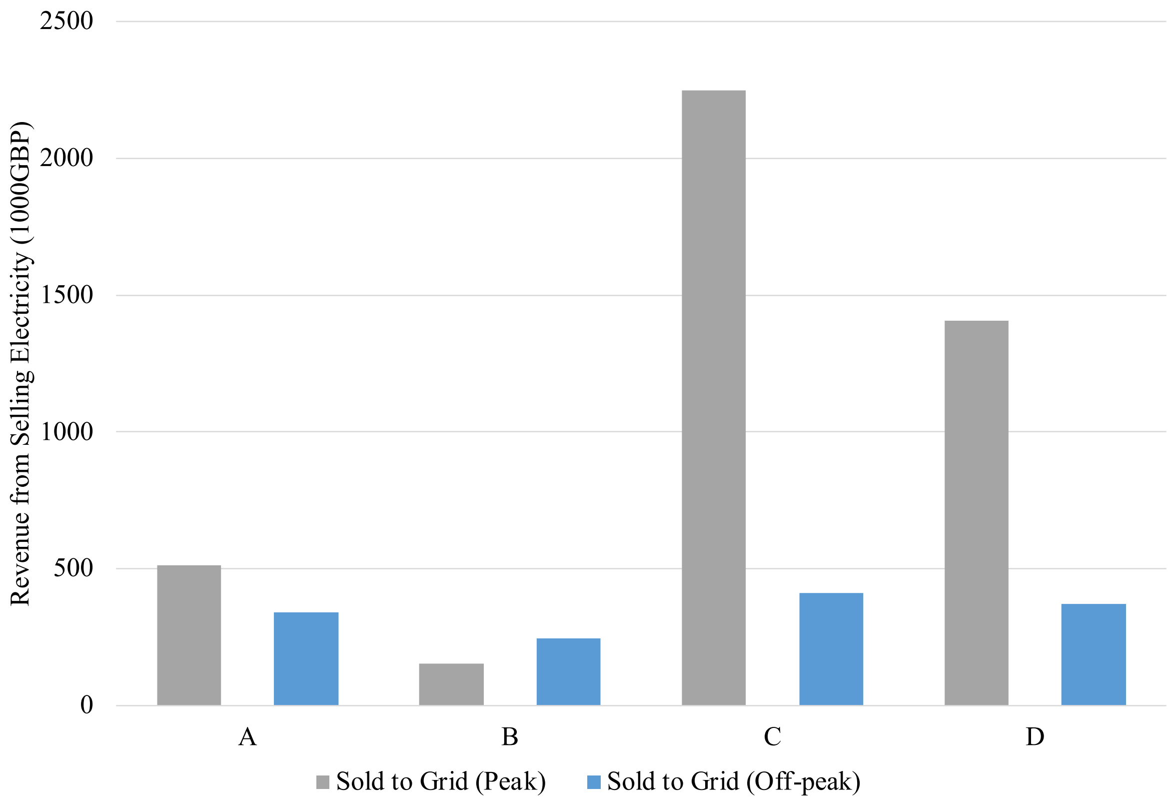

Figure 5-17 Annual electricity revenue from selling energy to the grid at GSP3

5.4.4.2 Regenerative Braking Energy Distribution

The results of the flow of regenerative braking energy from the simulation for each scheme are displayed in Table 5-8. For the GSP1, 40 per cent of the regen is consumed by the trains, and the excess regen of 60 per cent is fed to the grid in scheme A. With the integration of the ESS in scheme B, 24 per cent of the regen is stored in the ESS, and about a third goes to the grid. The integration of the PV farm alone does not change the flow of the regen in scheme C, thus the proportion of the regen flow is the same as in scheme A. Due to variations in solar irradiance, the flow pattern of energy from each source is also varied. Therefore, in scheme D, in which both the ESS and PV farm are included, the amount of energy distribution is represented as an average value. It has been found that the percentage of the regen that flows to the ESS in scheme D is considerably lower than in scheme B or around 8 per cent less. This happens because the ESS is fully charged by the PV power. Thus, it could not capture the regen afterwards. Similarly, the explanation from the GSP1 can be applied to describe the result from the GSP3. It should be noted that no regenerative energy exists in GSP2.

Table 5-8 Regenerative braking energy distribution

Grid Supply Points	Schemes	Regenerative energy Distribution (MWh)			Total (MWh)
		To Trains	To ESS	To Grid	
GSP1	Scheme A	16.82 [40%]	0	25.14 [60%]	41.96
	Scheme B	16.82 [40%]	10.13 [24%]	15 [36%]	41.96
	Scheme C	16.82 [40%]	0	25.14 [60%]	41.96
	Scheme D	16.82 [40%]	6.86 [16%]	18.28 [44%]	41.96
GSP3	Scheme A	6.16 [21%]	0	23.79 [79%]	29.95
	Scheme B	6.16 [21%]	9.03 [30%]	14.75 [49%]	29.95
	Scheme C	6.16 [21%]	0	23.79 [79%]	29.95
	Scheme D	6.16 [21%]	8.62 [29%]	15.17 [50%]	29.95

5.4.4.3 Solar PV Energy Distribution

When it comes to PV power distribution, the comparison between schemes C and D are made and shown in Figure 5-18. The amount of energy generated from PV farms in 24 hours with different solar irradiance profiles from 12 months for GSP1 is plotted. In scheme C, the PV power flows to the traction substation to supply the train load, and the remaining energy is sold to the grid. On the other hand, in scheme D, the excess energy from the PV farm has an additional route which is to be stored in the ESS, as can be observed by the orange bar in the figure. The amount of PV energy stored in the ESS is inversely proportional to the amount of energy produced by the PV farm. This is clearly seen between May and August. The reason behind this situation is that the ESS is fully charged due to too much excess power. Also, it means that the benefits of the ESS are smaller compared to when the PV farm generates less power. It is worth noting that the results from GSP2 and GSP3 give a similar trend and are not presented here.

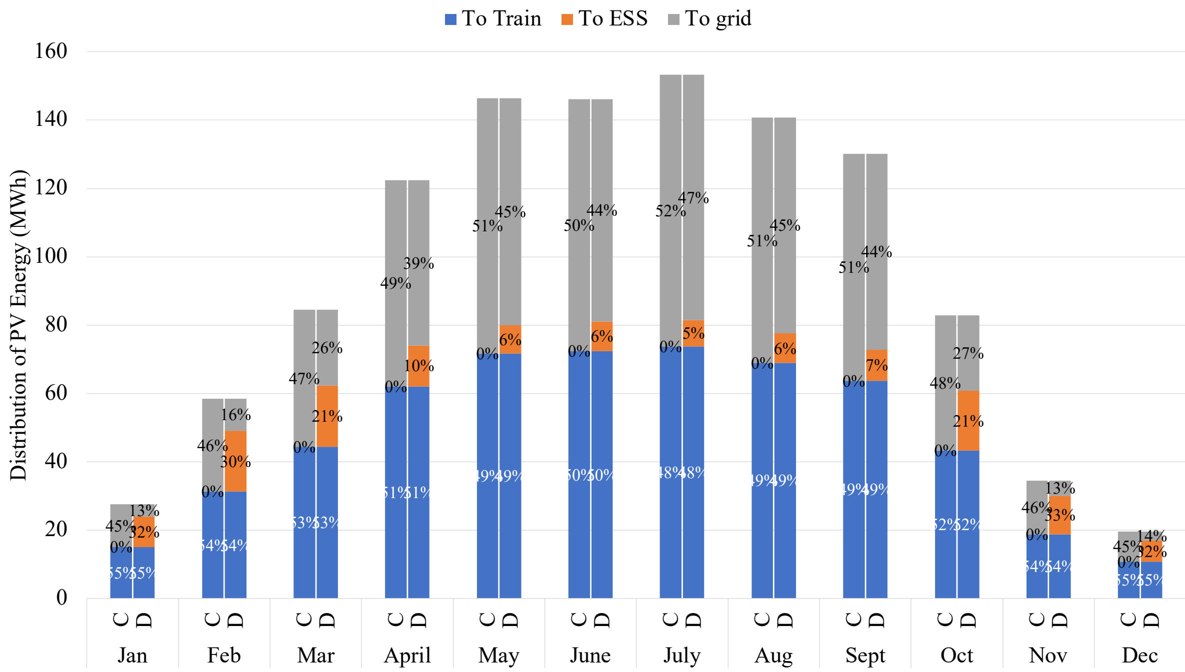

Figure 5-18 Distribution of energy generated from the PV farm in schemes C and D at GSP1

5.4.4.4 Energy Storage Charge and Discharge

In this chapter, the goal of energy storage is to capture the regenerative braking energy and supply the load during the peak period. Moreover, it absorbs the power from the grid at the off-peak time. The profile of the SOCs of ESS in scheme B of GSP1 is presented in Figure 5-19(a). The initial SOC of each ESS is set to 10 per cent and the simulation started at 00:00. On day 1 of the operation, the ESSs started to absorb the energy during the off-peak until reaching the upper limit at 90 per cent. Then, at 08:00 when the peak time of electricity price begins, the ESS started to release energy to supply traction load until it reached 10 per cent of SOC at around 16:00. From 09:00 to 16:00, it was charged by regenerative energy and then discharged when there was demand. After 16:00, it started charging again until 90 per cent and kept this energy level until the end of the day. Therefore, the SOC on the next day will be started at 90% and it will keep the same pattern for other days. The power profile of the ESS is provided in Figure 5-19(b) where the negative power presents charging power and the positive power presents discharging power. While power required from the grid is reduced during the peak time of electricity price, the grid supplied more power during the off-peak time mainly to charge the ESS as seen Figure 5-19(c). The total trainload at GSP 1 is shown in Figure 5-19(d).

The total amount of energy flowing in and out of the energy storage in scheme B for all GSPs is illustrated in Figure 5-20. The simulation result reveals that at GSP1 and GSP3, around 80 per cent of the energy charged to the energy storage on the first day came from the grid and the rest was from regenerative energy. This figure is decreased on the second day since there is energy stored from the first day. Due to no regen in GSP2, the grid is only the power source to charge the energy storage. When looking at the total energy charged to the energy storage, it is obvious that GSP2 is lower than others. Overall, there are about 32 MWh difference in energy changed to the ESS between day1 and day2.

In terms of discharge, GSP2 released the least amount of energy to the load as when the energy storage is depleted, it cannot be charged until the off-peak time due to the lack of regenerative braking from the train. Therefore, no energy is left to discharge.

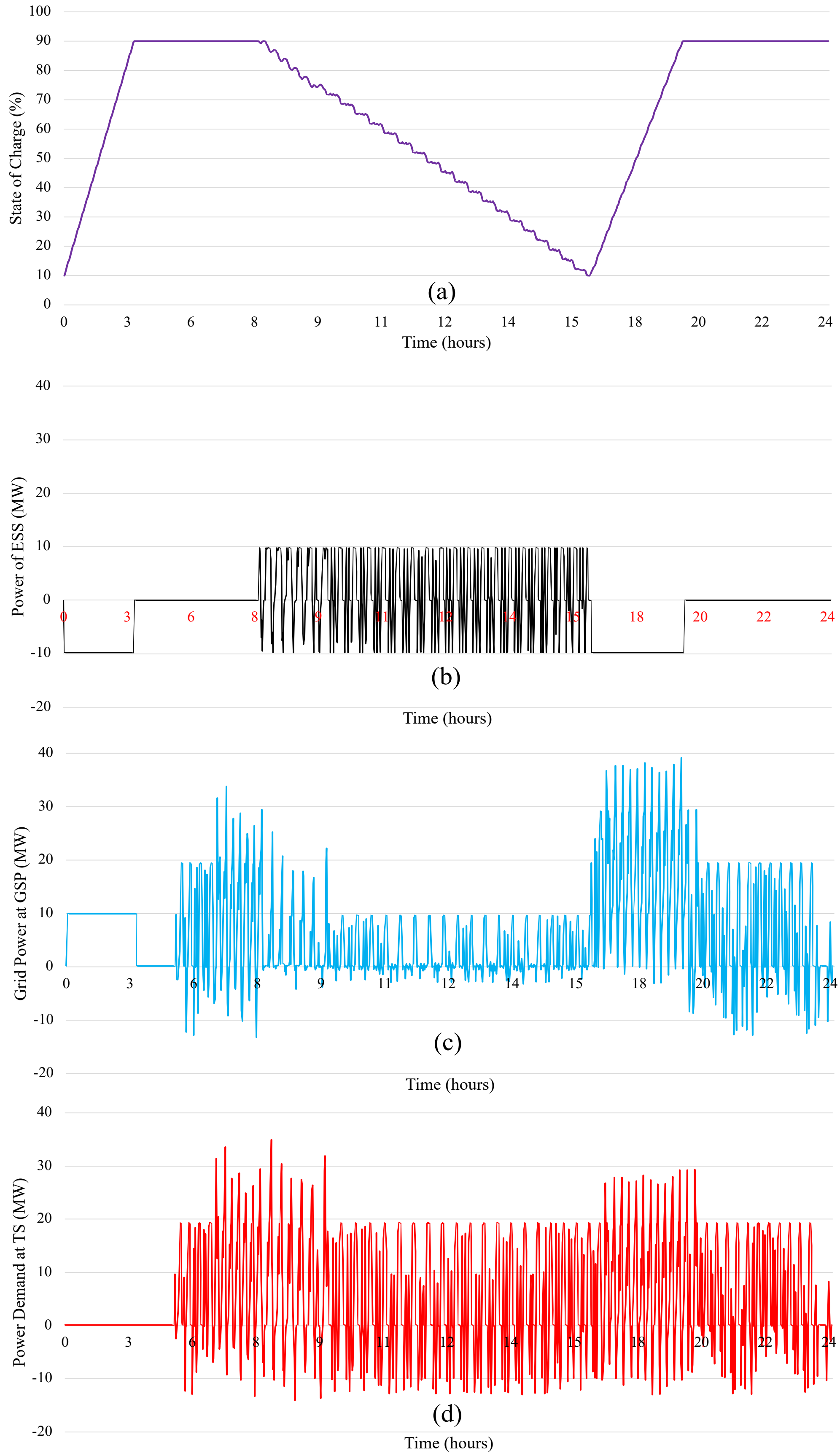

Figure 5-19 a) State of Charge b) Power of ESS c) Grid Power and d) Power demand at TS in scheme B at GSP1

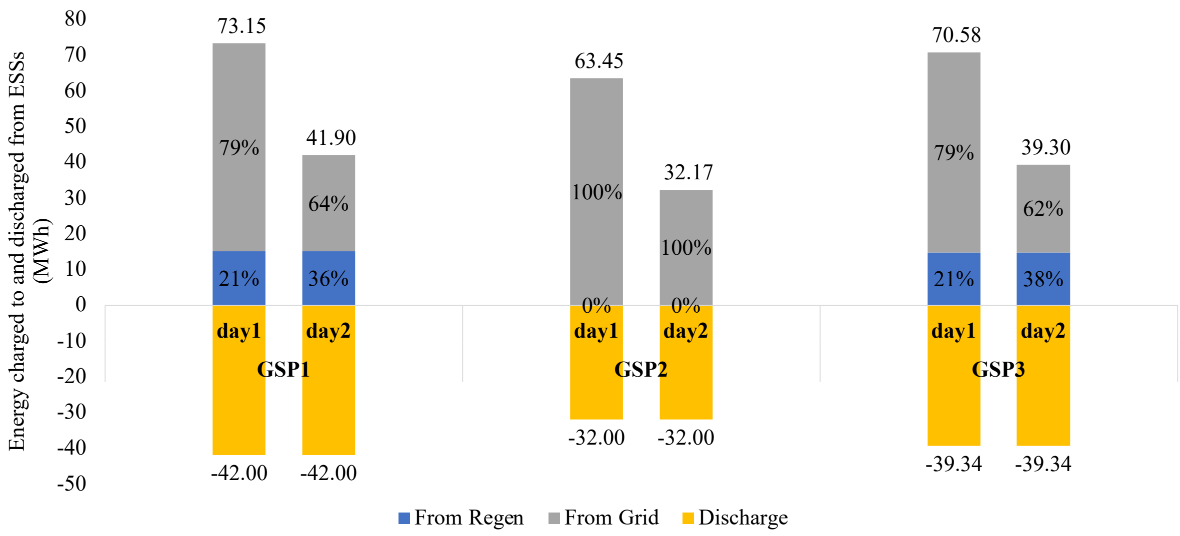

Figure 5-20 Percentage of energy charged to the ESS and amount of energy discharged from the ESS of scheme B

The state of charge results from scheme D with solar irradiance data from January at GSP1 is illustrated in Figure 5-21(a). It can be seen that the SOC profile is more fluctuating than scheme B and it does not reach the lower SOC limit at 10 per cent as the ESS also captured the excess energy from the renewable generation. The power profile of the ESS and the grid are given in Figure 5-21(b) and Figure 5-21(c), respectively. There are two periods that the grid power reached its peak; one is from 06:00 to 08:00 when the train service was busy and the demand was supplied by the grid only as the electricity price is low (off-peak electricity price) and another is between 16:00 and 20:00 when the grid needed to supply the train demand and also charged the ESS. Figure 5-21(d) and Figure 5-21(e) present the train power profile measured at traction substation 1 and PV generation at the PCC.

Figure 5-22 shows the results of the amount of charge and discharge from scheme D. GSP1, and GSP3 give a similar trend with more energy being charged and discharged from the energy storage in months when the power generated from the PV farm is low, i.e., in autumn and winter (Jan to Mar and Oct to Dec). From April to September, when the power from the PV is high, the energy storage is fully charged by the excess power, and it is rarely discharged as well. Thus, it cannot be charged anymore. In contrast, at GSP2, the charge and discharge energy tend to be higher in spring and summer (April to September). Due to the lack of support from regenerative energy, the energy storage is depleted quickly after supplying the load and then it is recharged by the excess power from the PV farm.

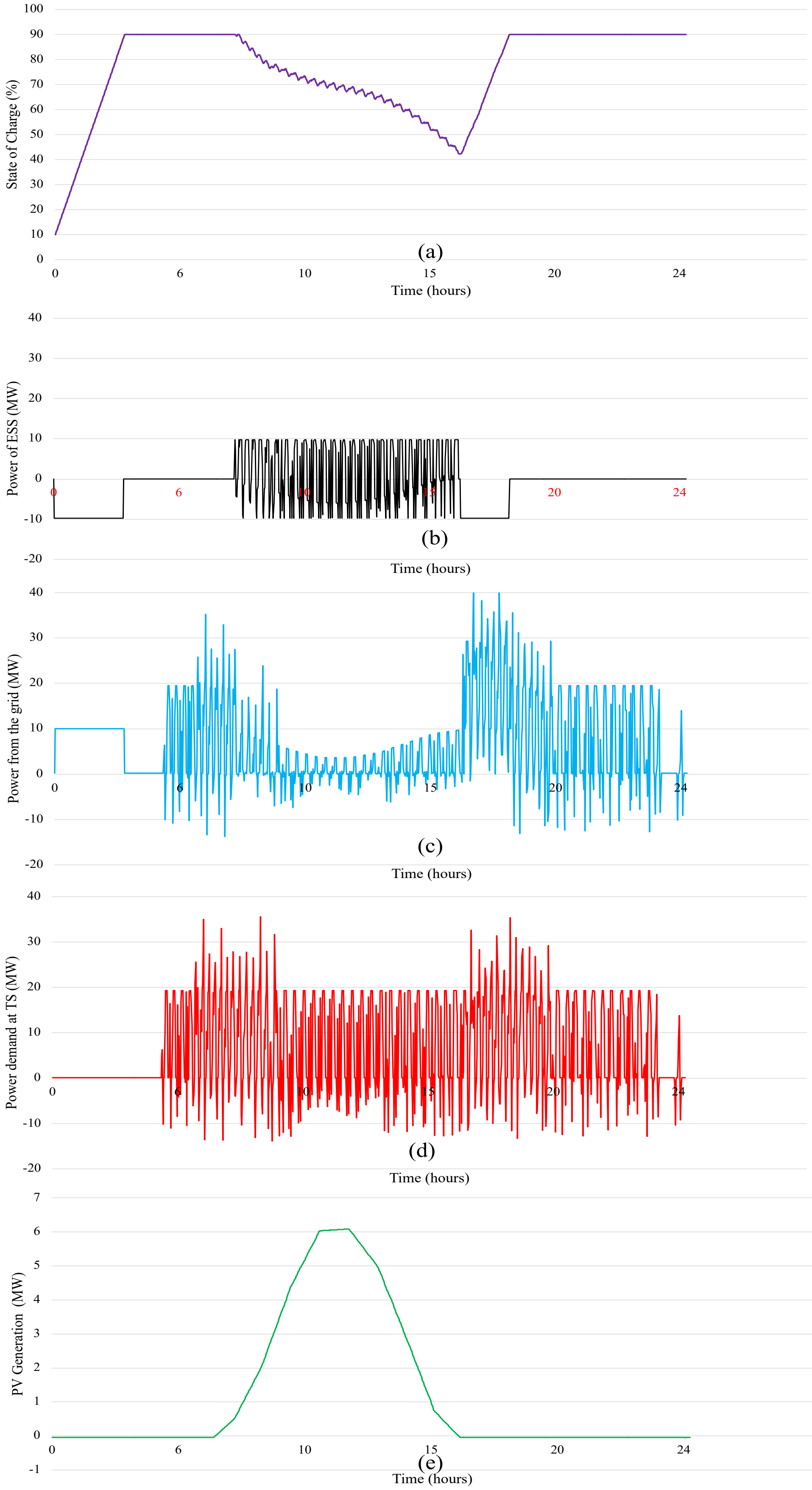

Figure 5-21 a) State of Charge b) Power of ESS c) Grid Power d) Power demand at TS and e) PV generation in scheme D at GSP1 (solar irradiance data of Jan)

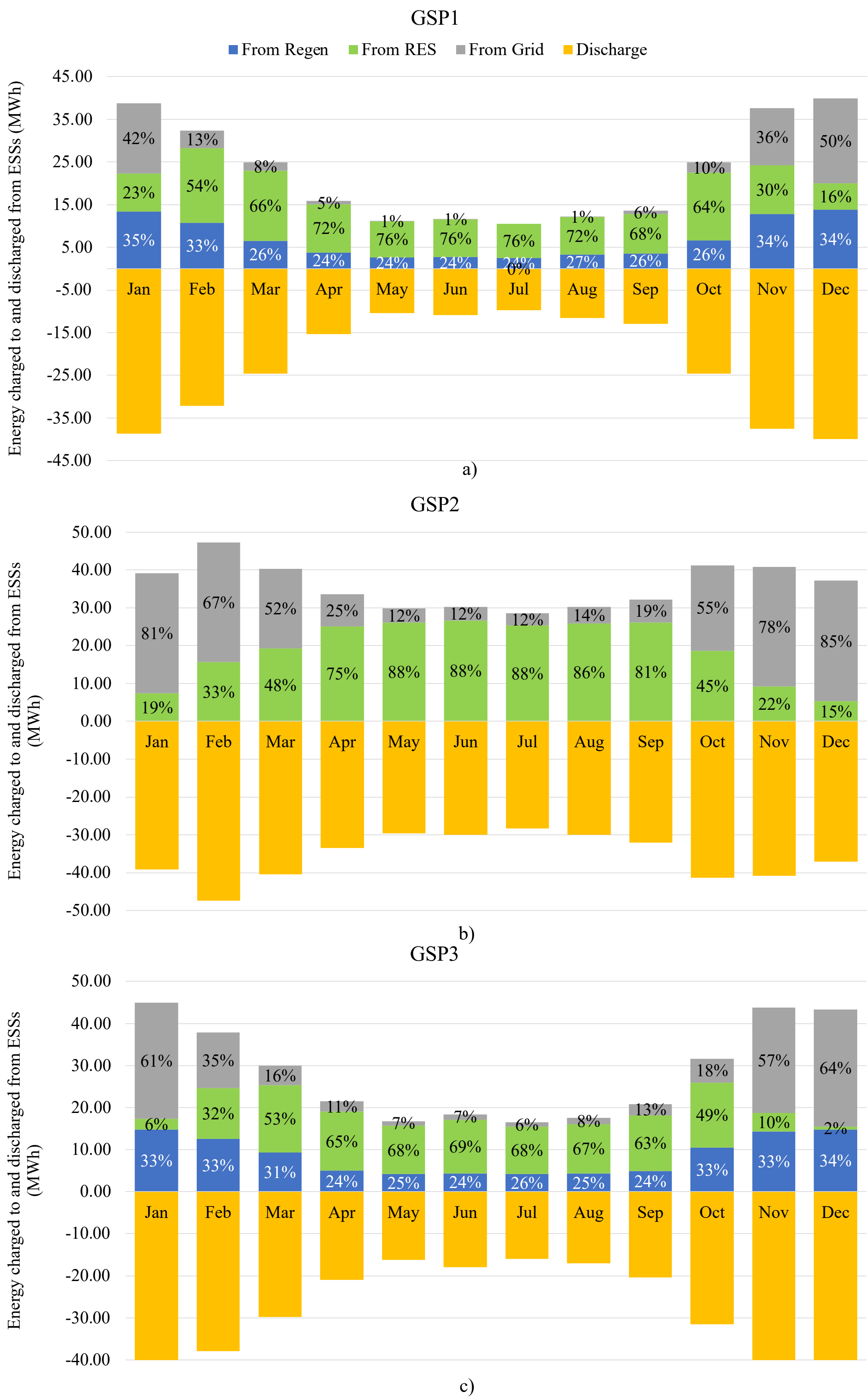

Figure 5-22 Percentage of energy charged to the ESS and amount of energy discharged from the ESS of scheme D in different months and GSPs

5.4.4.5 Share of Load Supply

Figure 5-23 presents how the load in each GSP is supplied. For scheme A, the load in the GSP1 and GSP3 is supplied mainly by the utility grid and a small amount of supply from regenerative energy and in GSP2, it is totally dependent on the grid power. For scheme B, with the support of the ESS, which stored the residual regen and grid power during the off-peak period, the amount of energy purchased from the grid is approximately between 11 and 21 per cent lower than scheme A. In scheme C, with the addition of the PV farm, the reliance on grid energy is notably reduced. Renewable energy supports around 22 to 25 per cent of the load. Furthermore, about 10 to 13 per cent of energy demand is supplied by the energy storage device in scheme D.

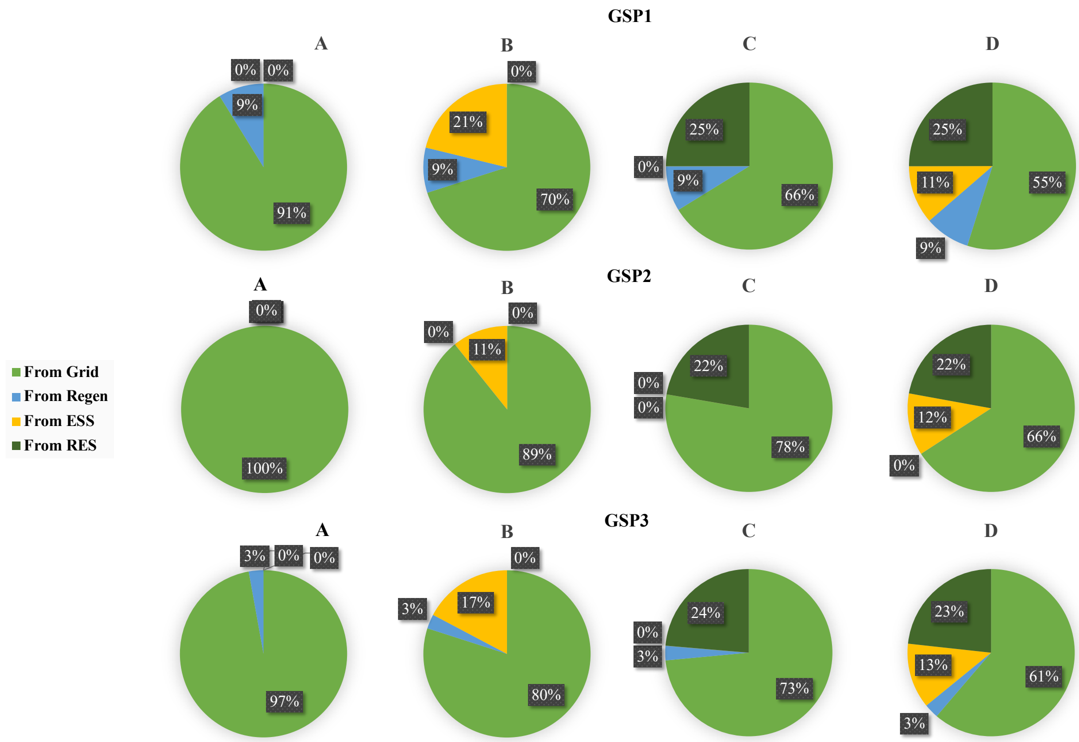

Figure 5-23 Percentage of each power source supplied to the load.

5.4.4.6 Electrical losses

There are always power losses in the power system. In this chapter, three types of power losses are considered. Firstly, transmission line loss, also known as power line loss, refers to the quantity of electrical energy that is lost during long-distance transmission across high-voltage power lines. This loss is caused by the resistance of the transmission lines, which converts some of the electrical energy into heat and dissipates it into the environment. The second one is transformer loss which is referred to the amount of power that is lost during the passage of electrical energy via a transformer. Core loss and winding loss are the two main forms of transformer loss. Finally, the amount of energy that is wasted when an inverter changes DC current into AC current is known as the inverter loss. The loss during the conversion process in a bi-directional converter is also included in the inverter loss.

The result of transmission line loss is illustrated in Figure 5-24(a). A black dashed line shows the percentage of renewable energy penetration which is a ratio of energy generated from solar PV farms and net energy demand. With the energy storage device, transmission line loss in scheme B is slightly lower than in scheme A. This is because it required less energy from the grid as the ESS supplied the energy that was captured during the train in regenerative mode. A decrease in line loss is obvious in schemes C and D in which the solar PV farms are integrated and are inversely proportional to the amount of solar power generated. Moreover, the advantage of the ESS is also clearly seen in scheme D, especially when the amount of renewable generation is high. However, as the voltage level of the transmission line is very high and the line impedance is also very low, the line losses from each scheme are not much different in terms of value.

In contrast to transmission line loss, transformer loss shows the opposite trend. Scheme A generated the lowest transformer loss, followed by scheme B, scheme C and lastly scheme D as can be seen in Figure 5-24(b). With additional components such as ESS and solar PV farms, the loss is considerably higher than the benchmark one. It is also observed that transformer loss is proportional to the RES energy penetration. Figure 5-24(c) presents inverter loss which exists in schemes B, C and D. it is obvious that schemes with the integration of solar PV generated higher inverter loss than others and the trend is similar to the transformer loss. In addition, when the ESS is included in scheme D, the highest inverter loss is seen. Finally, when it comes to total loss, it can be easily seen that scheme D is the highest among others.

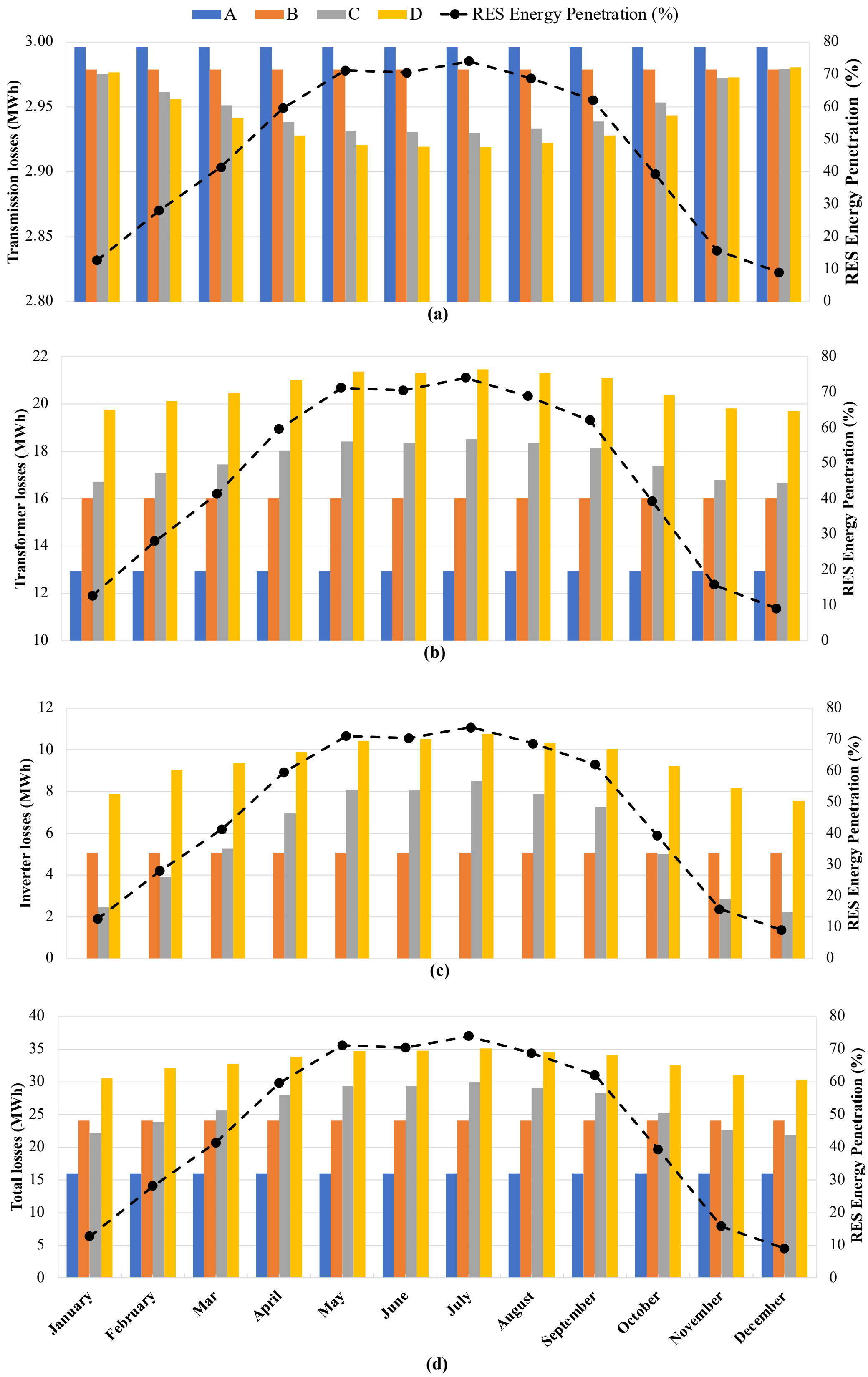

Figure 5-24 a) transmission losses, b) transformer losses, c) Inverter losses and d) Total losses

5.5 Summary

This chapter introduces a scheme for the integration of solar PV farms and large-scale energy storage system into the railway power supply. For the purposes of comparison, four schemes are included namely, scheme A (no ESS and no PV farm), scheme B (ESS included), scheme C (PV farm included) and scheme D (both ESS and PV farm included). The goal of this chapter is to study the energy flow in different parts of the system, the benefits of energy storage and renewable energy source.

In order to reuse the regenerative braking energy, the energy storage was added to the benchmark scheme and represented by scheme B. The result demonstrates that the energy storage captured the regen and effectively utilised it later. It cannot absorb the entire regenerative energy, however. Furthermore, a modest decline in electricity costs and carbon emissions is observed compared to the benchmark scheme. The PV farm integration has cost and carbon reduction advantages, as seen from scheme C. The net electricity cost dropped considerably with more energy sold to the grid and lower carbon tax due to the reduction of carbon emissions. The benefits of both energy storage and the PV farm are illustrated in scheme D in which the lowest electricity cost and carbon emissions were attained even total losses of scheme D is the highest due to a number of transformers and converters being installed.

To conclude, energy storage can provide various supports to the railway power supply system, especially, cost and carbon reductions. It also helps to reduce reliance on grid power and enhances the flexibility of the system. However, sizing to find the optimal capacity of energy storage is a critical topic. Renewable energy source provides similar benefits as energy storage, but a lot more impact in term of carbon emissions. In some situations, the integration of large capacity renewable farms at the transmission line or traction substation is not feasible since large area of land will be required. Therefore, in chapter 6, the new integration scheme will be introduced, and optimisation problem will be formulated to find the optimal capacity and location of renewable sources and energy storage device.

Chapter 6 Optimal Sizing and Location of Energy Storage System and Renewable Energy Sources to Minimize Railway Total Cost

6.1 Introduction

With the global trend to reduce carbon emissions, the UK government had set a goal to reach net-zero emissions by 2050 [49]. All industrial sectors, including the railway sector are seeking ways to achieve this goal. Transitioning from the reliance on fossil fuels is one of the most effective ways to reduce emissions. For an electrified railway system, carbon emissions are dependent on the source of electricity, which is supplied by the national grid. A lot of research contributes to carbon reduction with the integration of renewable energy sources (RES) into the railway power system and the utilization of energy storage systems (ESS) and regenerative braking energy (RBE).

Many research articles provided a study of the RES integration and ESS utilization for the AC railway systems. The advantages and disadvantages of various RES integration schemes for AC railway systems are discussed in [84] and [85]. Although RES integration to the medium voltage DC railway microgrid is most suitable, the potential to improve the energy performance for the AC railway microgrid cannot be neglected. Sida T. [24] presented a hybrid energy storage system (HESS) for a high-speed railway traction substation, which includes the supercapacitor and vanadium redox battery to capture the RBE. An improved mutation-based particle swarm optimization is introduced to obtain the optimal size of HESS with a minimum net present value. Wenli D. [38] proposed a hybrid traction substation with PV integration without altering the architecture. Boudoudouh et al. [30] proposed a distributed energy management for a railway microgrid with a hybrid substation, which includes a PV plant, wind farm, and ESS. The design can reduce the subscribed power and eliminate the voltage drop/rise along the line.

Energy management system (EMS) for railway systems has been widely researched to optimize energy consumption. Novak et al. [86] presented a railway EMS using hierarchical coordination of several trains' energy consumption and traction substation. Razik et al. [87] presented a prototype implementation of a railway EMS, which is a distributed system coordinating rolling stock, substations, and wayside resources. The overall energy demand, power consumption, and cost optimization can be performed in both offline and real-time processes. Tian et al. [43] proposed an integrated optimization method to solve the energy-saving problems of a multi-train traction power network, with consideration of train movement and electrical power flow. An electric railway smart microgrid system, with multiple RES and ESS integrated via a railway power conditioner (RPC), is proposed by Chen [32], to reduce railway energy consumption and improve the power quality. A power-to-gas (P2G) technology is introduced to absorb the excess energy from RES and RBE.

Several research articles studied the EMS considering the energy and cost evaluation. Yichen Y. [39] proposed a flexible smart traction power supply system (TPSS) with the utilization of an AC-DC-AC traction substation to solve the power quality issues, the low utilization rate of RBE, and the inability to use the distributed generation along the railway. The optimal operation cost can be reduced up to 42.17% compared with the traditional TPSS. D'Arco et al. [26] proposed PV integration schemes for AC railways and analyzed the cost and power losses. The study revealed that the PV farm power rating is the critical factor that determined the cost of the system. Liu et al. [34] proposed an EMS of a co-phase traction substation with PV and HESS, to minimize the operation cost. The results achieved a cost saving of 4.99%. Aguado et al. [29] proposed a railway model including PV, Wind, RBE and HESS, to optimize the total operation cost. With RES and ESS, there is an improvement of 33.22% and 9.63% in costs and energy savings, respectively. Salkuti [31] proposed an optimal railway operation by balancing the energy flow between the grid, traction and braking trains, RES, and ESS, to minimize the total operation cost. The optimization results, solved by using GAMS/CONOPT, are verified with a differential evolution algorithm. Park et al. [88] proposed an AC railway model with the integration of RES and HESS and the utilization of RBE to optimize the total operation cost. The proposed non-linear programming problem was solved by a differential evolution algorithm and achieved a total cost savings of 13.05%. Şengör et al. [28] suggested a mixed integer linear programming model of a railway station with ESS and PV integration. The impact of RBE and different pricing schemes are evaluated. The authors aimed to minimize the total daily cost of the station's electricity consumption as well as to evaluate the RBE, and ESS. The combination of PV, ESS and RBE reduces the cost by around 30% compared to the base case. Chen et al. [40] proposed a flexible TPSS with HESS and PV to improve the power quality and eliminate the neutral zone. A sparrow search algorithm is used to optimize for the lowest cost which includes the investment, the replacement, the operation and maintenance (O&M), and the electricity costs. The model could achieve a 13.55% cost reduction.

The integration of RES and ESS along with the utilization of RBE could improve the operational cost and reduce energy consumption, which can be proven by the various models of the research presented. However, most of these research articles have studied the integration of RES at the traction substation and the size of RES is greatly affected by the limited space. Nevertheless, by integrating the RES along the railway, the issue of the limited RES size could be alleviated. In addition, the aspect of contact wire loss was not considered in the above literature. Therefore, this study proposed the integration of distributed RES and ESS into the railway overhead line via a static frequency converter (SFC). The proposed model of the railway system includes the analysis of the contact wire loss. Moreover, the location and capacity of PV farms, wind farms, and ESS are optimized to obtain minimum global daily cost, which includes operation and investment costs. The main contributions of this study are:

1. A renewable energy sources and energy storage system integration scheme is proposed for retrofitting the conventional high-speed railway power system without modifying the architecture.
2. A comprehensive model with an energy management system is developed to calculate energy consumption and cost considering the operation and the investment, including the railway network contact wire loss.
3. Brute force method is used to optimize the sizing and location of the RES and ESS and minimize the total daily cost, which is verified in a case study.

6.2 Renewable Railway Modelling Method

The proposed RES and ESS integration scheme into an AC railway power supply system is presented in Figure 6-1. The AC railway is separated into multiple feeding sections by neutral sections. D_{ess1} and D_{ess2} are the installed ESS locations for the left and right feeding sections (km), respectively.

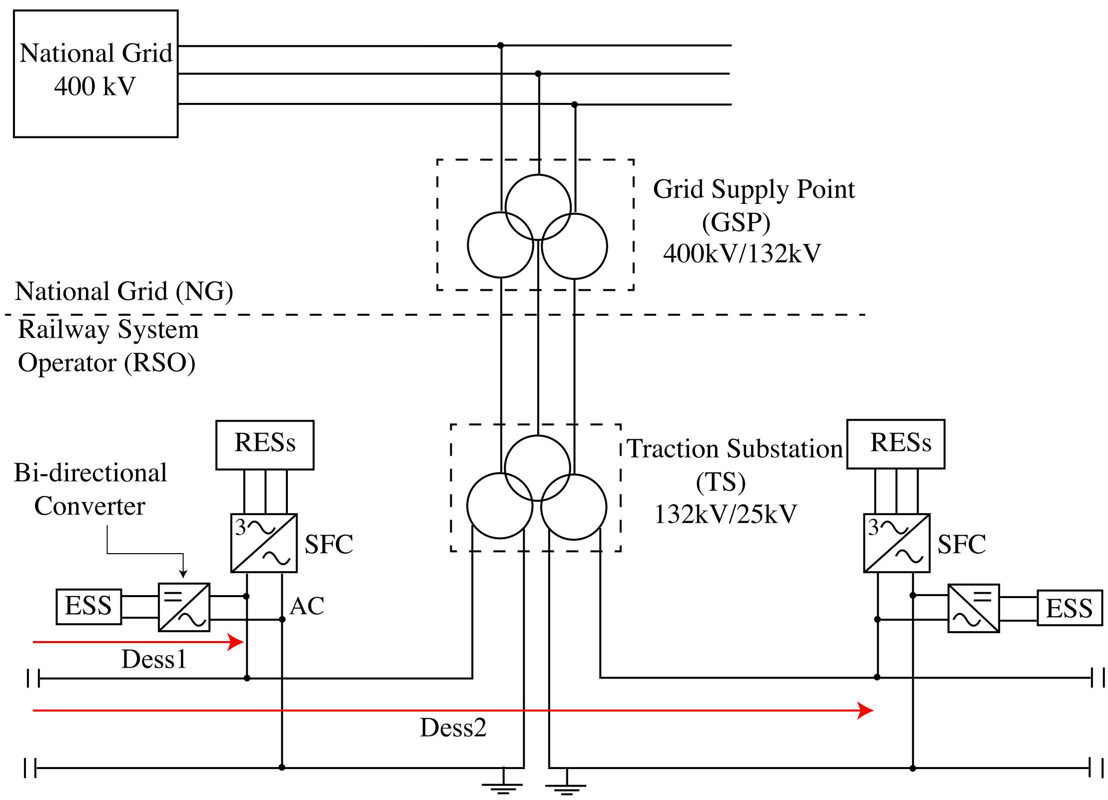

Figure 6-1 Integration scheme of RES and ESS into AC railway power supply system.

6.2.1 Train Movement Modelling

A train power profile is created considering neutral sections Figure 6-2 illustrates a single train profile with one traction substation and two feeding sections. To obtain the multiple train profile for an entire day, all train profiles in the same feeding section are combined into one single profile. Note that all trains are identical in terms of rolling stock specification, driving style and route.

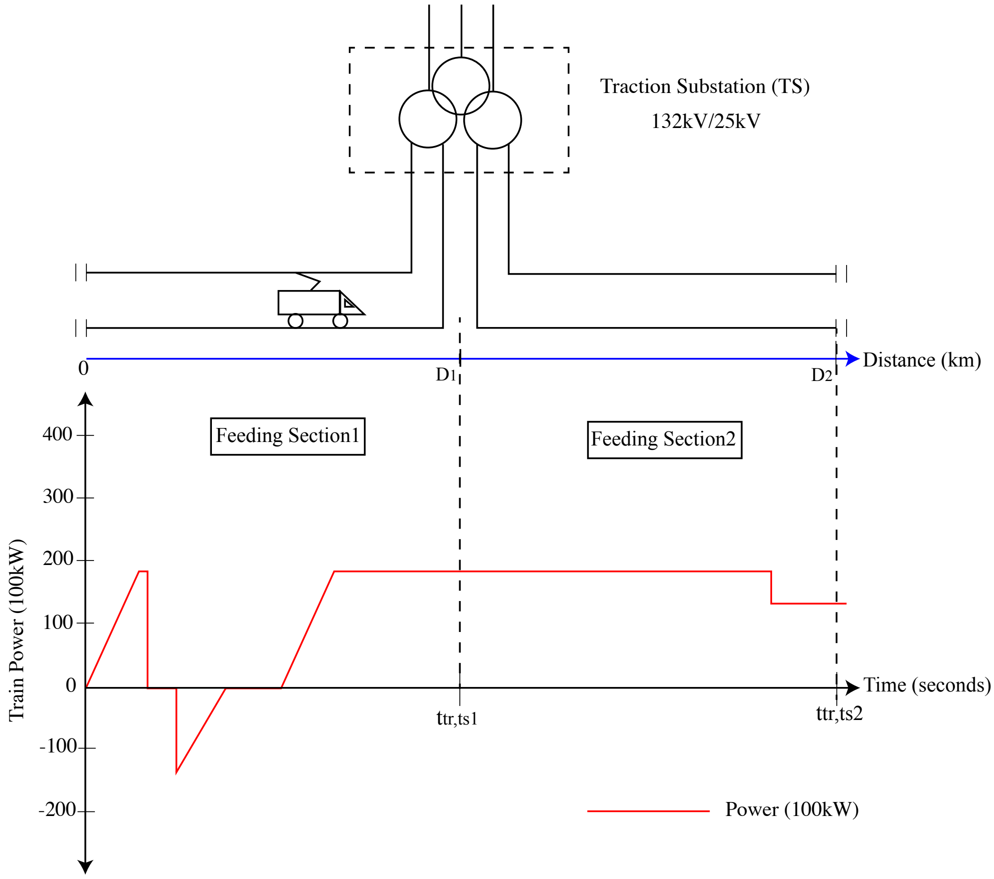

Figure 6-2 Single train power profile in two feeding sections.

6.2.2 RES Modelling

PV and wind farms are connected to an SFC via a three-phase 690V/33kV transformer, which is then integrated into the 25 kV railway power supply system, as shown in Figure 6-3

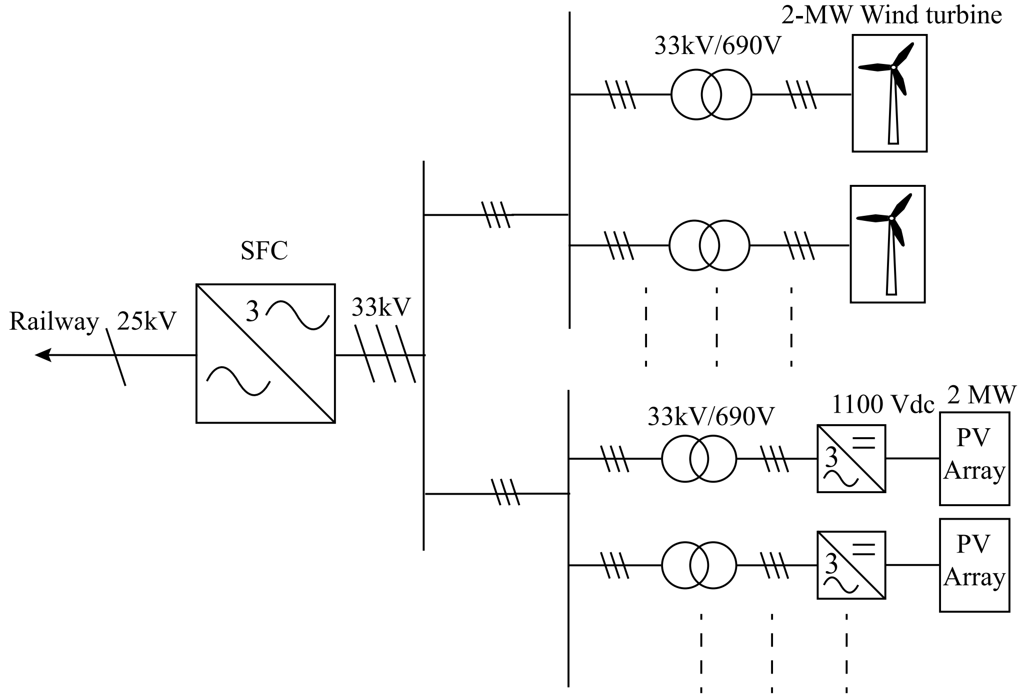

Figure 6-3 A single-line diagram of solar PV farm and wind farm connected to railway overhead line via SFC.

6.2.2.1 Solar PV model

A large-scale PV farm is formulated of several 2 MW PV arrays. The electrical power generated by a PV farm is given in (6-1).

$$P_{pv}^{t} = s^{t} \cdot A \tag{6-1}$$

where:

P_{pv}^{t} is the power produced by the PV farm at time t [W];

s^{t} is the solar irradiance at time t [W/m^2];

A is the surface area of the PV farm [m^2].

6.2.2.2 Wind turbine model

A large-scale wind farm is formulated of several 2 MW wind turbines. The electrical power generated by a wind turbine is given in (6-2) [54][16][48].

$$P_{wind}^{t} = \begin{cases} 0 & , \quad v_w^t < v_{ci} \\ P_{wind}^{rated} \cdot \dfrac{(v_w^t)^a - {v_{ci}}^a}{{v_r}^a - {v_{ci}}^a}, & \quad v_{ci} \le v_w^t \le v_r \\ P_{wind}^{rated} & , \quad v_r < v_w^t < v_{co} \\ 0 & , \quad v_w^t > v_{co} \end{cases} \tag{6-2}$$

where:

v_w^t is the wind speed at time t [m/s];

P_{wind}^{t} is the power output of the wind farm at time t [W];

P_{wind}^{rated} is the rated generation capacity of the wind farm [W] ;

v_{ci} is the cut-in wind speed [m/s];

v_{co} is the cut-out wind speed [m/s];

v_r is the rated wind speed [m/s];

a is the Weibull shape parameter.

6.2.3 Conversion Device Modelling

For a grid-connected PV farm, an inverter is necessary to convert DC to AC power. Equation (6-3) is utilized to simulate the inverter loss [62]. For ESS, a bi-directional converter, which acts as a rectifier during the charging process and an inverter during the discharging process, is required [89]. The efficiency of the bi-directional converter can be calculated using (6-4). Equation (6-5) shows that the rated power of the converter is equivalent to the rated power of the energy storage.

$$\eta_{inv,pv}(P_{dc,pu}) = A_{inv,pv} + B_{Inv,pv} \cdot P_{dc,pu} + \frac{C_{inv,pv}}{P_{dc,pu}} \tag{6-3}$$

$$\eta_{conv,ess}(P_{ess,pu}) = A_{conv,ess} + B_{conv,ess} \cdot P_{ess,pu} + \frac{C_{conv,ess}}{P_{ess,pu}} \tag{6-4}$$

$$S_{conv,ess} = P_{ess}^{rated} \tag{6-5}$$

where:

$\eta_{inv,pv}$ and $\eta_{conv,ess}$ are the PV inverter efficiency and the bi-directional converter efficiency [%];

$P_{dc,pu}$ is ratio of the DC input power and the inverter rated power [p.u.];
$P_{ess,pu}$ is the ratio of the ESS input power and the converter rated power [p.u.];
$A_{inv,pv}$, $B_{inv,pv}$, $C_{inv,pv}$, $A_{conv,ess}$, $B_{conv,ess}$ and $C_{conv,ess}$ are the parameters determined using information and the method in [62][90].
It should be noted that the three parameters for the bi-directional converter are given the same values as the PV inverter.

6.2.4 Transformer

Transformers are not ideal due to copper and core losses. The transformer efficiency is given by (6-6) [45].

$$\eta_{tf}(k) = \frac{k \cdot S_{tf}}{k \cdot S_{tf} + k^2 \cdot P_k + P_0} \quad (6\text{-}6)$$

where:
$\eta_{tf}(k)$ is the transformer efficiency at load factor k [p.u.];
S_{tf} is the transformer rated power based on P_k [MVA];
P_0 is the core loss at the rated voltage and frequency [W];
P_k is the load loss at the rated current and frequency [W].

6.2.5 Static frequency converter

SFC is utilized to convert a three-phase to a single-phase power without changing the frequency [56]. In this study, the three-phase output powers from the PV and wind farms are converted to DC voltages via a DC link and then inverted to single-phase AC powers. The rated capacity of an SFC is a sum of PV and wind farm capacity as presented in (6-7). Assuming that the efficiency curve of the SFC has the same characteristic as the PV inverter efficiency curve, (6-8) is derived from (6-3).

$$S_{sfc} = P_{pv}^{rated} + P_{wind}^{rated} \quad (6\text{-}7)$$

$$\eta_{sfc}(P_{3p-AC,pu}) = A_{sfc} + B_{sfc} \cdot P_{3p-AC,pu} + \frac{C_{sfc}}{P_{3p-AC,pu}} \quad (6\text{-}8)$$

where:

S_{sfc} is the SFC rated capacity [MVA];

η_{sfc} is the static frequency converter efficiency [%];

$P_{3p-AC,pu}$ is a ratio of the three-phase AC input powers of SFC [p.u.];

S_{sfc} (p.u.), A_{sfc}, B_{sfc}, and C_{sfc} are assumed the same values as the PV inverter.

Based on an assumption that they are modular systems, the number of units can be customized to obtain the required power rating. For instance, a 10 MW energy storage will require 5 units of bi-directional converters. All parameters for the conversion devices are displayed in Table 6-1.

Table 6-1 Parameters for the conversion devices

Inverters and SFC per unit		Transformers for PV and Wind farms	
Capacity (MVA)	2	S_{tf} (MVA)	2.1
$A_{inv,pv}, A_{conv,ess}, A_{sfc}$	99.34	Voltage (V)	690/33000
$B_{inv,pv}, B_{conv,ess}, B_{sfc}$	-1.472	P_o (kW)	2.1
$C_{inv,pv}, C_{conv,ess}, C_{sfc}$	-0.1694	P_k (kW)	24.34

6.3 Energy Management System

6.3.1 Operation Strategies of Energy Storage System (ESS)

ESS is utilized to absorb excess energy from RES and residual RBE. The flowchart of the 19 ESS working modes is illustrated in Figure 6-4. Several parameters define the ESS working modes, i.e., the train driving modes, the RES size, the State of Charge (SOC), and the ESS power.

The ESS working modes are grouped in three states, as presented in Table 6-2 and the stored energy for each state is calculated by (6-9). In *idle state*, the ESS has no operation, and the energy level does not change, for instance, when trains require no power or are in coasting mode. In *charging state*, the ESS charges and the energy level increases. In *discharging state*, the energy level decreases as it releases energy to supply loads.

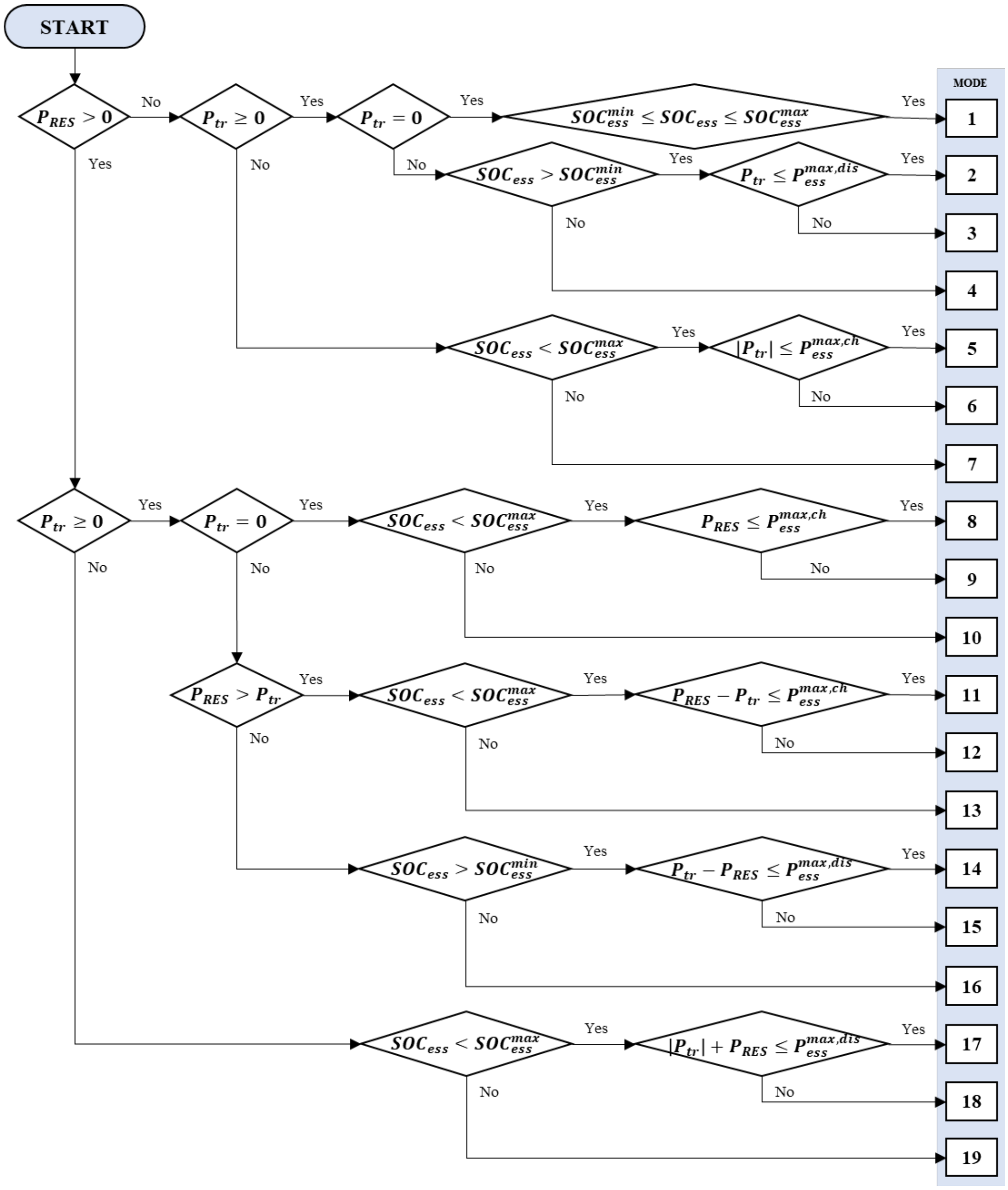

Figure 6-4 The flowchart of the ESS control strategy

Table 6-2 Power and energy for each mode of the ESS

State	Mode	Power
Idle	1, 4, 7, 10, 13, 16, 19	$P_{ess}^{ch,t} = P_{ess}^{dis,t} = 0$
Charging	6, 9, 12, 18	$P_{ess}^{ch,t} = P_{ess}^{max,ch}$
	5	$P_{ess}^{ch,t} = P_{tr}^{t}$
	8	$P_{ess}^{ch,t} = P_{res}^{t}$
	11	$P_{ess}^{ch,t} = P_{res}^{t} - P_{tr}^{t}$
	17	$P_{ess}^{ch,t} = P_{res}^{t} + \lvert P_{tr}^{t} \rvert$
Discharging	3, 15	$P_{ess}^{dis,t} = P_{ess}^{max,dis}$
	2	$P_{ess}^{dis,t} = P_{tr}^{t}$
	14	$P_{ess}^{dis,t} = (P_{tr}^{t} - P_{res}^{t})$

$$E_{ess}^{t+1} = \begin{cases} E_{ess}^{t} + \dfrac{P_{ess}^{ch,t} \cdot \eta_{ess}^{ch} \cdot \Delta t}{3600}, & \text{charging} \\ E_{ess}^{t} \qquad\qquad\qquad\quad , & \text{idle} \\ E_{ess}^{t} - \dfrac{P_{ess}^{dis,t} \cdot \Delta t}{3600 \cdot \eta_{ess}^{dis}} \quad , & \text{discharging} \end{cases} \tag{6-9}$$

Equation (6-10) denotes the SOC of the ESS. The limits of charging and discharging power are shown in (6-11) and (6-12. Additionally, it is assumed that the upper limits are identical to the rated power capacity as shown in (6-13). Equations (6-14) and (6-15) indicated that the SOC and the stored energy should be in a suitable range to prevent the over-charge and over-discharge.

$$SOC_{ess}^{t} = \frac{E_{ess}^{t}}{E_{ess}^{rated}} \cdot 100 \tag{6-10}$$

$$0 \le P_{ess}^{ch,t} \le P_{ess}^{max,ch} \tag{6-11}$$

$$0 \le P_{ess}^{dis,t} \le P_{ess}^{max,dis} \tag{6-12}$$

$$P_{ess}^{max,ch} = P_{ess}^{max,dis} = P_{ess}^{rated} \tag{6-13}$$

$$SOC_{ess}^{min} \le SOC_{ess}^{t} \le SOC_{ess}^{max} \tag{6-14}$$

$$SOC_{ess}^{\min} \cdot E_{ess}^{rated} \leq E_{ess}^{t} \leq SOC_{ess}^{\max} \cdot E_{ess}^{rated} \tag{6-15}$$

where:

$P_{ess}^{ch,t}$ is the charging power at time [W];

$P_{ess}^{dis,t}$ is the discharging power at time t [W];

$P_{ess}^{max,ch}$ is the maximum charging power [W];

$P_{ess}^{max,dis}$ is the maximum discharging power [W];

P_{ess}^{rated} is the rated power capacity of the energy storage [W];

P_{res}^{t} is the total power from RES [W];

P_{tr}^{t} is the net power of trains in the feeding section at time t [W];

E_{ess}^{t} and E_{ess}^{t+1} are the stored energy in the ESS at time t and $t+1$ [Wh];

η_{ess}^{ch} and η_{ess}^{dis} are the charge and discharge efficiency [p.u.];

E_{ess}^{rated} is the rated capacity of the ESS [Wh];

SOC_{ess}^{t} is the state of charge at time t [%];

SOC_{ess}^{min} and SOC_{ess}^{max} are the lower and upper limits of SOC [%];

Δt is the time interval which is set to 20 [s].

6.4 Energy Evaluation

6.4.1 Contact wire loss calculation

The contact wire loss is dependent on two main factors; the magnitude of the conductor resistance and the current flows from/to trains. With RES and ESS, the current flows depend on the ESS working modes and the integrating location affects the contact wire losses as denoted in (6-16). The total energy loss in the contact wire is given in (6-17).

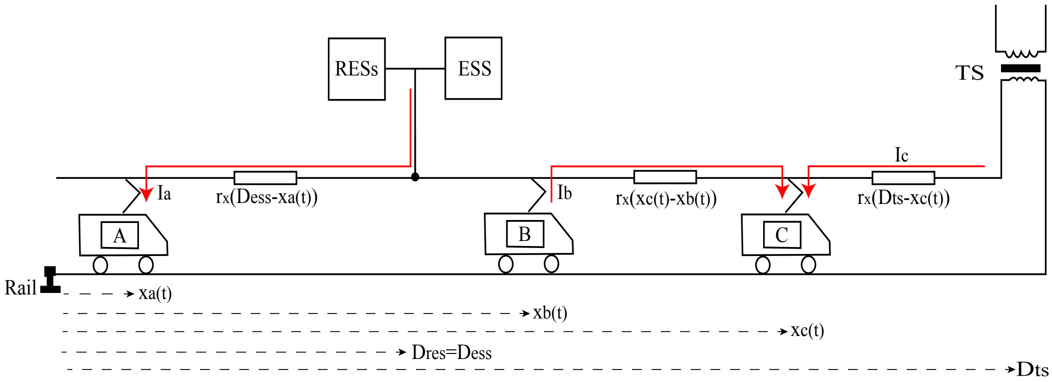

Figure 6-5 Current flows with multiple trains in a feeding section.

$$P_{CWloss}^{t} = I_a^{t\,2} \cdot r \cdot (D_{ess} - x_a^t) + I_b^{t\,2} \cdot r \cdot (x_c^t - x_b^t) + I_c^{t\,2} \cdot r \cdot (D_{ts} - x_c^t) \tag{6-16}$$

$$E_{CWloss} = \sum_{t=1}^{N} P_{CWloss}^{t} \cdot \Delta t/3600 \tag{6-17}$$

where:

P_{CWloss}^{t} is the electrical loss on the contact wire [W];

I_a^t is the current required by traction train A [A];

I_b^t is the current supplied from braking train B to traction train C [A];

I_c^t is the current supplied to train C by the grid [A];

x_a^t is the location of train A [km];

x_b^t is the location of train B [km];

x_c^t is the location of train C at time t [km];

D_{ess} is the location of the ESS and RES [km];

D_{ts} is the location of traction substation [km];

r is the electrical resistance of contact wire per unit length [Ω/km];

E_{CWloss} is the energy loss in contact wire [Wh].

6.4.2 Train energy consumption

The electrical traction energy and the RBE can be calculated using (6-18) and (6-19), respectively.

$$E_{traction} = \sum_{t=1}^{N} P_{traction}^{t} \cdot \Delta t/3600 \qquad (6\text{-}18)$$

$$E_{regen} = \sum_{t=1}^{N} P_{regen}^{t} \cdot \Delta t\ /3600 \qquad (6\text{-}19)$$

where:

$E_{traction}$ is the energy required by traction trains [Wh];

E_{regen} is the RBE from time index t = 1 to N [Wh].

6.4.3 Solar PV energy

The generated electrical energy of a solar PV is computed by (6-20), where E_{pv} is the energy of the PV farm during time index $t = 1$ to N [Wh].

$$E_{pv} = \sum_{t=1}^{N} P_{pv}^{t} \cdot \Delta t\ /3600 \qquad (6\text{-}20)$$

6.4.4 Wind energy

The energy from the wind turbine is calculated by (6-21), where E_{wind} is the energy from a wind farm during time index $t = 1$ to N [Wh].

$$E_{wind} = \sum_{t=1}^{N} P_{wind}^{t} \cdot \Delta t/3600 \qquad (6\text{-}21)$$

6.5 Total Cost Optimization

The main goal of the optimization is to find the best location and size for the RES and ESS. Therefore, the total cost which is the sum of the daily operation and investment cost becomes minimum.

6.5.1 Objective Function

Minimization of:

$$C_{total} = C_{buy} + C_{ess} + C_{sfc} + C_{pv} + C_{wind} + C_{carbon} - C_{sell} \tag{6-22}$$

where:

C_{total} is the total cost;

C_{buy} is the total cost of purchasing power from the grid;

C_{ess} is the total cost of ESS;

C_{sfc} is the cost of the SFC;

C_{pv} is the cost of PV farm;

C_{wind} is the cost of wind farm;

C_{carbon} is the carbon emissions cost;

C_{sell} is the total revenue from selling power back to the grid.

All costs are based on £/day.

Equation (6-23) presents the total daily cost of purchasing power from the grid. The total cost of ESS is a sum of the capital cost and the O&M cost, which can be calculated using (6-24). It can be seen from (6-25) that there are two parts of ESS cost; one is the cost of energy capacity (£/MWh) and the other is the cost of power capacity (£/MW) [91]. Equation (6-26) is used to calculate the ESS storage time t_{ess} (hr). The O&M cost is assumed 10% of the ESS capacity cost per year. Hence, for the entire operation lifetime, the O&M cost can be computed using (6-27). The SFC cost per unit is shown in (6-28).

$$C_{buy} = \sum_{t=1}^{N} \frac{P_{buy}^{t} \cdot \Delta t \cdot c_{buy}}{3600 \cdot 10^6} \quad (6\text{-}23)$$

$$C_{ess} = \left(C_{ess}^{cap} + C_{ess}^{om}\right) \cdot \frac{1}{365 \cdot T_{ess}} \quad (6\text{-}24)$$

$$C_{ess}^{cap} = (c_{ess,MWh} + \frac{c_{ess,MW}}{t_{ess}}) \cdot \frac{E_{ess}^{rated}}{10^6} \quad (6\text{-}25)$$

$$t_{ess} = \frac{E_{ess}^{rated}}{P_{ess}^{rated}} \quad (6\text{-}26)$$

$$C_{ess}^{om} = 0.1 \cdot c_{ess,MW} \cdot P_{ess}^{rated} \cdot T_{ess} \quad (6\text{-}27)$$

$$C_{sfc} = \frac{S_{sfc} \cdot c_{sfc}}{365 \cdot 10^6 \cdot u_{sfc} \cdot T_{sfc} \cdot} \quad (6\text{-}28)$$

Solar PV farm and wind farm costs are presented in (6-29) and (6-30). There are three main costs considered, i.e., the pre-development cost, the construction and infrastructure cost, and the O&M cost [70]. Furthermore, as power from the grid is not wholly generated from clean energy sources, the carbon cost is considered as seen in (6-31). The carbon emission is estimated using average carbon intensity (CI, gCO2/kWh).

$$C_{pv} = \frac{P_{pv}^{rated}\left(c_{pd,pv} + c_{con,pv} + c_{om,pv} \cdot T_{pv}\right)}{365 \cdot T_{pv}} \quad (6\text{-}29)$$

$$C_{wind} = \frac{P_{wind}^{rated}\left(c_{pd,wind} + c_{con,wind} + c_{om,wind} \cdot T_{wind}\right)}{365 \cdot T_{wind}} \quad (6\text{-}30)$$

$$C_{carbon} = \sum_{t=1}^{N} \frac{P_{buy}^{t} \cdot \Delta t \cdot CI \cdot c_{carbon}}{3600 \cdot 10^6} \quad (6\text{-}31)$$

Finally, due to the intermittency of renewable generation, there is a mismatch between demand and supply resulting in excess energy, which is sold to the grid at a lower rate than the purchasing price. Equation (6-32) shows the revenue from selling the excess energy.

$$C_{sell} = \sum_{t=1}^{N} \frac{P_{sell}^{t} \cdot \Delta t \cdot c_{sell}}{3600 \cdot 10^6} \quad (6\text{-}32)$$

where:

c_{buy} is the cost per MWh of buying energy from the grid;

c_{sell} is the cost per MWh of selling power to the grid;

C_{ess}^{cap} is the capital cost of energy storage;

C_{ess}^{om} is the operation and maintenance cost of energy storage;

$c_{ess,MW}$ is the cost of ESS power capacity;

$c_{ess,MWh}$ is the cost of ESS energy capacity;

T_{ess} is the operational lifetime of the ESS;

c_{sfc} is the SFC cost per unit, u_{sfc} is the capacity per unit of SFC;

T_{sfc} is the operational lifetime of the SFC;

P_{buy}^{t} is the power purchased from the grid at time t [MW];

P_{sell}^{t} is the excess power sold to the grid at time t [MW];

N is the total number of time intervals in a day (4320).

It should be noted that C_{ess}, C_{sfc}, C_{pv} and C_{wind} are scaled down to one-day time horizon to match C_{buy}, C_{sell} and C_{carbon} and to reduce the computational burden.

6.5.2 Variables

There are five variables to be optimized as follows:

1. *Location of the energy storage system and renewable energy sources* (D_{ess}, km): This variable indicates the integrating location of the ESS, PV and wind farm.

2. *Rated energy capacity of the energy storage* (E_{ess}^{rated}, Wh): This variable indicates how much energy can be stored from empty until fully charged.

3. *Rated power capacity of the energy storage* (P_{ess}^{rated}, W): This variable indicates how much power can flow in and out of the energy storage in any given instant.

4. *Rated power of the PV farm* (P_{pv}^{rated}, W): This variable presents the maximum power produced by the PV farm.

5. *Rated power of the wind farm* (P_{wind}^{rated}, W): This variable presents the maximum power produced by the wind farm.

6.5.3 Constraints

6.5.3.1 Constraints of the ESS

Equations (6-11) to (6-15) present the constraints of the ESS. In addition, (6-33) and (6-34) present the upper limits of the energy and power capacity. Moreover, to ensure that the energy storage can supply the train during travelling in the section in case of a power outage, equation (6-35) is applied.

$$0 \leq E_{ess}^{rated} \leq E_{ess}^{limit} \tag{6-33}$$

$$0 \leq P_{ess}^{rated} \leq P_{ess}^{limit} \tag{6-34}$$

$$t_{ess} \geq T_{tr,fs} \tag{6-35}$$

where:

E_{ess}^{limit} is the maximum rated energy capacity [Wh];

P_{ess}^{limit} is the maximum power capacity of the ESS [W];

$T_{tr,fs}$ is the duration of a train traveling in the feeding section [hr].

6.5.3.2 Constraints of solar PV and wind farms

Equation (6-36) indicates that power generated from solar PV must not exceed the rated capacity which is limited by (6-37). Similarly, (6-38) and (6-39) are constraints of the wind farm.

$$0 \leq P_{pv}^{t} \leq P_{pv}^{rated} \tag{6-36}$$

$$0 \leq P_{pv}^{rated} \leq P_{pv}^{limit} \tag{6-37}$$

$$0 \leq P_{wind}^{t} \leq P_{wind}^{rated} \tag{6-38}$$

$$0 \leq P_{wind}^{rated} \leq P_{wind}^{limit} \tag{6-39}$$

where:

P_{pv}^{rated} is the rated capacity of PV [W];

P_{wind}^{rated} is the rated capacity of wind farms [W];

P_{pv}^{limit} and P_{wind}^{limit} is the upper limit of the PV farm and wind farm capacity [W].

6.5.3.3 Constraints of the contact wire

To prevent the contact wire from overloading, the maximum current carrying capacity is set. Therefore, the capacity of PV and wind farms must be less than this limit, as shown in (6-40), where P_{cw}^{rated} is the maximum capacity of the contact wire (W).

$$P_{pv}^{rated} + P_{wind}^{rated} \leq P_{cw}^{rated} \qquad (6\text{-}40)$$

The current carrying capacity of the conductor used in contact wire in this study is 1594 A with a wind velocity of 1 m/s, conductor temperature of 80 degrees Celsius at an ambient temperature of 20 degrees Celsius [55]. The type of conductor is 626-AL1. Therefore, with a working voltage of 25 kV, this conductor can carry approximately 40 MW of power.

6.5.3.4 Power balance

Equation (6-41) describes the power balance that the demand must be met by the supply. Any excess power is sold to the grid. On the other hand, power is required from the grid in case of insufficiency.

$$\begin{aligned} &P_{traction}^{t} + P_{cwloss}^{t} + P_{conv}^{t} + P_{ess}^{ch,t} + P_{sell}^{t} \\ &\qquad = P_{buy}^{t} + P_{pv}^{t} + P_{wind}^{t} + P_{ess}^{dis,t} + P_{regen}^{t} \end{aligned} \qquad (6\text{-}41)$$

where:

P_{conv}^{t} is power losses in the conversion devices i.e., inverter, transformer and the SFC [W].

6.6 Case Study

6.6.1 Description

The route and overhead line information from the first phase of the HS2 project in the UK is used. The feeding sections are divided into six sections for the entire route from London to Birmingham, as illustrated in Figure 6-6. The route and infrastructure information are presented in

Table 6-3 and Table 6-4. Nevertheless, only the first two feeding sections with a total length of 48 km are considered in the case study. The same methodology can be applied to obtain optimization results for other feeding sections.

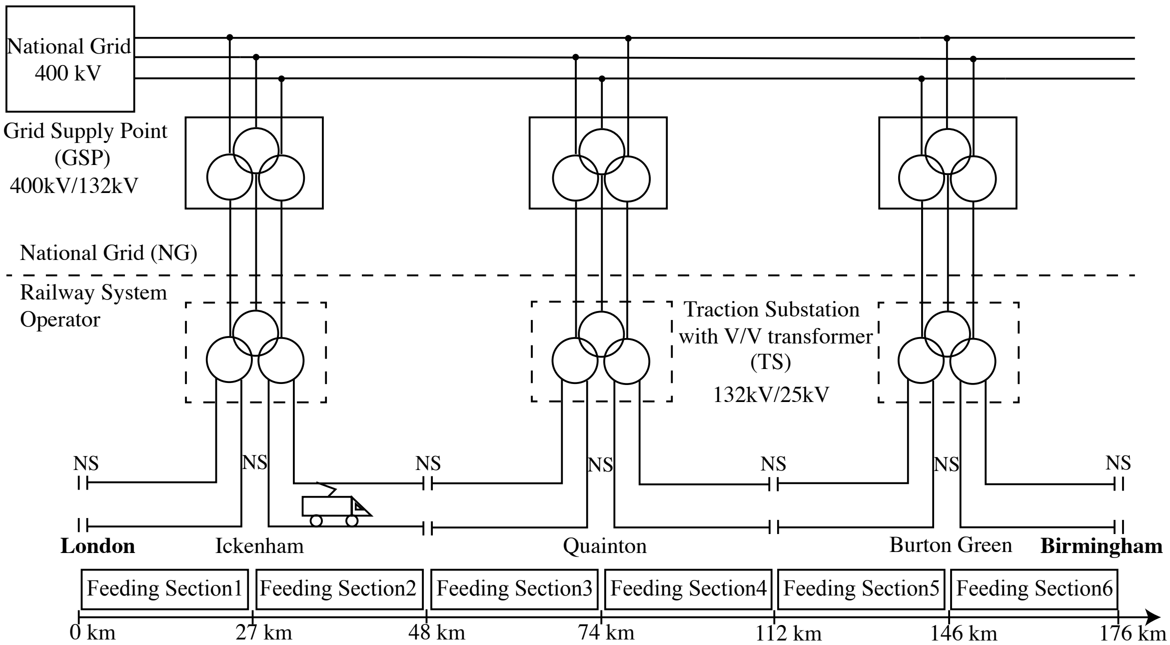

Figure 6-6 A conventional connection scheme showing the entire power system connection of the case study

Table 6-3 HS2 PHASE 1: Route and station information [75]

Location (km)	Station
0	Euston
9.5	Old Oak Common
156.7	Birmingham Interchange
176	Birmingham Curzon Street

Table 6-4 HS2 PHASE 1: Grid supply points (GSP), traction substations and section information [75]

Location (km)	GSP&TS	Neutral Section	Feeding Section
0	-	NS	FS1
27	Ickenham	NS	FS2
48	-	NS	FS3
74	Quainton	NS	FS4
112	-	NS	FS5
146	Burton Green	NS	FS6
176	-	NS	-

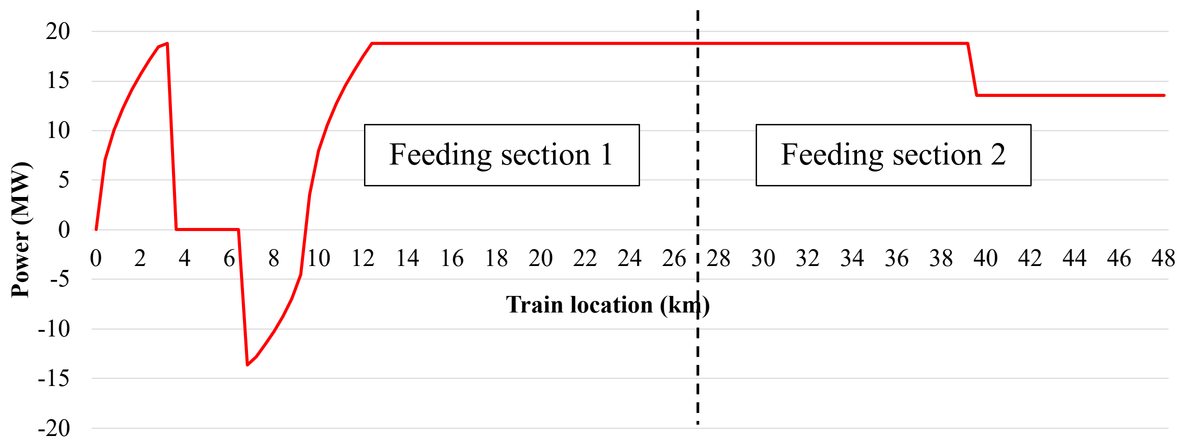

Figure 6-7 The power profile of a single train travelling through the FS1 (left) and FS2 (right)

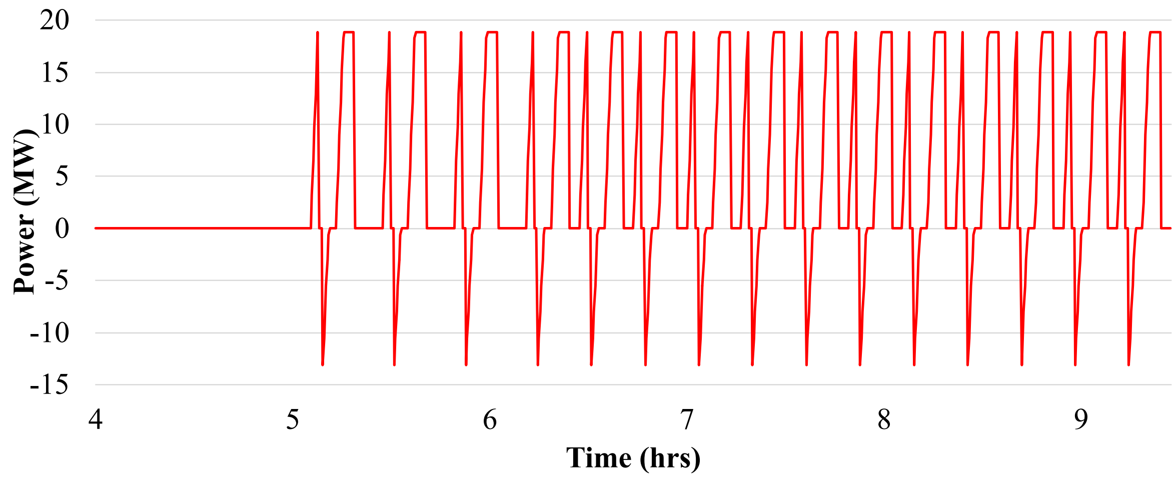

(a)

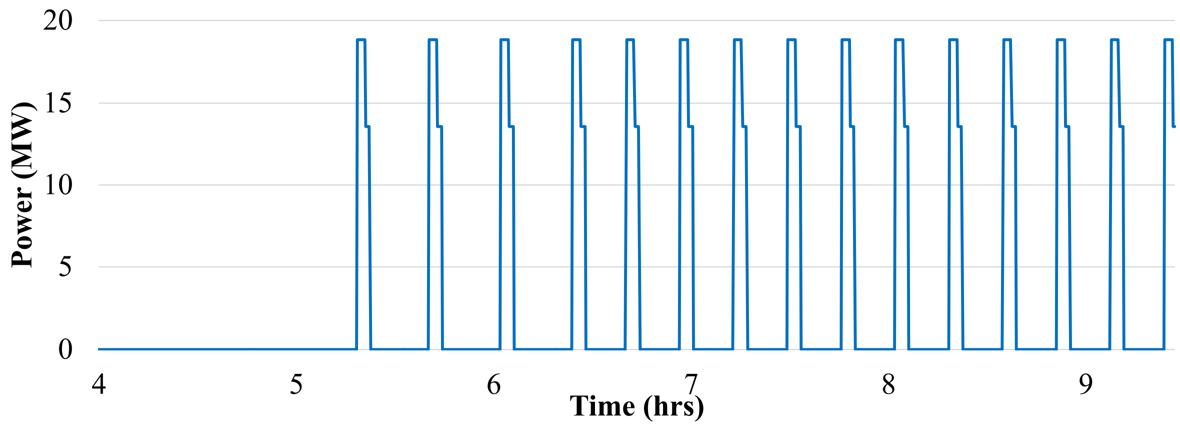

(b)

Figure 6-8 Multiple-train power profiles from 4 AM to 9 AM in a) FS1 and b) FS2.

Figure 6-7 displays an example of the train power profile supplied by the FS1 while traveling from 0 km to 27 km and the FS2 from 27 km to the next neutral section at 48 km. It can be noticed that the RBE is produced during the train travel in FS1, which is the negative power from 6 km to 9 km. On the other hand, the train is in traction mode in FS2. Moreover, the multiple-train power profile of the FS1 and FS2, illustrated in Figure 6-8(a) and Figure 6-8(b), is used for the optimization. It should be noted that reactive power is not considered in this study.

6.6.2 Scenarios and parameters

To compare the daily total cost for various combinations of energy sources – grid, ESS, PV farm and wind farm, eight scenarios are created and summarized in Table 6-5. Scenario 1 represents the base scenario where all train demands are supplied by the grid. ESS is installed to capture and reuse the RBE when available in Scenario 2. A solar PV farm is installed to reduce the reliance on grid power in Scenario 3. Then, the addition of ESS is presented in Scenario 4. In Scenario 5, the load demand is supplied by the grid and the wind farm. Similarly, ESS is added in Scenario 6. Next, the grid, PV farm and wind farm are considered in Scenario 7 and lastly, all energy sources are integrated into the system.

Table 6-5 Scenario description

Scenarios	Grid	ESS	PV	Wind
1	✓	-	-	-
2	✓	✓	-	-
3	✓	-	✓	-
4	✓	✓	✓	-
5	✓	-	-	✓
6	✓	✓	-	✓
7	✓	-	✓	✓
8	✓	✓	✓	✓

The lower and upper limits of each variable are tabulated in Table 6-6. The hourly meteorological data for five years from 2015 to 2019 is averaged to reduce uncertainty and computational burden. Then, hourly solar irradiance and wind speed data are interpolated before being applied as input for solar PV and wind farms, as shown in Figure 6-9. The solar PV and wind farm parameters are displayed in Table 6-7 and Table 6-8. Additionally, parameters for the energy cost, the carbon cost, the ESS cost and the SFC cost are shown in Table 6-9. In order to ensure that the global optimum is found, a Brute Force (BF) search, which is the algorithm that attempts all conceivable solutions in a problem in order to identify the extrema of the objective function, is adopted. As an exact algorithm, BF guarantees that the best solutions will be found if they exist [92].

Table 6-6 Lower limits, upper limits and step size for variables

Variable	Lower Limit	Upper limit	Step size
E_{ess}^{rated} (MWh)	0	40	2
$P_{ess}^{rated}(MW)$	0	40	2
$P_{pv}^{rated}(MW)$	0	40	2
$P_{wind}^{rated}(MW)$	0	40	2
$D_{ess1}(km)$	0	27	0.5
$D_{ess2}(km)$	27	48	0.5

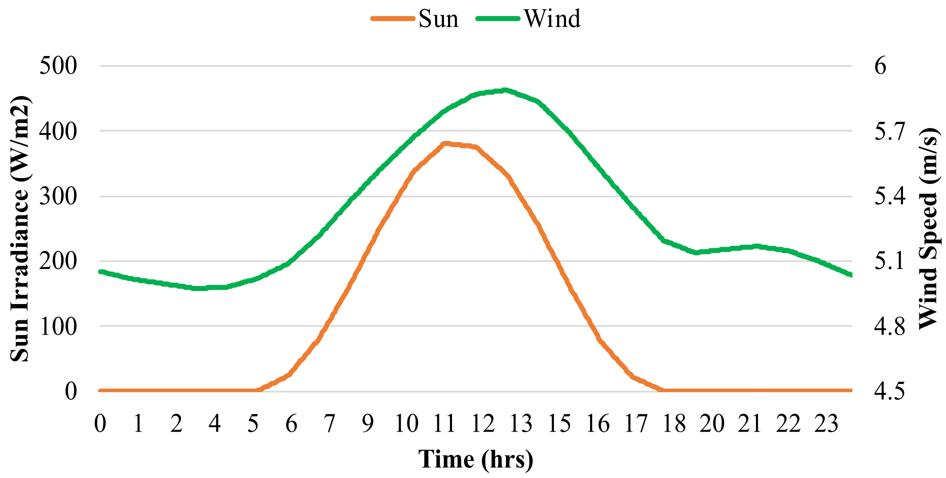

Figure 6-9 Average sun irradiance and average wind speed [77]

Table 6-7 Solar PV farm parameters

Parameters	Values [70]	Descriptions
$c_{pd,pv}$	50×10^3 £/MW	Pre-development cost
$c_{con,pv}$	400×10^3 £/MW	Construction cost
$c_{om,pv}$	$6700 \cdot T_{pv}$ £/MW	O&M Cost
T_{pv}	35 years	Lifetime of PV farm

Table 6-8 Wind farm parameters

Parameters	Values [70][54]	Descriptions
$c_{pd,wind}$	120×10^3 £/MW	Pre-development cost
$c_{con,wind}$	1000×10^3 £/MW	Construction cost
$c_{om,wind}$	$23500 \cdot T_{wind}$ £/MW	O&M cost
T_{wind}	25 years	Lifetime of Wind farm
v_{ci}	4 m/s	Wind Cut-in speed
v_r	13 m/s	Rated wind speed
v_{co}	23 m/s	Wind Cut-out speed
a	2	Weibull shape parameter
a	0.159	Hellman Height exponent

Table 6-9 Parameters for energy cost, SFC cost, carbon cost, and energy storage system

Parameters	Values [91], [72]	Descriptions
c_{buy}	140 £/MWh	Cost of grid energy
c_{sell}	70 £/MWh	Cost of selling energy to grid
CI	30.8 gCO_2/kWh	Average Carbon intensity
c_{carbon}	18 £/ton	Cost of Carbon emissions
$c_{ess,MWh}$	192 £/MWh	Energy Capacity Cost of ESS
$c_{ess,MW}$	184 £/MW	Power Capacity Cost of ESS
P_{cw}^{rated}	40 MW	Maximum Power Capacity of Contact Wire
r	0.15 Ω/km	Contact wire resistance
SOC_{ess}^{min}	10%	Minimum state of charge
SOC_{ess}^{max}	90%	Maximum state of charge
$T_{tr,fs}$	1/5 and 1/15 hr	Duration in section1 and 2
T_{ess}	10 years	Lifetime of ESS
c_{sfc}	3.46×10^5 £/unit	Cost of SFC per unit
U_{sfc}	2 MVA	Capacity of SFC per unit
T_{sfc}	25 years	Lifetime of SFC

6.6.3 Cost analysis

The optimization results for FS1 are displayed in Table 6-10. The highest daily cost belongs to Scenario 1 where the load is solely supplied by the grid. Scenario 2 is 200 £/day lower than Scenario 1 with an ESS (2 MWh, 4 MW) installed 10.5 km away from London Euston. The cost is reduced because the RBE is used to supply the upcoming trains. Moreover, with the optimal location of the ESS, the contact wire losses are reduced by around 8 % compared to Scenario 1.

With the PV integration in Scenario 3, the optimal size and location of the PV farm are 40 MW and 20 km. The cost dropped to 9890 £/day, which is significant compared to the first and the second scenarios. It is noticed that the contact wire losses slightly go up as the excess power flowed to the grid dissipated as losses. Further cost saving is observed with the integration of the ESS in Scenario 4, where 1020£/day is saved, and the contact wire loss is the lowest among all scenarios. This results from excess power and RBE are absorbed by the ESS. For this scenario, the installation of a PV farm (40 MW) and an ESS (24 MWh, 10 MW) are required at 15.5 km to achieve the optimal solution.

Without the ESS, the total cost notably decreased by 6330 £/day despite the higher contact wire losses compared to the previous case. To attain this cost saving, a 40 MW wind farm must be connected at 20.5 km. Additionally, the ESS and wind farm are considered in Scenario 6 and the result reveals that by installing the ESS (2 MWh, 10 MW) and a 40 MW wind farm at 20 km, the total cost is remarkably reduced to 954 £/day or approximately 62 % reduction and a decline of 0.95 MWh/day of contact wire losses relative to the case without the ESS.

The rated capacities of both PV and wind farms are considered in Scenario 7. However, the result reveals that to minimize the total cost, only a 40 MW wind farm is required to integrate at 20.5 km. This result provides the same outcome as Scenario 5. Considering all variables i.e., the RES location, the energy and power capacity of ESS, and the rated power of PV and wind farms in Scenario 8, the optimization result indicates that installing a 40 MW wind farm and an ESS (2 MWh, 10 MW) at 20 km, is the most economical scheme. It is observed that the result from this scenario is identical to Scenario 6.

Table 6-11 presents the results of FS2. The advantages of the RES and ESS are shown, and the same trend is observed. It is worth to note that the negative value of total cost indicates that there is excess energy sold to the power grid. However, because the train travelling in this section is in traction mode, the ESS is not essential in Scenario 2; hence, the cost and losses in Scenarios 1 and 2 are identical. The main difference is that instead of purchasing, the railway operator can sell the power, which can be seen as a negative cost in Scenarios 5 to 8.

Table 6-10 Optimization result of feeding section 1

Scenarios	C_{total} (£/day)	E_{cwloss} (MWh/day)	D_{ess} (km)	E_{ess}^{rated} (MWh)	P_{ess}^{rated} (MW)	P_{pv}^{rated} (MW)	P_{wind}^{rated} (MW)
1	15800	6.11	-	-	-	-	-
2	15600	5.64	10.5	2	4	-	-
3	9890	6.46	20	-	-	40	-
4	8870	4.64	15.5	24	10	40	-
5	2540	7.20	20.5	-	-	-	40
6	954	6.25	20	2	10	-	40
7	2540	7.20	20.5	-	-	0	40
8	954	6.25	20	2	10	0	40

Table 6-11 Optimization result of feeding section 2

Scenarios	C_{total} (£/day)	E_{cwloss} (MWh/day)	D_{ess} (km)	E_{ess}^{rated} (MWh)	P_{ess}^{rated} (MW)	P_{pv}^{rated} (MW)	P_{wind}^{rated} (MW)
1	10300	3.10	-	-	-	-	-
2	10300	3.10	27	0	0	-	-
3	5330	3.41	30	-	-	40	-
4	4960	2.60	40.5	6	4	40	-
5	-966	3.50	28.5	-	-	-	40
6	-1622	3.57	30.5	2	8	-	40
7	-966	3.50	28.5	-	-	0	40
8	-1622	3.57	30.5	2	8	0	40

6.6.4 Energy flow analysis

The energy demand in FS1 is broken down according to loads, depicted in Figure 6-10(a), where the traction load accounts for approximately 95 % or 112.8 MWh/day in the scenarios without the ESS. Conversion loss (E_{conv}) exists only when the conversion devices are operated, and it is proportional to the amount of power generated by RES and the charging and discharging power of the ESS. The green bars represent the energy charged (E_{ch}) into the ESS. With RES, the ESS is charged with a large amount of excess energy.

The breakdown of the energy supply is illustrated in Figure 6-10(b). In the scenarios without RES, the demand is met by the power purchased from the grid. However, there is a small amount of energy sold to the grid, as seen in Scenarios 1 and 2 in Figure 6-10(c), which is the unused RBE. Despite having the ESS in Scenario 2, there is a small amount of RBE that is not captured since the ESS reached the upper limit capacity. With RES integration, the required power from the grid falls considerably. In Scenarios 4 and 5, the PV farm produced 98.6 MWh/day. Furthermore, from Scenarios 5 to 8, the energy from the wind farm dominates the grid power, causing a large amount of excess power sold to the grid. As seen in Figure 6-10(c), the energy sold to the grid is greater than the energy purchased from the grid. Additionally, the carbon emissions significantly declined in cases with the RES and ESS. Scenarios 4, 6 and 8 depict the benefits of the ESS in reducing the required power from the grid, hence lowering carbon emissions. It is worth mentioning that the attribute of energy flow of FS2 is similar to FS1.

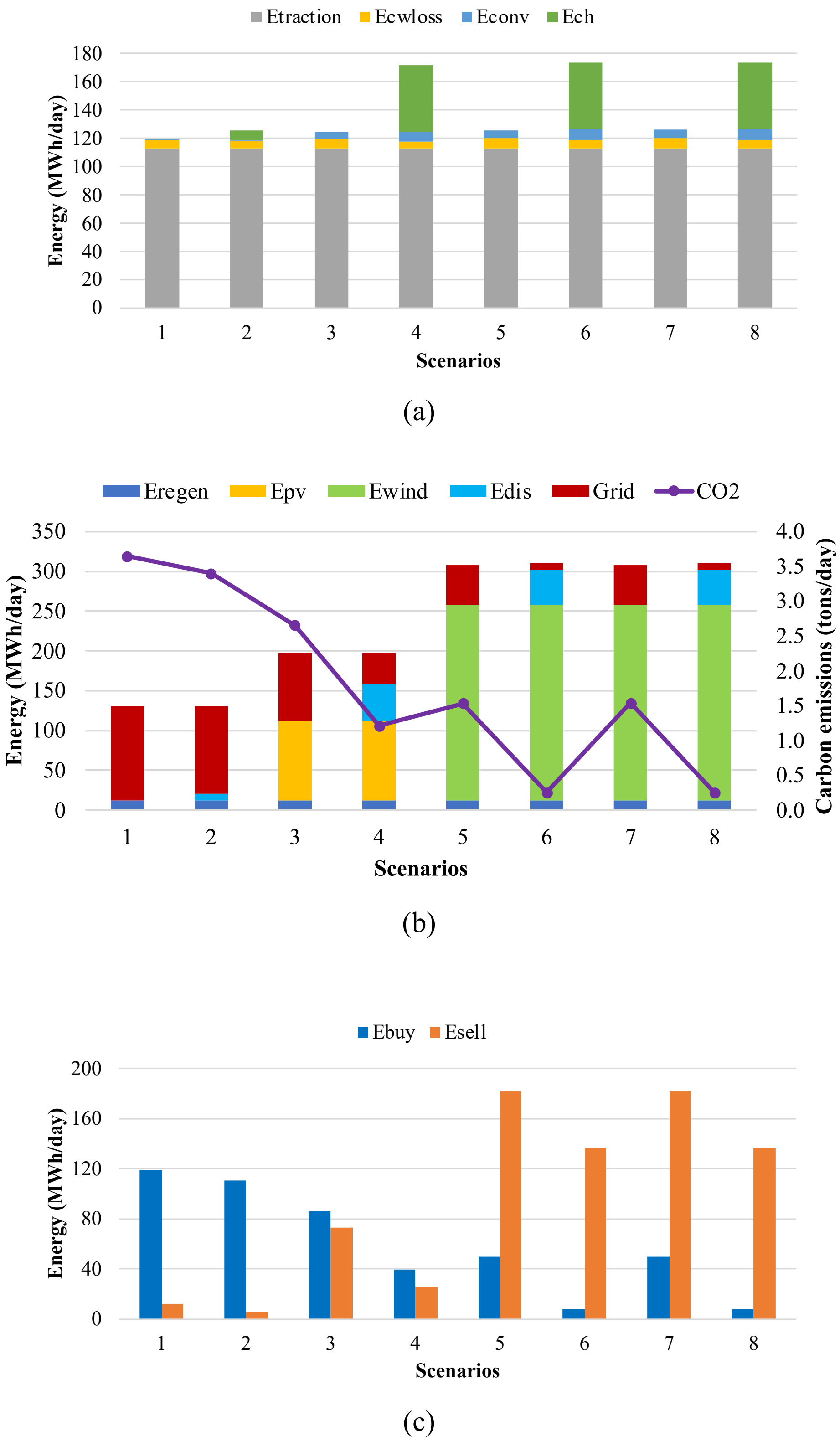

Figure 6-10 Energy flow charts of FS1 a) energy demand b) energy supply and c) exchange energy with the grid.

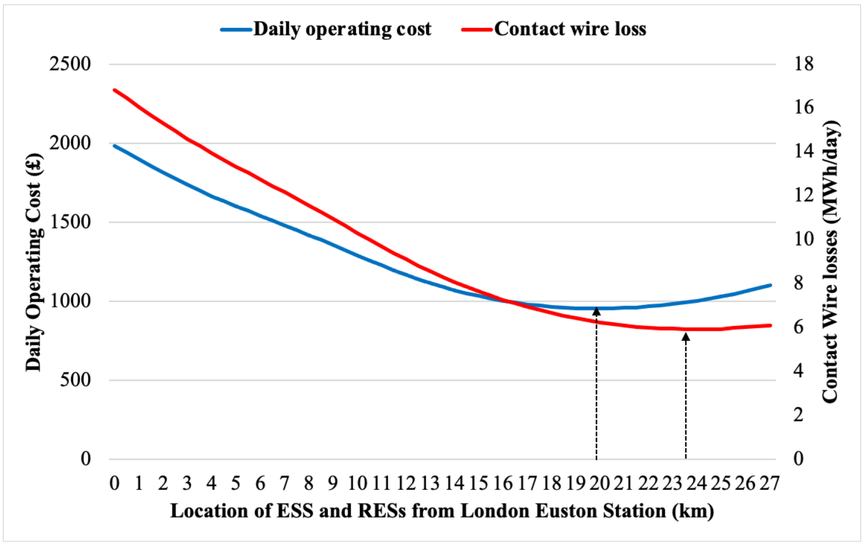

(a)

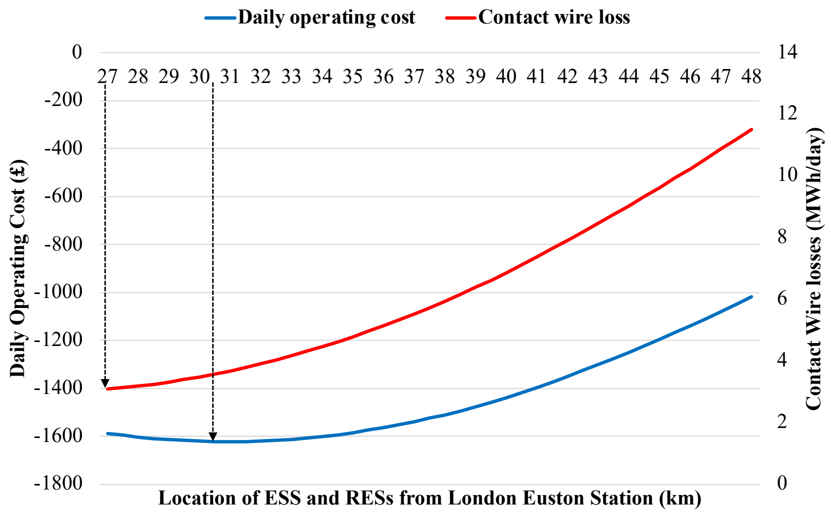

(b)

Figure 6-11 Total daily cost and contact wire losses with different RES and ESS locations a) feeding section 1, based on a 2 MWh, 10 MW ESS and a 40 MW wind farm b) feeding section 2, based on a 2 MWh, 8 MW ESS and a 40 MW wind farm.

Figure 6-11 illustrates the total daily cost and the contact wire losses for different ESS and RES locations in feeding sections 1 and 2. It can be seen that the location with the minimum total cost is different from the location with the minimum contact wire loss. For instance, in Figure 6-11(a), the lowest contact wire loss is found where the ESS and wind farm in feeding section 1 are installed at 23.5 km. Nevertheless, the total cost in this location is higher than installing at 20 km, which is the optimal location. The contact wire losses can be separated into two parts:

loss due to the flow of current to trains and loss due to the flow of current to the grid (excess power from renewables). Hence, more energy is needed to compensate for the loss when the current is supplied to trains, and less energy is fed to the grid after subtracting the loss. The results reveal that the locations where the minimum contact wire losses are found tend to be near or at the traction substation. This is because a major proportion of contact wire losses is generated by excess energy flow to the grid from the wind farm. Thus, if the renewables are installed close to the traction substation, the reduction of contact wire losses will be observed. Nonetheless, this increases another part of contact wire losses (current flow to trains) and slightly increases demand. The railway system operator will need to buy more energy in case power from the wind farm and energy storage are insufficient. Therefore, the total cost is rising. This is a reason why the lowest contact wire loss location is not the same spot as the lowest total cost location.

6.7 Summary

This chapter proposed the integration scheme for renewable energy sources and energy storage systems into the AC railway power supply system. Additionally, a comprehensive model with an energy management system is developed to reduce the daily total cost. Finally, the Brute Force method is employed to optimize the best integrating location, ESS power and energy capacity, including PV and wind farm sizes that achieve minimum total daily cost.

The result from the case study shows that energy storage played a crucial role in storing the regenerative braking energy and excess energy from renewable energy sources. From the case study, the global cost could be saved around 1.3 % if the ESS is installed to capture the regenerative energy and 10 % and 58 % to absorb excess energy from the PV and wind farm, compared to the same scenarios without the ESS. With the optimal location, the contact wire losses are considerably reduced in the scenarios with the ESS. The PV and wind farms are the main contributor to reducing the reliance on grid energy and carbon emissions. However, it has been found that integrating a wind farm is a better way to reduce and/or gain money and reduce carbon emissions compared to a PV farm. It should be noted that the solar irradiance and wind speed data used in this study are based on the UK location. Therefore, the result may differ in a different location.

Chapter 7 Conclusions and Future Work

7.1 Conclusions

This thesis introduced ways to integrate renewable energy sources into the 25-kV AC railway power network and efficiently utilise regenerative braking energy with goals to decarbonise power generation and reduce electricity costs and also global costs. A number of literature related to renewable energy and energy storage applications in the electrified railway system were reviewed and investigated in Chapter 2.

Chapter 3 described the details of each component in the railway power system and also the description of electrical parameter calculation. Furthermore, this chapter demonstrates the development of the 25-kV AC traction network model that was used for the whole research. The schemes for connecting the solar PV farm and wind farm were offered in Chapter 4. This chapter also revealed the comparison results between each integration scheme. Many parameters output from the simulation were analysed. Chapter 5 demonstrated the integration of energy storage devices and solar PV farms. The ESS working modes were proposed to reduce the electricity cost by charging the excess energy from both solar PV farms and regenerative braking and then using it when the electricity price is high. Additionally, the ESS was absorbing energy from the grid when the electricity price is low. In Chapter 6, Brute Force approach was applied to search for the best solution in which the global cost is minimum. The contact wire loss was included in this search. From the study presented in Chapter 4 to Chapter 6, it is clearly seen that the hypothesis made at the start of the thesis is validated. Carbon emissions are decreased significantly with the integration of renewable energy sources and energy storage systems.

7.2 Main Contributions

7.2.1 Renewable Integration Schemes for AC Traction Power Network

In order to lessen the reliance on power from the national grid and carbon emissions, three schemes for integrating renewable energy sources were introduced for the AC traction power supply system. Power losses, voltage unbalance factor, lifetime cost and carbon emissions were compared using High Speed 2 rail service and route data as a case study.

7.2.2 AC Traction Power Network with Energy Storage System

An energy storage system with the proposed control strategy is introduced and connected to the three-phase railway power network. The main objective of this ESS is to help reduce the total electricity cost on the railway side. This ESS captured the non-utilised regenerative braking energy and excess energy from the solar PV farm and then reused it when the electricity price is high. It is clear from the simulation results that the ESS played a crucial role in cost-saving and energy management.

7.2.3 Renewable and Energy Storage System Optimisation Study for AC Railway Applications

The scheme for connecting the renewable power plants and energy storage system to the railway contact wire was proposed, and the contact wire loss was calculated. In an effort to reduce the global cost, the Brute Force algorithm was employed to find the optimal capacity and installed location along the contact wire of solar PV farms, wind farms and ESS.

7.3 Recommendations for Further Research

7.3.1 AC Railway Feeding Systems and Optimization Algorithms

This research adopted a direct feed system to calculate the contact wire loss. More complicated feeding systems, such as booster transformers and autotransformers, could be used by the application of the multi-conductor transmission line model. In addition, while the Brute Force approach is simple and guarantees finding the solutions, it requires much computational time. Therefore, future work could focus on those two topics.

7.3.2 Solar Irradiance and Wind Speed Data

Available data for solar irradiance and wind speed is based on an hourly basis datapoint which means that in order to obtain a 20-second interval data, the interpolation was carried out. This can cause the model to underestimate or overestimate the power generation. Thus, it is worth searching for methods to process the data.

7.3.3 Future Power Supply System for AC High-Speed Rail

There are a number of researchers who studied and proposed new power supply systems for high-speed rail, for instance, co-phase power supply systems, converter-based power supply systems, and high-voltage direct current (HVDC) power supply systems. The main objective of those proposed systems is to mitigate the issue of load imbalance. In the future, those power supply systems may be the new standard for high-speed rail. However, the topic of renewable integration for the new proposed railway power supply system is barely studied and modelled. Therefore, it is a very interesting subject and worth researching.

References

[1] International Energy Agency, “The Future of Rail - Opportunities for energy and the environment,” 2019.

[2] C. Carr and J. Doppelbauer, “Fostering the Railway Sector Through the European Green Deal,” 2020.

[3] R. J. Hill, “Electric railway traction. Part 3: Traction power supplies,” *Power Engineering Journal*, vol. 8, no. 6, pp. 275–286, 1994.

[4] R. D. White, “AC 25kV 50 Hz electrification supply design,” *IET Seminar Digest*, vol. 2011, no. 14203, pp. 92–130, 2011.

[5] F. Ciccarelli, M. Fantauzzi, D. Lauria, and R. Rizzo, “Special transformers arrangement for AC railway systems,” in *Electrical Systems for Aircraft, Railway and Ship Propulsion, ESARS*, 2012, pp. 1–6.

[6] D. Serrano-Jiménez, L. Abrahamsson, S. Castaño-Solís, and J. Sanz-Feito, “Electrical railway power supply systems: Current situation and future trends,” *International Journal of Electrical Power and Energy Systems*, vol. 92, pp. 181–192, 2017.

[7] M. Shafighy, S. Khoo, and A. Z. Kouzani, “Modelling and simulation of regeneration in AC traction propulsion system of electrified railway,” *IET Electrical Systems in Transportation*, vol. 5, no. 4, pp. 145–155, 2015.

[8] “Engineering Recommendation P24 Issue 2 2020 AC supplies to railway systems,” 2020.

[9] International Energy Agency, “Renewables 2022,” 2022.

[10] International Renewable Energy Agency (IRENA), “World energy transitions outlook 2022,” 2022.

[11] K. Ramalingam and C. Indulkar, “Chapter 3 - Solar Energy and Photovoltaic Technology,” in *Distributed Generation Systems*, Elsevier Inc, 2017, pp. 69–147.

[12] S. Shields, “Cells, Modules, Panels and Arrays - FSEC®.” Florida’s Premier Energy Research Center at the University of Central Florida, 2023.

[13] Y. Yang, K. A. Kim, F. Blaabjerg, and A. Sangwongwanich, “2 - Power electronic technologies for PV systems,” in *Advances in Grid-Connected Photovoltaic Power Conversion Systems*, Y. Yang, K. A. Kim, F. Blaabjerg, and A. Sangwongwanich, Eds. Woodhead Publishing, 2019, pp. 15–43.

[14] G. A. Puche, P. G. Vidal, and E. Muñoz-Cerón, “Large-Scale Photovoltaic Power Plants,” in *Solar Energy*, pp. 125–169.

[15] Y. Yang, K. A. Kim, F. Blaabjerg, and A. Sangwongwanich, “1 - Introduction,” in *Advances in Grid-Connected Photovoltaic Power Conversion Systems*, Y. Yang, K. A. Kim, F. Blaabjerg, and A. Sangwongwanich, Eds. Woodhead Publishing, 2019, pp. 1–13.

[16] A. Rashad, S. Kamel, and F. Jurado, “Chapter 2 - The Basic Principles of Wind Farms,” in *Distributed Generation Systems*, G. B. Gharehpetian and S. M. Mousavi Agah, Eds. Butterworth-Heinemann, 2017, pp. 21–67.

[17] T. Burton, N. ; Jenkins, D. Sharpe, and E. Bossanyi, “10. Wind Energy and the Electric Power System,” *Wind Energy Handbook (2nd Edition)*. John Wiley & Sons, pp. 569–570, 2011.

[18] T. Bowen, I. Chernyakhovskiy, and P. Denholm, “Grid-Scale Battery Storage: Frequently Asked Questions,” *National Renewable Energy Laboratory*, no. 2013, pp. 1–8, 2018.

[19] A. H. Fathima and K. Palanisamy, “8 - Renewable systems and energy storages for hybrid systems,” in *Hybrid-Renewable Energy Systems in Microgrids*, A. H. Fathima, N. Prabaharan, K. Palanisamy, A. Kalam, S. Mekhilef, and J. J. Justo, Eds. Woodhead Publishing, 2018, pp. 147–164.

[20] T. Ratniyomchai, S. Hillmansen, and P. Tricoli, “Recent developments and applications of energy storage devices in electrified railways,” *IET Electrical Systems in Transportation*, vol. 4, no. 1, pp. 9–20, 2014.

[21] D. W. Gao, “Chapter 3 - Interfacing Between an ESS and a Microgrid,” in *Energy Storage for Sustainable Microgrid*, D. W. Gao, Ed. Oxford: Academic Press, 2015, pp. 79–121.

[22] Z. Hu, *Energy Storage for Power System Planning and Operation*. Newark, SINGAPORE: John Wiley & Sons, Incorporated, 2020.

[23] S. De La Torre, A. J. Sánchez-Racero, J. A. Aguado, M. Reyes, and O. Martínez, “Optimal Sizing of Energy Storage for Regenerative Braking in Electric Railway Systems,” *IEEE Transactions on Power Systems*, vol. 30, no. 3, pp. 1492–1500, 2015.

[24] S. Tang, X. Huang, Q. Li, N. Yang, Q. Liao, and K. Sun, “Optimal Sizing and Energy Management of Hybrid Energy Storage System for High-Speed Railway Traction Substation,” *Journal of Electrical Engineering and Technology*, vol. 16, no. 3, pp. 1743–1754, 2021.

[25] H. Hayashiya *et al.*, "Potentials, peculiarities and prospects of solar power generation on the railway premises," in *2012 International Conference on Renewable Energy Research and Applications, ICRERA 2012*, 2012, pp. 1–6.

[26] S. D'Arco, L. Piegari, and P. Tricoli, "Comparative Analysis of Topologies to Integrate Photovoltaic Sources in the Feeder Stations of AC Railways," *IEEE Transactions on Transportation Electrification*, vol. 4, no. 4, pp. 951–960, 2018.

[27] Z. Chen *et al.*, "Using existing infrastructures of high-speed railways for photovoltaic electricity generation," *Resources, Conservation and Recycling*, vol. 178, no. June 2021, p. 106091, 2022.

[28] I. Şengör, H. C. Kiliçkiran, H. Akdemir, B. Kekezoğlu, O. Erdinç, and J. P. S. Catalão, "Energy Management of a Smart Railway Station Considering Regenerative Braking and Stochastic Behaviour of ESS and PV Generation," *IEEE Transactions on Sustainable Energy*, vol. 9, no. 3, pp. 1041–1050, 2018.

[29] J. A. Aguado, A. J. S. Racero, and S. De La Torre, "Optimal operation of electric railways with renewable energy and electric storage systems," *IEEE Transactions on Smart Grid*, vol. 9, no. 2, pp. 993–1001, 2018.

[30] S. Boudoudouh and M. Maaroufi, "Renewable Energy Sources Integration and Control in Railway Microgrid," *IEEE Transactions on Industry Applications*, vol. 55, no. 2, pp. 2045–2052, 2019.

[31] S. R. Salkuti, "Optimal Operation of Electrified Railways with Renewable Sources and Storage," *Journal of Electrical Engineering and Technology*, no. 0123456789, 2020.

[32] C. Feng, Z. Gao, Y. Sun, and P. Chen, "Electric railway smart microgrid system with integration of multiple energy systems and power-quality improvement," *Electric Power Systems Research*, vol. 199, no. May, p. 107459, 2021.

[33] H. Ehteshami, H. Hashemi-Dezaki, and S. Javadi, "Optimal linearized operation of electric railway system in the presence of flexible renewable sources and switchable capacitor banks considering supply and demand sides' uncertainties," *Electric Power Systems Research*, vol. 211, no. November 2021, p. 108254, 2022.

[34] Y. Liu, M. Chen, Z. Cheng, Y. Chen, and Q. Li, "Robust Energy Management of High-Speed Railway Co-Phase Traction Substation With Uncertain PV Generation and Traction Load," *IEEE Transactions on Intelligent Transportation Systems*, vol. 23, no. 6, pp. 5079–5091, 2022.

[35] S. Akbari, S. S. Fazel, and S. Jadid, "Optimal operation of a smart railway station based on a multi-energy hub structure considering environmental perspective and regenerative

braking utilization," *Energy Science and Engineering*, vol. 9, no. 9, pp. 1614–1631, 2021.
[36] M. Chen, Z. Cheng, Y. Liu, Y. Cheng, and Z. Tian, "Multitime-Scale Optimal Dispatch of Railway FTPSS Based on Model Predictive Control," *IEEE Transactions on Transportation Electrification*, vol. 6, no. 2, pp. 808–820, 2020.
[37] Y. Liu, M. Chen, S. Lu;, Y. Chen;, and Q. Li;, "Optimized Sizing and Scheduling of Hybrid Energy Storage Systems for High-Speed Railway Traction Substations," *Energies*, 2018.
[38] W. Deng, C. Dai, W. Chen, and S. Gao, "Experimental Investigation and Adaptability Analysis of Hybrid Traction Power Supply System Integrated with Photovoltaic Sources in AC-Fed Railways," *IEEE Transactions on Transportation Electrification*, vol. 7, no. 3, pp. 1750–1764, 2021.
[39] Y. Ying, Q. Liu, M. Wu, and Y. Zhai, "The Flexible Smart Traction Power Supply System and Its Hierarchical Energy Management Strategy," *IEEE Access*, vol. 9, pp. 64127–64141, 2021.
[40] M. Chen, Z. Liang, Z. Cheng, J. Zhao, and Z. Tian, "Optimal Scheduling of FTPSS with PV and HESS Considering the Online Degradation of Battery Capacity," *IEEE Transactions on Transportation Electrification*, vol. 8, no. 1, pp. 936–947, 2022.
[41] S. Hillmansen, "Electric railway traction systems and techniques for energy saving," *IET Seminar Digest*, vol. 2012, no. 14922, pp. 19–23, 2012.
[42] M. Chymera and C. J. Goodman, "The calculation of train performance," in *IET Conference Publications*, 2014, vol. 2014, no. CP690.
[43] Z. Tian, P. Weston, N. Zhao, S. Hillmansen, C. Roberts, and L. Chen, "System energy optimisation strategies for metros with regeneration," *Transportation Research Part C: Emerging Technologies*, vol. 75, pp. 120–135, 2017.
[44] H. S. T. (HS2) Limited, "Grid Supply Point Connection at Parkgate."
[45] S. Hadi, *Power System Analysis*. McGraw-Hill, 1999.
[46] J. Wang and R. Hamilton, "A review of negative sequence current," in *2010 63rd Annual Conference for Protective Relay Engineers*, 2010, pp. 1–18.
[47] A. Schaffarczyk, *Understanding Wind Power Technology : Theory, Deployment and Optimisation*. Newark, UNITED STATES: John Wiley & Sons, Incorporated, 2014.
[48] G. L. Johnson, *Wind Energy Systems*. Manhattan, Kansas, 2006.
[49] C. on C. Change, "Net Zero: The UK's contribution to stopping global warming," 2019.
[50] International Energy Agency, "Renewables 2020," 2020.

[51] National Statistics, “UK Energy In Brief 2021,” 2009.

[52] Office of Rail and Road, “Rail Emissions 2019-20,” 2020.

[53] SMA Solar Tecnology, “The new Sunny Central : more power per cubic meter SUNNY CENTRAL 2200 - Datasheet,” 2021.

[54] Vestas, “General Specification V90–1.8/2.0 MW 50 Hz VCS Vestas,” 2010.

[55] E. Kiessling, Friedrich; PUSCHMANN,Rainer; SCHMIEDER, Axel; SCHNEIDER, *Contact Lines for Electric Railways Planning, Design, Implementation, Maintenance.*, vol. 1, no. 3. 2018.

[56] ABB, “More power for railway lines: Dynamic shunt compensation and static frequency conversion for the 50 Hz traction power supply,” 2016.

[57] ABB, “ABB to provide innovative traction power solution for UK railway network,” 2018.

[58] Rail Industry Association, “RIA Electrification Cost Challenge,” 2019.

[59] G. Goodman and V. Martin, “Wind powered electricity in the UK,” 2019.

[60] IEC, “IEC 60076-20 TS: Power Transformers – Part 20: Energy Effi- ciency,” 2016.

[61] B. J. Bayliss, C.R.;Hardy, “Power Transformers,” in *Transmission and Distribution Electrical Engineering*, no. 1, 2007, pp. 499–564.

[62] C. Demoulias, “A new simple analytical method for calculating the optimum inverter size in grid-connected PV plants,” *Electric Power Systems Research*, vol. 80, no. 10, pp. 1197–1204, 2010.

[63] SMA Solar Tecnology, “Sunny Tripower 15000TL/ 20000TL/ 25000TL,” 2014.

[64] ABB, “ABB wind turbine converters PCS6000, full power converter, up to 12 MW,” 2019.

[65] National Grid ESO, “Geometries of power lines,” 2023. [Online]. Available: https://www.emfs.info/sources/overhead/ohl-calculating/geometries/.

[66] A. I. El Gayar, Z. Abdul-Malek, and I. F. El-Shami, “Wind-Induced Clearances Infringement of Overhead Power Lines,” in *International Journal of Computer and Electrical Engineering*, 2014, vol. 6, no. 4, pp. 275–282.

[67] Clydesdale, “ABC, Copper, AAAC & ACSR Conductor SpecificationsTechnical,” 1990.

[68] F. Ghassemi and M. Perry, “Review of Voltage Unbalance Limit in The GB Grid Code CC . 6 . 1 . 5 (b),” *National Grid*, vol. 5, no. October. pp. 1–32, 2014.

[69] N. Grid *et al.*, “The Grid Code,” no. 5. p. 140, 2017.

[70] UK Department for Business Energy and Industrial Strategy, “Electricity Generation

Cost Report 2020,” 2020.
[71] Department of Energy and Climate Change, “Review of Renewable Electricity Generation Cost and Technical Assumptions,” 2022.
[72] National Grid ESO, “Appendix E1 Overhead Lines,” 2014.
[73] E. & I. S. Department for Business, “Quarterly Energy Prices: UK January to March 2021,” 2021.
[74] H. S. T. (HS2) Limited, “Realising the Potential,” 2018.
[75] “HS2 Phase One plan and profile maps: London to the West Midlands - GOV.UK.”
[76] H. S. T. (HS2) Limited, “London to the West Midlands and Beyond - HS2 Technical Appendix,” 2009.
[77] I. Pfenninger, S., Staffell, “Renewables.ninja.” [Online]. Available: https://www.renewables.ninja/.
[78] SP Energy Networks, “Calculation of system fault levels,” 2008.
[79] National Grid ESO, “Introducing our 2021 Future Energy Scenarios | National Grid ESO.” .
[80] E. Pilo De La Fuente, S. K. Mazumder, and I. G. Franco, “Railway Electrical Smart Grids: An introduction to next-generation railway power systems and their operation,” *IEEE Electrification Magazine*, vol. 2, no. 3, pp. 49–55, 2014.
[81] Y. Jiang, J. Liu, W. Tian, M. Shahidehpour, and M. Krishnamurthy, “Energy Harvesting for the Electrification of Railway Stations: Getting a charge from the regenerative braking of trains,” *IEEE Electrification Magazine*, vol. 2, no. 3, pp. 39–48, 2014.
[82] Y. C. and Q. L. Yuanli Liu, Minwu Chen, Shaofeng Lu, “Optimized Sizing and Scheduling of Hybrid Energy Storage Systems for High-Speed Railway Traction Substations,” *Energies*, 2018.
[83] L. P. Di Noia and R. Rizzo, “Analysis of Integration of PV Power Plant in Railway Power Systems,” in *Proceedings of 2019 8th International Conference on Modern Power Systems, MPS 2019*, 2019, pp. 1–5.
[84] B. An, Y. Li, J. M. . Guerrero, W.-J. Lee, L. Luo, and Z. Zhang, “Renewable Energy Integration in Intelligent Railway of China : Configurations, Applications and Issues,” no. March, pp. 2–22, 2020.
[85] M. Brenna, F. Foiadelli, and H. J. Kaleybar, “The Evolution of Railway Power Supply Systems Toward Smart Microgrids: The concept of the energy hub and integration of distributed energy resources,” *IEEE Electrification Magazine*, vol. 8, no. 1, pp. 12–23, 2020.

[86] H. Novak, V. Lešić, and M. Vašak, "Hierarchical coordination of trains and traction substation storages for energy cost optimization," in *IEEE Conference on Intelligent Transportation Systems, Proceedings, ITSC*, 2018, vol. 2018-March, pp. 1–6.

[87] L. Razik, N. Berr, S. Khayyam, F. Ponci, and A. Monti, "REM-S-Railway energy management in real rail operation," *IEEE Transactions on Vehicular Technology*, vol. 68, no. 2, pp. 1266–1277, 2019.

[88] S. Park and S. R. Salkuti, "Optimal energy management of railroad electrical systems with renewable energy and energy storage systems," *Sustainability (Switzerland)*, vol. 11, no. 22, 2019.

[89] H. Abdi, B. Mohammadi-ivatloo, S. Javadi, A. R. Khodaei, and E. Dehnavi, "Chapter 7 - Energy Storage Systems," in *Distributed Generation Systems*, G. B. Gharehpetian and S. M. Mousavi Agah, Eds. Butterworth-Heinemann, 2017, pp. 333–368.

[90] ABB, "ABB solar inverters - One of the broadest offerings in the industry," 2015.

[91] W. Cole and A. W. Frazier, "Cost projections for utility-scale battery storage," 2019.

[92] Z. Tian, "System Energy Optimisation Strategies for DC Railway Traction Power Networks," University of Birmingham, 2017.